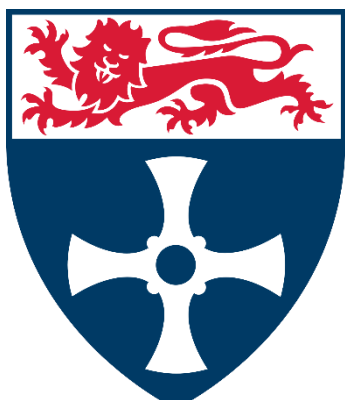


# **Biosynthetic Materials to Mimic the Musculoskeletal Environment**



# **Newcastle University**

**Kegan McColgan-Bannon**

Thesis Submitted for the title of Doctor of Philosophy (Integrated)

Newcastle University

School of Engineering

School of Mechanical Engineering

March 2021

## **Acknowledgements**

I would like to thank my supervisors, Dr Ferreira-Duarte, Prof Kenneth Dalgarno, and Dr Piergiorgio Gentile for helping me through the PhD process. Thanks too, for the support of my major funding and supporting bodies, EPSRC, Versus Arthritis, and the AMCDT at the University of Nottingham. To the academic collaborators who helped bring together the work on Fibre Scaffolds, Dr Sarah Upson and Dr Muhammad Tausif. Thanks to the Bioimaging Unit at Newcastle University for their expertise and support, and to the many other technicians and academics who agreed to let me use their equipment. To all of Cohort 2 from the AMCDT for making my time in Nottingham as fun as it was educational. Lastly thanks to my PhD compatriots at Newcastle University, whose company made the entire process infinitely more enjoyable.

## **Abstract**

Gaps in the current capabilities of Tissue Engineering approaches to treat musculoskeletal conditions has driven research into biosynthetic materials for use in scaffolds. The natural ECM polymers used in these have beneficial surface chemistry for the adhesion and proliferation of cells, but lack in mechanical integrity and stability. Synthetic polymers PCL and PHBV, selected for their biocompatibility and degradation properties, are examined as base materials for the fabrication of biosynthetic scaffolds with Collagen.

This study aims to develop new biosynthetic materials, design synthetic techniques, characterize the materials, and evaluate the fabrication techniques through which the materials are processed. Based on existing work in 3D printed and fiber polymer scaffolds we ask: can the viability of these scaffolds be enhanced by the incorporation of natural ECM proteins?

The optimized synthesis of biosynthetic materials and their scaffold fabrication process strategies are outlined in the thesis, and their viability assessed through physicochemical, mechanical, and biological characterization. Optimised fabrication pathways to the creation of collagen functionalized scaffolds of PCL, PHBV, and PCL / PHBV through Fused Filament Fabrication and Forcespinning are detailed.

The results of characterizing these scaffolds found that different manufacturing routes prove suitable for different tissue engineering applications, FFF printed robust flexible log pile structures to articular cartilage, force spun fragile high surface area fibers to dermal regeneration. In both instances collagen functionalization increased favourable cellular behaviour on the scaffolds.

## Contents

Acknowledgements .....	2
Abstract .....	3
Contents .....	4
List of Acronyms aAbbreviations .....	11
Chapter 1: Introduction .....	12
Aims and Objectives .....	15
Chapter 2: Literature Review .....	17
2.1 Introduction .....	17
2.2 Osteoarthritis and cartilage damage .....	17
<b>Figure 2.1</b> .....	18
2.3 Tissue Engineering and Regenerative Medicine .....	18
2.3.1 History of Tissue Engineering.....	18
2.3.2 Tissue Engineering applied to treat musculoskeletal defects and diseases .....	20
2.4 Scaffold Characteristics.....	21
<b>Table 2.1</b> .....	22
2.5. Biomaterials for TE Musculoskeletal Applications .....	22
2.5.1 The Use of Synthetic Polymers.....	22
<b>Table 2.2</b> .....	23
2.5.2 Poly- $\epsilon$ -Caprolactone (PCL) .....	23
2.5.3 Poly – L – Lactic acid (PLA) & Poly (lactic-co-glycolic acid) (PLGA) .....	24
2.5.4 Poly(3-hydroxybutyrate-co-3-hydroxy valerate) (PHBV) .....	25
2.5.5 Polyurethanes (PU).....	25
2.6 Use of Natural Polymers and ECM-derived Materials .....	25
<b>Table 2.3</b> .....	26
2.6.1 Collagen.....	26
<b>Figure 2.2</b> .....	27
2.6.2 Elastin.....	27
2.6.3 Fibrin .....	28
2.6.4 Hyaluronic Acid .....	28
2.6.5 Chondroitin Sulphate.....	28
2.6.6 Chitosan.....	28
2.7 The Use of Functionalised and Biosynthetic Scaffolds .....	29
<b>Table 2.4</b> .....	29
<b>Figure 2.3</b> .....	31
2.8 Collagen Functionalisation of Polymer scaffolds. ....	32

<b>Figure 2.4</b>	33
2.9. Scaffold Fabrication Methods and Their Use in Musculoskeletal Applications	34
2.9.1 Additive Manufacturing for Tissue Engineering	34
2.9.2 Fused Filament Fabrication	34
<b>Figure 2.5</b>	35
2.9.3 Electrospinning and Forcespinning	35
<b>Figure 2.6</b>	36
<b>Figure 2.7</b>	37
3. Summary	37
Chapter 3: Methods and Materials	38
3.1. Materials	38
3.1.1 General Reagents	38
3.1.2 Scaffold Materials	38
3.1.3 Solvents	39
3.1.4 Coupling Reagents	39
3.1.5 Cell Culture and Cytocompatibility Reagents	39
3.2 Methods	40
3.2.1 Biosynthetic Materials Based on PCL and Collagen	40
3.2.1.1 PCL-g-Collagen Bulk Functionalisation	40
3.2.1.2 PCL-s-Collagen Films Surface Functionalisation	40
3.2.1.3 PCL / Collagen Biosynthetic Blend	40
3.2.1.4 PCL-g-Gelatin Films Surface Functionalisation	41
3.2.1.5 Surface Functionalisation of PCL with Hyaluronic Acid (PCL-g-HA) Films and Scaffolds	41
3.2.2 Biosynthetic Materials Based on PHBV and Collagen	41
3.2.2.1 PCL / PHBV Blends Functionalised with Collagen	41
3.2.2.2 Surface Functionalisation of PHBV with Collagen	42
3.3 Materials Processing	42
3.3.1 Hot Compression Moulding	42
3.3.2 Filament Extrusion	42
<b>Figure 3.1</b>	43
<b>Table 3.1</b>	43
3.3.3 3D Printing – Fused Filament Fabrication (FFF)	43
<b>Table 3.2</b>	44
3.3.4 Laser Cutting of PCL and PCL / PHBV Scaffolds and Films	44
3.3.5 Preparation PHBV Fibre Membranes and Films	44
<b>Figure 3.2</b>	45
3.3.6 Spin Coating	45

3.4 Physicochemical Characterisation and Analysis .....	45
3.4.1 Scanning Electron Microscopy (SEM).....	45
3.4.2 Optical Microscopy and Fluorescence Analysis .....	45
3.4.3 Confocal Microscopy .....	46
3.4.4 Image Processing and Analysis.....	46
3.4.5 Sirius Red Staining.....	46
3.4.6 Fourier Transform Infrared – Attenuated Total Refraction (ATR-FTIR) .....	46
3.4.7 Differential Scanning Calorimetry (DSC).....	46
3.4.9 Contact Angle.....	46
3.4.10 Degradation Studies .....	47
3.4.11 Mechanical Analysis .....	47
3.5 Biological Analysis .....	47
3.5.1 Cell Culture and Expansion.....	47
3.5.2 Cell Counting using Haemocytometer .....	48
3.5.3 Cell Freezing and Defrosting .....	48
3.5.4 Technique for Cell Seeding onto Scaffolds.....	48
3.5.5 Cytoskeletal and Nucleus Staining.....	49
3.5.6 Metabolic Activity Analysis by Presto Blue Assay .....	49
3.5.7 Analysis of Cell Viability by LIVE / DEAD Assay.....	50
3.5.8 Statistical Analysis .....	50
Chapter 4: Evaluation of Conjugation Methods for 3D Structures.....	51
4.1 Introduction .....	51
4.2 Synthesis of Biosynthetic Materials Based on PCL and Collagen.....	51
4.2.1 PCL-g-Collagen Bulk Material .....	51
<b>Table 4.1</b> .....	52
<b>Figure 4.1</b> .....	52
4.2.2 PCL and Collagen Blend Material (PCL / Collagen Blends).....	53
<b>Figure 4.2</b> .....	53
4.2.3 Chemical Analysis by ATR-FTIR.....	53
<b>Figure 4.3</b> .....	55
<b>Figure 4.4</b> .....	56
4.3 Material Processing Development and Analysis.....	57
4.3.1 Assessment of collagen content and wettability changes onto Spin Coated thin-films .....	57
<b>Table 4.2</b> .....	57
<b>Figure 4.5</b> .....	58
4.3.2 PCL and Collagen Modified Samples Processed by Hot Moulding .....	58
<b>Figure 4.6</b> .....	59

4.3.3 Extrusion of PCL and Collagen Modified Samples.....	59
<b>Table 4.3 .....</b>	60
<b>Figure 4.7.....</b>	61
4.3.4 Processing PCL and Collagen Modified Samples by Fused Filament Fabrication (FFF) Printing .....	62
<b>Table 4.4 .....</b>	62
<b>Figure 4.8.....</b>	64
4.3.5 Hydrolytic Degradation Studies of PCL-Collagen films and Scaffolds .....	64
<b>Figure 4.9 .....</b>	65
4.3 Discussion.....	66
4.3.1 PCL-Collagen Synthesis and Analysis .....	66
<b>Table 4.5 .....</b>	66
<b>Figure 4.10 –.....</b>	67
4.3.2 Chemical Analysis by ATR-FTIR of Produced PCL and Collagen Materials .....	68
4.3.3 Assessing the Solubility Properties of PCL-Collagen Biosynthetic Materials.....	68
4.3.4 Creation of PCL and PCL-Collagen Films by Hot Moulding .....	69
4.3.5 Assessment of the Wettability Characteristics of PCL and PCL-Collagen by Contact Angle.....	70
4.3.6 Creation of PCL and PCL-Collagen Filaments by Extrusion.....	70
4.3.7 Printing of PCL and PCL-Collagen Scaffolds; Optimisation and Results .....	73
<b>Figure 4.11.....</b>	74
4.3.8 Assessing the Decomposition of PCL and PCL-Collagen through Hydrolytic Degradation.....	75
4.4 Chapter Conclusion.....	76
<b>Table 4.7 .....</b>	78
Chapter 5: PCL / PHBV-Collagen Materials Development and Scaffold Production .....	79
5.1. Introduction.....	79
<b>Figure 5.1.....</b>	79
5.2. PCL / PHBV blend at different ratios: blend selection analysis .....	79
5.2.1. Contact Angle .....	79
5.2.2. Tensile Strength .....	79
5.2.3. Tensile Modulus .....	80
5.2.4. ATR-FTIR Characterisation of PCL / PHBV Blends.....	80
<b>Figure 5.2.....</b>	81
<b>Figure 5.3.....</b>	82
5.3. PCL / PHBV and PCL / PHBV-Collagen films: physical-chemical properties .....	82
5.3.1. Contact Angle .....	82
<b>Figure 5.4.....</b>	83
5.3.2. ATR-FTIR chemical analysis .....	83

<b>Figure 5.5</b> .....	84
5.4. Manufacturing of PCL / PHBV and PCL / PHBV-Collagen scaffolds by FFF printing .....	84
5.4.1. Filament Extrusion .....	84
5.4.2. FFF Printing .....	84
<b>Table 5.6</b> .....	84
<b>Figure 5.6</b> .....	85
5.4.3. Compressive Modulus .....	85
<b>Figure 5.7</b> .....	86
5.4.5. Degradation Studies .....	86
<b>Figure 5.8</b> .....	87
5.5. Discussion .....	87
5.5.1. PCL / PHBV Material Analysis .....	87
5.5.1. PCL / PHBV-Collagen Discussion .....	88
5.5.2. Wettability .....	88
5.5.3. ATR-FTIR .....	89
5.5.4. Extrusion .....	89
<b>Table 5.8</b> .....	90
5.5.5. FFF Printing of Scaffolds .....	90
5.5.6. Compression Testing .....	91
5.5.7. Hydrolytic Degradation .....	91
5.5.8. Summary .....	92
Chapter 6: Biological Performance of 3D Printed PCL and PCL / PHBV Scaffolds	
Functionalised with Collagen .....	93
6.1. Introduction .....	93
6.2. 3D printed porous PCL-scaffolds functionalised with Collagen .....	93
6.2.1. Cell viability by LIVE / DEAD assay .....	93
<b>Figure 6.1</b> .....	94
<b>Figure 6.2</b> .....	95
6.3. 3D printed PCL films functionalised with Collagen .....	95
6.3.1. Neo-NHDF fibroblasts viability by LIVE / DEAD assay .....	96
<b>Figure 6.3</b> .....	96
6.3.2. Neo-NHDF fibroblasts Metabolic Activity .....	96
<b>Figure 6.4</b> .....	97
6.3.3. Cell Morphology of Tc28a2 chondrocytes .....	97
<b>Figure 6.5</b> .....	98
6.4. 3D printed PCL / PHBV-scaffolds functionalised with Collagen .....	98
6.4.1. TC28a2 chondrocytes viability by LIVE / DEAD assay .....	98
<b>Figure 6.6</b> .....	99

6.4.2. TC28a2 chondrocytes Metabolic Activity by presto blue assay.....	99
<b>Figure 6.7.....</b>	100
6.4.3. Cell Morphology of Tc28a2 chondrocytes onto 3D printed Discs .....	100
<b>Figure 6.8.....</b>	101
6.5. Discussion .....	101
6.5.1. 3D printed porous PCL-scaffolds functionalised with Collagen .....	101
6.5.2 3D printed PCL discs functionalised with Collagen.....	103
6.5.3. 3D printed PCL / PHBV discs functionalised with Collagen.....	104
6.5.4. 3D printed PCL / PHBV scaffolds functionalised with Collagen .....	105
6.5.5. Comparison between cell morphology of Tc28a2 chondrocytes onto 3D printed PCL and PCL / PHBV scaffolds functionalised with Collagen .....	106
6.6. Summary and interim conclusions.....	106
Chapter 7: Biomimetic PHBV-Collagen Forcespun Membranes.....	107
7.1. Introduction.....	107
7.2. Collagen functionalisation of PHBV Forcespun membranes .....	107
<b>Figure 7.1.....</b>	107
7.3. Physical-chemical characterisation of functionalised PHBV-collagen membranes ...	108
7.3.1. Fibre Collagen Content and Morphology .....	108
<b>Figure 7.2.....</b>	109
7.3.2. Chemical analysis by ATR-FTIR .....	109
<b>Figure 7.3.....</b>	110
7.3.3. Chemical analysis by X-Ray Photoelectron Spectroscopy (XPS).....	110
<b>Figure 7.4.....</b>	111
7.3.4. Thermal analysis by Differential Scanning Calorimetry (DSC).....	111
<b>Figure 7.5.....</b>	112
7.3.5. Contact Angle .....	112
7.3.6. In Vitro Hydrolytic Degradation Study .....	112
<b>Figure 7.6.....</b>	113
7.4. Cytocompatibility studies of functionalised PHBV-collagen membranes .....	113
7.4.1. Cellular Metabolic Activity .....	113
<b>Figure 7.7.....</b>	114
7.4.2. Cell viability and morphology .....	114
<b>Figure 7.8.....</b>	115
<b>Figure 7.9.....</b>	116
7.5. Discussion .....	116
7.6. Summary and interim conclusion .....	119
Chapter 8: Summary Discussion, Conclusions, and Future Work .....	121
8.1. Introduction.....	121

8.2. Summary Discussion .....	121
8.2.1. Material Processing .....	121
8.2.2. Route to the Scaffold.....	121
8.2.3. Building logpiles and spinning fibers.....	121
8.2.4. Cytocompatibility, morphology, and metabolism studies.....	124
8.3. Conclusions .....	124
8.4. Future work .....	126
8.4.1. Continued support .....	126
8.4.2. Wider application .....	127
Appendix: References .....	128

## **List of Acronyms aAbbreviations**

ABS – Acrylonitrile butadiene styrene

ATR-FTIR – Attenuated Total Refraction – Fourier Transform Infrared

DAPI – 4',6-diamidino-2-phenylindole dihydrochloride

DCC – Dicyclohexylcarbodiimide

DCM – Dichloromethane

DMA – Dynamic Mechanical Analysis

DMEM – Dulbecco's Modified Eagle Medium

DMF – Dimethylformamide

DSC – Differential Scanning Calorimetry

ECM – Extra Cellular Matrix

EDC – N-(3-Dimethylaminopropyl)-N'-ethylcarbodiimide hydrochloride

FFF – Fused Filament Fabrication

HFP – 1,1,1,3,3,3-Hexafluoro-2-propanol

MES – 2-(N-Morpholino) ethanesulfonic acid hydrate

NaOH – Sodium Hydroxide

PBS – Phosphate Buffered Saline

PCL – Poly  $\epsilon$ -Caprolactone

PHBV – Poly (3-hydroxybutyrate-co-3-hydroxy valerate)

PLA – Poly Lactic Acid

PLGA – Poly (lactic-co-glycolic acid)

PU – Poly Urethane

TE – Tissue Engineering

THF – Tetrahydrofuran

## **Chapter 1: Introduction**

Tissue Engineering (TE) has been in the scientific vernacular since the 1980's, albeit in loose referral to the use of prosthetics and surgical modification of tissue. According to Vacanti<sup>1</sup>, (and in contention with other historical accounts of the discipline) the earliest use of the term in the modern sense was in a 1991 paper "Functional Organ Replacement: The New Technology of Tissue Engineering" in the *Surgical Technology Today* journal.

In his 1993 paper "Tissue Engineering", Langer<sup>2</sup> defined the nascent subject: "Tissue engineering is an interdisciplinary field that applies the principles of engineering and the life sciences towards the development of biological substitutes that restore, maintain, or improve tissue function." He also set out three core components of TE for the creation of new tissue, which largely resemble the body of current literature, even 25 years after initial publication. These are as follows:

1. Isolated cells or cell substitutes.
2. Tissue-inducing substances.
3. Cells placed on or within matrices.

It is widely accepted in the scientific community that Tissue Engineering strategies are those that combine the principles of all three of the above.

The primary nature of the work covered in this thesis covers the development of scaffolds constructed from biocompatible materials that help induce cellular growth and the analysis of cells seeded within these matrices. The proposed purpose of these biomaterial scaffolds is the healing of musculoskeletal tissues damaged through conditions such as osteoarthritis (OA), where tissue damage can range from hyaline cartilage through subchondral bone.

Current therapies in the treatment of cartilage defects are primarily surgical (late-stage progression) or preventative (early-stage progression), leaving broad segments of patients with unmet needs. There is a gap for mid stage therapies in the treatment paradigm, and the TE approach is one route that could address this gap. TE therapies have been approved for the treatment of cartilage damage in the form of Autologous Chondrocyte Implantation, a wholly cell-based therapy. This treatment, however, has limitations in terms of the mechanical support provided to implanted cells.

To this point, this thesis details the examination of a range of biomaterials processed into scaffolds in different configurations. The project encompasses multiple aspects of medical

device development, materials science, scaffold design and fabrication, and *in vitro* biological characterisation. The primary materials under examination are Poly- $\epsilon$ -Caprolactone (PCL), Poly (3-hydroxybutyrate-*co*-3-hydroxy valerate) (PHBV), and Type I Collagen. PCL and PHBV were selected for their mechanical properties, biocompatibility, and neutral degradation characteristics, while Collagen was selected to enhance the surface properties of the scaffolds, due to its versatility in conjugation and excellent cellular adhesion promotion. The work consists of three projects that centre on the theme of developing 3D biomaterial scaffolds from biocompatible synthetic polymers that have been functionalised with collagen.

The first two projects focusing on the development of PCL and PCL / PHBV logpile scaffolds utilise the additive manufacturing technology Fused Filament Fabrication (FFF) to produce 3D porous scaffolds. The proposed application of these scaffolds is in developing a treatment for the cartilage damage seen in osteoarthritis.

The Thesis will follow the following structure:

Chapter 1: Introduction

Chapter 2: Literature Review

Chapter 3: Methods and Materials

Chapter 4: Evaluation of Conjugation Methods for 3D Structures

Chapter 5: PCL / PHBV Materials Development and Scaffold Production

Chapter 6: Biological performance of 3D printed PCL and PCL / PHBV scaffolds  
functionalised with Collagen

Chapter 7: Biomimetic PHBV – Collagen Forcespun Membranes

Chapter 8: Summary Discussion, Conclusions, and Future Work

Appendix: References

### ***Chapter 2: Literature Review***

The literature review begins by examining the context to developing a TE therapy for cartilage repair in the context of patient unmet needs, and the requirements and specifications for scaffolds to fit this purpose. The review then examines commonly used synthetic, natural, and biosynthetic polymers used in cartilage TE research. After examining the materials, common processing techniques are detailed, including both processing technology, such as 3D printing, and the chemical conjugation techniques used in building biosynthetic materials.

### ***Chapter 3: Methods and Materials***

An exhaustive list of materials used in the experiments, along with a detailed description of the methodologies at each stage. Covering material processing, analysis, and cellular assays.

### ***Chapter 4: Evaluation of Conjugation Methods for 3D Structures***

The first of the results / discussion chapters, this chapter describes the experiments used to define the fabrication process to create PCL-Collagen scaffolds from biosynthetic material synthesis to final product. The content of this chapter begins with a description of five different synthetic techniques used to create the different forms of biosynthetic PCL-collagen materials. The physicochemical characterisation, mechanical properties, processing optimization, and development of printing parameters for these materials are detailed in the results section. The chapter concludes with a discussion on the experiments to point, with a critique of the properties of each material and the challenges involved in their production. Summarising the rationale behind the selection of processing methods carried forward to future experiments. In addition, the challenges involved in process optimisation for extrusion and 3D printing are also discussed.

### ***Chapter 5: PCL / PHBV-Collagen Materials Development and Scaffold Production***

This chapter covers the development of PCL / PHBV blended materials from base polymers into PCL / PHBV-collagen biosynthetic logpile scaffolds. The chapter details the assessment of PCL / PHBV blends through physical and mechanical testing, before settling on a ratio to carry forward with. The blend ratio of 60 / 40 w / w PCL / PHBV was used to fabricate filaments and then scaffolds, which were further conjugated with Collagen. The results section details the examination of the physicochemical and mechanical properties, and optimisation of fabrication processes. The chapter closes with discussion of the physicochemical and mechanical properties of the PCL / PHBV scaffolds, both as a distinct project and within the context of the broader work conducted in the previous chapter on developing PCL-Collagen materials and scaffolds.

### ***Chapter 6: Biological Performance of 3D Printed PCL and PCL / PHBV Scaffolds Functionalised with Collagen***

This chapter describes the biological testing of the biosynthetic material scaffolds detailed in the prior two chapters. The cytocompatibility and metabolic properties of fibroblastic and chondrocytic cells seeded on 3D “logpile” scaffolds and 3D printed flat discs of conjugated PCL and PCL / PHBV were examined. The cytocompatibility, morphology, and metabolism of seeded cells were examined to understand the biological behaviour of conjugated and

unconjugated scaffolds. The chapter closes with a discussion of the results detailed in the chapter and interim conclusions.

### ***Chapter 7: Biomimetic PHBV – Collagen Forcespun Membranes***

The third project investigates the use of Forcespinning technology in the fabrication of 3D nanofibre PHBV webs, conjugated with collagen post fabrication. The intended application of these webs is musculoskeletal, but not in load-bearing tissues. The chapter details the results of the physicochemical testing to examine the chemical composition, surface, and mechanical properties, in addition to using cellular assays to assess the cytocompatibility, morphology and metabolism of cells seeded onto scaffolds. The chapter closes with a discussion of the results in the context of biocompatible fibre membrane literature.

### ***Chapter 8: Summary Discussion, Conclusions, and Future Work***

This chapter begins with a high-level overview discussion in comparing the results of the 4 previous chapters. The physicochemical, mechanical, and biological properties of PCL logpile, PCL / PHBV logpile, and PHBV fibre scaffolds are contrasted, along with discussion on the suitability for application, and advantages / disadvantages of each process and product. The chapter then lists the conclusions of the work detailed in the thesis, centered around the materials processing journey, biological behaviour, and recommendations for application. The chapter closes with recommendations for future work to refine the findings of this thesis, and the impact of the work in the wider field.

#### ***Aims and Objectives***

##### ***Aims:***

To develop new biosynthetic material scaffolds with enhanced surface properties, to investigate for potential use in musculoskeletal tissue engineering applications. The tissue of specific interest is articular cartilage but also in skin. As such methods of advanced manufacture, cell lineage choice and analysis will be tailored to investigate both outcomes. The aim is to achieve this by assessing different fabrication routes to producing tissue engineering scaffolds, on which the biological properties will be assessed using seeded cells and analytical assays. Fabrication will be assessed at the point of synthesis/ blending/ conjugation, the physicochemical properties of the materials, processing of materials into filaments, optimised 3D printing method, and the mechanical and biological properties of printed scaffolds.

***Objectives:***

1. Develop new biosynthetic polymer materials for potential application in cartilage tissue engineering utilising 3D printing and advanced manufacturing techniques.
2. To develop novel conjugation methods to functionalise the base polymers with proteins relevant to the cartilage application.
3. Assess the material fabrication strategies through which the new biosynthetic materials were processed into 3D scaffolds.

## **Chapter 2: Literature Review**

### ***2.1 Introduction***

Musculoskeletal defects represent a unique and pressing problem, with over a million new cases requiring bone graft procedures reported annually in the US and EU. Though not associated with as high an impact on quality of life (QOL) as rheumatoid arthritis, osteoarthritis (OA) is socioeconomically a greater concern due to the higher population morbidity<sup>3</sup>, and is recognised as a major public health concern. In 2013, there were approximately 9 million individual reported<sup>4</sup> cases of OA in the UK, the total direct costs<sup>5</sup> of which are estimated at over £1 billion to the NHS and speculative indirect costs of £6 billion to the wider market due to labour exclusion, caused by sick days, doctors' appointments, developing adjacent illnesses, etc. Of direct costs to the NHS, £850 million is primarily attributed to arthroplasty (Total Joint Replacement) and other surgical treatments, with the remaining £160 million primarily spent on non-steroidal anti-inflammatory drugs (NSAIDs). The combination of advances in medical technology and increasingly sedentary lifestyles brought about by shifts from manual labour to office based jobs has led to increases in the elderly and obese demographics across the western world which has in turn, projected massive increases in the prevalence of OA in coming years<sup>6</sup>. OA presents in many joints, most commonly in the knee and hip, but often presenting in the hands. OA accounts for approximately 50% of the total musculoskeletal patients in the UK with 33% of adults over the age of 45 diagnosed with the condition in one or more joints.

### ***2.2 Osteoarthritis and cartilage damage***

OA is a common joint disease associated with the degradation of cartilage and bone tissue<sup>4</sup>; it is typically associated with repetitive mechanical stress and aging, however, it is also strongly tied to gender, body mass, increasing age, physical activity levels, and can be induced by severe joint trauma. Over a duration of time , OA is exhibited by the progressive deterioration of tissues in the joint, leading to symptoms of pain, stiffness and swelling, fatigue, and functional limitation<sup>7</sup>. OA typically begins with cartilage wear leading to small defects in the tissue and as the disease progresses, leads to an overall thinning of the cartilage layer. As a result of the damaged layer, tissue growth is accelerated in the joint as the body tries to repair the damaged tissue, causing osteophyte formation and inflamed synovium, resulting in joint swelling and stiffness. In the late stages of OA, areas of the cartilage are completely worn away, leaving the underlying bone tissue exposed with no shielding against other bone tissue, causing debilitating bone defects to form through the wear of regular movement. Once defects reach critical size (defined as the point at which defects cannot heal without intervention<sup>8</sup>, between 2-3 cm<sup>2</sup><sup>9</sup>), significant pain, swelling and reduced range of motion are observed in patients, causing a

significant degradation on the patient's QOL, increasing risk of developing depression and cardiovascular disease<sup>10</sup>.

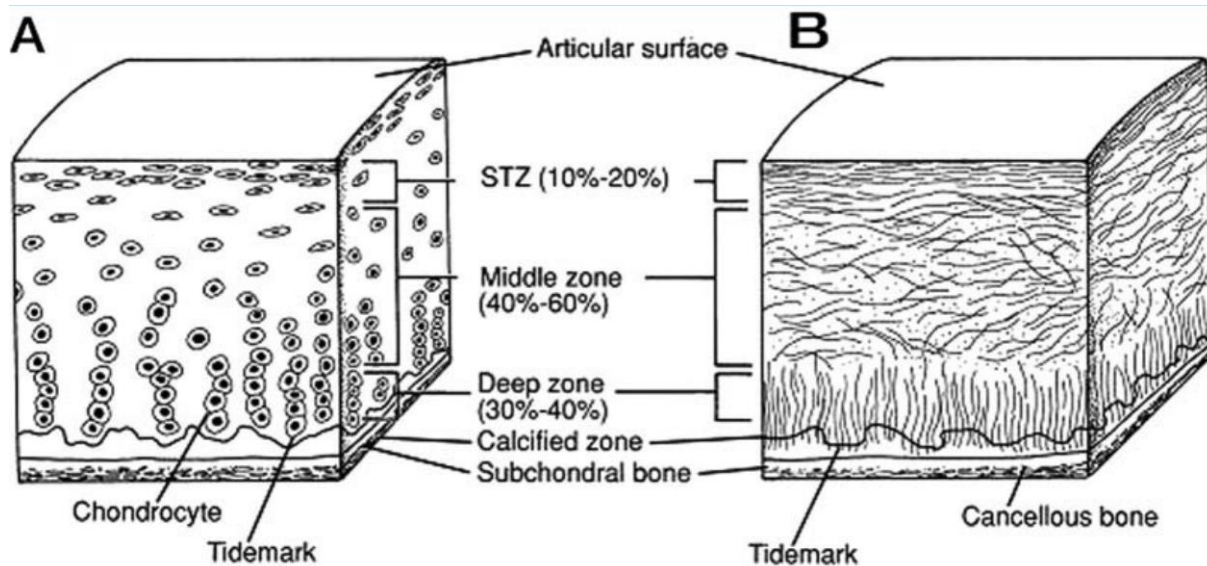


**Figure 2.1:** Cross sectional representation of the structure of articular cartilage. A. Representation of the structure by cellular morphology and distribution; B. Representation of the structure by the alignment and density of collagen ECM fibrils<sup>11</sup>.

Articular cartilage is hyaline in morphology (not fibrous, like the cartilage in the ear or nose), and varies in depth from c. 2-4mm<sup>11</sup>. Articular cartilage is avascular and without innervation, and as such lack the ability to bring in (or remove) nutrients like other tissues. The tissue is composed of chondrocytes that deposit an extracellular matrix composed primarily of collagen and proteoglycans, with other proteins in lower quantities. Chondrocytes (Figure 2.1 A) are stratified throughout articular cartilage, forming different layers; described in Figure 2 as STZ (superficial tangential zone), middle zone, and deep zone. The alignment of cells in the STZ causes the collagenous ECM to deposit in a horizontal fashion, providing sheer stress protection on the surface of the tissue. The middle zone chondrocytes are more sparsely distributed and less aligned, with thicker collagen fibrils. The deep zone has densely packed chondrocyte formations and provides the tissues most strong resistance to compressive forces, with vertically aligned collagen fibrils. Below the deep zone, the tissue becomes calcified and transitions into cells of a bone morphology lineage. =

### 2.3 Tissue Engineering and Regenerative Medicine

#### 2.3.1 History of Tissue Engineering

Tissue Engineering (TE) is a multidisciplinary area within the Regenerative Medicine field that has emerged over the past 4 decades, which seeks to create and apply new therapies based upon integrating the fabrication of biological mimicking scaffolds, the growth of tissue appropriate

cells within these scaffolds and the incorporation of growth promoting substances, with the intent of regenerating injured tissues. The relatively new discipline incorporates expertise from the fields of medicine, engineering, and biology, expanding rapidly since its inception with applications from the growth of artificial organs and skin to cartilage repair. Evidence of the historical implementation of TE principles and techniques can be dated back to 3000 BCE<sup>12</sup>, with evidence of skin grafts appearing in ancient India, however, the etymology of TE as we know it currently began to circulate in the late 1980's. According to the 2011 historical account of TE by Yarmush et al.<sup>13</sup>, the coinage of the term can be attributed to Dr Y.C. Fung in a 1985 proposal for funding while at the University of California at San Diego, though this is disputed by Vacanti's 2006 history<sup>1</sup> of the field in which he attributes the roots of the term to his own work with Robert Langer in the mid-80's. The term then popularised in the modern scientific vernacular through Vacanti's '91 publication "Functional Organ Replacement: The new technology of Tissue Engineering" and Vacanti and Langer's '93 article in *Science*: "Tissue Engineering".

Before the term tissue engineering was associated with the science, work in the 70's by James Rheinwald and Howard Green<sup>14</sup> at Harvard described the extraction and use of keratinocytes, from patient derived biopsied skin samples, to regrow epidermal skin layers for burns victims, leading to the commercialisation of the first cell-based TE product "Genzyme". Genzyme was used to treat burns patients without enough remaining skin to perform an autograft, however, the dermal layer formed was found to be thin and brittle, resulting in the treatment not being widely administered.

An early example of combining natural and synthetic polymers in a TE scaffold, a product under the name "Dermal Regeneration Template" was developed by MIT engineer Ioannis Yannas with burns surgeon John Burke<sup>15</sup>, which consisted of a freeze-dried, porous matrix of bovine type I collagen and shark chondroitin sulphate mounted on silicone sheets. In their '81 paper describing the development of a "physiologically acceptable" artificial skin substitute, the authors outline a set of biochemical, mechanical and physicochemical criteria to which the treatment substrate should abide. The list of criteria can broadly be observed in modern TE articles and include the need for skin property mimicking in: bending rigidity, tear strength, modulus of elasticity, surface energy, control of pore structure, controlled rate of biodegradation, non-toxic metabolites, low or absent antigenicity, absent inflammatory or foreign body reaction, facilitating the entry of intended tissues, synthesis of neo-dermal tissue. The authors also cite the requirement of maintaining the native triple helical structure of

collagen as a necessary consideration in the manufacturing process, though given the sterilisation conditions of 105°C, there is room for interpretation as to their success in this.

A key study by Langer and Vacanti in '88<sup>16</sup> tested the efficacy of a selection of “bioerodable” and “biodegradable” artificial polymers to act as vectors for selective cell transplantation. The study examined scaffolds of polyglactin, polyanhydrides, and poly orthoesters cultured for 4 days with hepatocytes, pancreatic islets, and small intestinal cells, then transplanted into animal recipients. The study showed the cells proliferated on the synthetic scaffolds, however, only the hepatocytes survived transplantation. Nonetheless, successfully transplanted cultured scaffolds showed evidence of vascularisation of the cell masses post-transplant in the host animal, demonstrating proof of concept for using synthetic scaffolds as a delivery vector for harvested cells, further opening further possibilities for research in the field.

Since the early days of the field, TE has seen application to a wide variety of tissues using a range of therapeutic delivery devices. For the sake of brevity, this review will focus primarily on the development of treatments involving biocompatible polymer scaffolds and work relevant to cartilage TE.

### ***2.3.2 Tissue Engineering applied to treat musculoskeletal defects and diseases***

Given the expense and complications associated with conventional approaches to treatment, tissue engineering (TE) has emerged as a method of repairing damaged tissues through regeneration instead of replacement. Over the course of TE’s development, numerous attempts have been made to circumvent the inherent shortcomings of traditional Osteoarthritis treatments, with the intention of using earlier stage, less invasive intervention to regenerate cartilage layers before the necessity of total joint replacement.

Two of the major considerations in developing TE treatments are the use of cell therapies and scaffolds<sup>17</sup>, and the two in conjunction. Each approach comes with its own set of considerations and must be examined individually. As the field of stem cells is relatively new and the best method of manipulating the cells is still under debate, with attempts to guide the cell into tissue regeneration through environmental conditions such as media additives or the tailoring of scaffold properties. In vivo, the ECM is the primary source of signals for cell transformation, providing a 3D structural matrix for cells to proliferate, abundant in chemical signalling molecules such as growth factors. The goal of many TE strategies is to replicate or mimic the ECM conditions of the target tissue, inducing it to regenerate through natural mechanisms. These strategies have led to research on the use of many combinations of growth factors and scaffold materials to emulate the osteochondral environment.

## **2.4 Scaffold Characteristics**

The concept of a TE scaffold is to act as the base for tissue regeneration, guiding the growth of new cells to form functional tissue, then decomposing at a rate which allows the new tissue to integrate and proliferate, leaving a repaired and functional tissue at the site of injury. With such a complex role, the choice of materials, geometry, manufacturing process and design of the scaffold are critical to TE efforts.

Table 1<sup>17</sup> (below) highlights the primary scaffold design considerations and the biological requirements they service. To allow for cellular infiltration, a scaffold must have an internally interconnected porous structure, which will determine the geometry of regenerated tissue.

Studies<sup>18</sup> on pore size have noted a significant increase in cell growth and proliferation on the surface of scaffolds with average pore sizes >100 µm. Scaffolds with an average pore size in the range of 300-400 µm were observed to develop vascularity in new tissue growth. Vascularisation is extremely important in the growth of new tissues as it allows for the delivery of nutrients and the removal of waste products<sup>18,19</sup>. A study by Lien et al.<sup>20</sup> noted that chondrocytes proliferated more favourably on scaffolds with pores sizes between 250-500 µm. Manufacturing method is a major influence over control of porosity, with methods such as salt leaching or freeze drying using porogens of differing size to control scaffold porosity. Porosity and pore size can be altered in methods like electrospinning or centrifugal spinning by altering the base polymer solution concentration or using polymers of varying molecular weight.

The degradation rate of the scaffold material will dictate the rate of regrowth of native tissue and ECM, and the of structural integrity over time of the material. Material choice is the most important factor when assessing degradation properties, with the rate and decomposition into non-toxic and non-inflammatory by-products largely determined by the base materials. Manufacturing methods also play a role in the rate of degradation, as pore size and porosity can determine the rate at which degrading factors infiltrate the scaffold. In the case of using blended materials in scaffolds, variation in degradation rates must be acknowledged, as one may degrade significantly faster, and causing faster than expected degradation in the other material.

The mechanical strength of scaffolds will dictate where a scaffold can be appropriately used, a scaffold must possess sufficient tensile or compressive strength to support the weak tissue's growth in the injured site, failure to do so would ruin the healing. As such, a scaffold's mechanical properties must match or exceed the mechanical properties of the native tissue, maintaining its geometric structure during the growth of a new 3D cell-matrix. This is another consideration largely governed by the choice of material and manufacturing method, for

example, Polycaprolactone scaffolds that have been produced by electrospinning and fused filament fabrication have vastly different mechanical properties, with the former being significantly more flexible, with weaker tensile and compressive properties. In the context of Osteoarthritis, the range of acceptable mechanical properties is broad, with values ranging from the millipascal in the soft cartilage layer to gigapascals in cortical bone tissue. As the intended target is the regeneration of cartilage, a value aligned with softer tissues is acceptable.

The incorporation of chemical stimuli can alter the adhesion, differentiation, and proliferation characteristics of cells. Molecules such as RGD, BMPs, IGFs, Collagens, Hyaluronan, Chitosan, etc. have been incorporated into osteochondral scaffolds in various manners.

**Table 2.1** – Considerations and requirements in design for musculoskeletal applications.

Scaffold Considerations	Biological Requirements
- Choice of Material & Biocompatibility • PCL, PLA, PHBV, PLGA, etc.	- Supports Cells Proliferation & Differentiation - Suitable for <i>in vivo</i> implantation
- Geometry & Architecture • Porous, biodegradable, mechanically compatible	- Support 3D Tissue Growth - Control of tissue morphology - Support desired cell differentiation
- Porosity • Pore size >100 µm, 250-500 µm preferential for chondrocytes <sup>21</sup>	- Support cell differentiation - Support recruitment - Support aggregation - Support vascularisation
- Mechanical Properties	- Support mechanical loading
- Degradation Rate	- Permit new tissue to fill the site of injury - Permit remodelling of the ECM - Match the healing rate of the new tissue
- Biochemical Stimuli	- Incorporation of appropriate chemical stimuli to direct tissue growth

## 2.5. Biomaterials for TE Musculoskeletal Applications

As discussed in the previous section, many important factors are governing the design of a targeted tissue engineering scaffold. This section will focus on the materials commonly found (but not exclusively) in the construction of osteochondral scaffolds, with a focus on biocompatible synthetic polymers and natural polymers found in the ECM of chondrocytes and chondrogenic cells.

### 2.5.1 The Use of Synthetic Polymers

Synthetic polymers are what is thought of traditionally as plastics, whether naturally or synthetically manufactured. Synthetic polymers are highly versatile materials, with an enormous range of tailorabile properties. To design a scaffold, the first property assessed must be biocompatibility, ensuring cellular growth and proliferation are unhindered by the material,

and the host is not affected by the degradation by-products. With this are also the mechanical properties, which must match the tissue they seek to regenerate, and bioresorbability, the aim of TE being to leave behind a regenerated section of functional living tissue. These characteristics can be found across synthetic polymers or can be induced through the choice of manufacturing technique, blending with other polymers (block or co-polymers), chemical treatment, or there is also of the possibility of combining synthetic polymers with natural ECM molecules to enhance its cellular properties.

There is a wide range of biocompatible synthetic polymers available, which expands greatly when taking into consideration blends and co-polymers, as such I will cover the most used base polymers in TE.

**Table 2.2 – Recent advances in the use of synthetic polymers for tissue engineering therapies**

Material	Importance	Year
PCL & Alginate	Multi-head AM used to print scaffold 3D structure and Cell-Alginate hydrogel <sup>22</sup>	2015
PCL & Hydroxyapatite composite	Nano HA / PCL melt blended scaffolds, printed by Fused filament fabrication <sup>23</sup>	2019
PCL & PLA	Multi process fabrication, bi-material with multiple pore size ranges <sup>24</sup>	2016
PHBV & SrCO <sub>3</sub> / PRP	Electrospun particle loaded PHBV fibre scaffolds <sup>25</sup>	2016

### **2.5.2 Poly- $\epsilon$ -Caprolactone (PCL)**

PCL is a biocompatible, biodegradable, thermoplastic polymer with an extensive history of use in medical devices, from tissue scaffolds to timed release drug delivery systems<sup>26,27,28</sup>. PCL has a glass transition and melting point of -60°C and 60°C respectively, bringing it comfortably into the range of processing temperatures for Fused Filament Fabrication. PCL is a softer thermoplastic than PLA or PHB, making it less suitable for the regeneration of load-bearing osseous bone tissue, however, its physical properties have made it more suitable for cartilage mimicking scaffolds.

Although PCL is a commonly used biopolymer, it is not biodegradable in the human body as we do not possess the correct enzymes, however, it is bioresorbable<sup>29</sup>; PCL implants have been

shown to hydrolytically degrade over time, the by-products passing harmlessly into the surrounding tissue, the process taking over 24 months<sup>30</sup>. Bioresorbability<sup>31</sup> refers to the overall removal of a foreign entity and degradation products *in vivo*, with no lasting effects. What is biodegradable is not necessarily bioresorbable and vice versa. While not technically biodegradable, a degradation process<sup>32</sup> by which hydrolytic cleavage of the poly ( $\alpha$ -hydroxyl) esters into acid by-products does occur *in vivo*. Degradation can occur on the surface of the material and involves the slow erosion of molecules from the surface of the PCL scaffold. This erodes the surface of a scaffold without significantly reducing the molecular weight of the PCL bulk and allows for the slow diffusion and removal of by-products from the surrounding tissue. Degradation can also occur at a much faster rate in the bulk of the scaffold material if significant cracks or defects are produced in the manufacturing process. Water infiltration inside the bulk of the PCL scaffold can lead to an autocatalytic response, wherein acidic by-products can further hydrolyse the bulk material, creating additional cracks and allowing in more water, causing an accelerated degradation rate. The rapid release of by-products in this second degradation model can cause inflammatory responses *in vivo*<sup>33</sup>, which is undesirable the inflammatory aspect of OA.

PCL has been investigated for osteochondral implants for quite some time<sup>26,34,35</sup>, with promising results. As with other synthetic polymers, PCL suffers from low cellular adhesion and literature has shown that PCL's cellular viability can be increased with the grafting of collagen<sup>36–38</sup>.

### **2.5.3 Poly – L – Lactic acid (PLA) & Poly (lactic-co-glycolic acid) (PLGA)**

PLA is perhaps the most commonly used polymer in 3D printing (alongside acrylonitrile butadiene styrene, ABS), due to its relatively strong mechanical properties and cheap availability from renewable resources. PLA has a glass transition and melting point of 60-65° and melting of 150-160°, again bringing it within the FFF printable range. PLA is degraded enzymatically and hydrolytically, with its crystalline form LPLA taking over 24 months to degrade<sup>30</sup>. PLA is often copolymerised with glycolic acid in medical devices, which brings degradation time down from >24 months to 12-16 months and increases the elasticity of the polymer. Both lactic acid and glycolic acid are natural by-products<sup>39</sup> of metabolic activity in the body and so have no toxic effects on the surrounding tissues. Due to its more rigid mechanical properties, PLA is a candidate for investigation in the regeneration of load-bearing bone tissue, and studies have shown its enhanced biological properties upon grafting with collagen<sup>40,41</sup>.

#### **2.5.4 Poly(3-hydroxybutyrate-co-3-hydroxy valerate) (PHBV)**

Polyhydroxyalkanoates (PHAs) are a class of biocompatible, biodegradable polyesters produced by a variety of microorganisms<sup>42</sup> and through plant-based fermentation<sup>43</sup>. Of this class, one of the most well-studied variants is poly (3-hydroxybutyric-co-3-hydroxyvaleric acid) (PHBV), a copolymer of polyhydroxybutyrate and polyhydroxyvalerate. PHBV is a biodegradable, non-antigenic, biocompatible type of microbial polyester, where low molecular weight PHB (polyhydroxybutyrate) has been found in cells. Due to its favourable biological properties, PHBV has been targeted for applications in a range of tissue engineering (TE) and in vivo applications, including wound dressings, neural, dermal, osseous and cardiovascular tissues<sup>44-47</sup>. PHBV was first marketed under the trade name “Biopol” in the 1980s, seeing use in drug delivery systems and medical implants. With a history of use in medical applications and its biodegradable / biocompatible properties, PHBV has already been investigated for its application in tissue engineering<sup>45,48</sup> and is a target for research with as a base for biosynthetic scaffolds. PHBV has previously been processed by SLS and has only been fabricated by FFF when blended with PCL<sup>49</sup>.

#### **2.5.5 Polyurethanes (PU)**

Polyurethanes, like PLA and PCL, are polyesters with a segmented chemical backbone consisting of polymerised polyol and di- or triisocyanate, joined by a carbamate link. This combination of chemical segments is classified as an alternating co-polymer and as such there is large variation in the physical properties of polyurethanes, induced by varying the polymer constituents, granting versatility beyond simply modifying molecular weight or crystallinity as with other polyesters. Polyurethanes are also available as both thermoset and thermoplastic<sup>50</sup>. Bioresorbable PU often contains block constituents from PCL and PLA. Historically PU scaffolds have been used in the regenerative treatments for dermal tissue<sup>51</sup>, vascular tissue<sup>52</sup>, nerve cells<sup>53</sup>, bone<sup>54</sup> and osteochondral scaffolds<sup>55</sup>. PU’s versatility means it has been fabricated into scaffolds by methods such as solvent casting / particle leaching, thermally induced phase separation, freeze-drying, melt moulding, gas foaming and can be 3D printed using FFF in blends with other polymers (known as Ninjaflex).

### **2.6 Use of Natural Polymers and ECM-derived Materials**

Proteins and polysaccharides found in the ECM are some of the most potent and highly researched biomaterials. Proteins such as collagen, elastin and fibrin, or polysaccharides such as hyaluronic acid and chondroitin are major constituents of the ECM of natural tissues and are heavily used in tissue engineering scaffolds for their ability to cause cell adherence,

proliferation and transformation. These polymers undergo natural enzymatic breakdown, yielding non-toxic by-products, fulfilling multiple scaffold design criteria.

**Table 2.3 – Key works using natural polymers in musculoskeletal TE from the last 5 years.**

Materials	Relevance	Year
Collagen & Alginate	Boosted mechanical properties & cell proliferation <sup>56</sup>	2018
Collagen & Alginate	3D printed hydrogels giving control to the hydrogel macrostructure <sup>57</sup>	2016
Hyaluronic Acid, hydroxyethyl acrylate, gelatin-methacryloyl	Innovative graft / free radical polymerisation system, good printability <sup>58</sup>	2019
Chitosan & Hyaluronic Acid	Highly porous cryogels <sup>59</sup>	2017

### **2.6.1 Collagen**

Collagen is the most abundant protein in the human ECM and is a major constituent of musculoskeletal tissues such as cartilage and bone. Collagen is a rod shaped, 300nm long and typically around 300 kDa in molecular weight<sup>60</sup>. There are 22 types of collagen identified in the human body, with types I-IV being most prevalent. Of all types, collagen type I is the most prevalent variant in the human ECM and is composed of three polypeptide units arranged in a triple helix. The total amino acid content of collagen is approximately 33% glycine, 25% proline, and 25% hydroxyproline. Collagen's primary structure has a predominant repeating triplet structure of glycine-proline-hydroxyproline, with a glycine unit found at every third residue. This primary structure pattern accounts for collagen's inherent structure and mechanical properties<sup>61</sup>. The secondary structure of collagen is an  $\alpha$ -helix, which take shape from the proline / hydroxyproline content of the glycine-proline-hydroxyproline triplet primary structure; three of these  $\alpha$ -helices form the tertiary structure, triple helix. The C and N terminus of the secondary  $\alpha$ -helix serve as points of interaction for covalent bonding with other ECM molecules<sup>62</sup>. The tertiary triple helix consists of a three  $\alpha$ -helices, two of which are identical  $\alpha_1$  chains, and one  $\alpha_2$  chain. The three chains maintain the tertiary structure through inter-chain hydrogen bonding. Collagen has a quaternary structure in the form of fibrils, which self-assemble from the triple helical tertiary structures.

Collagen type-I possesses structural motifs to which cell integrins bind<sup>63</sup>, mediating cellular adhesion and migration in the native ECM<sup>64</sup>. The high glycine content gives collagen its flexibility, and it has been manufactured into scaffolds as sheets, tubes, foams, powders and fibres. The exposed N-terminus and C-terminus offer platforms for chemical modification and crosslinking for collagen, such as carbodiimide crosslinking or modifying the collagen with photolabile groups for UV crosslinking<sup>65</sup>.

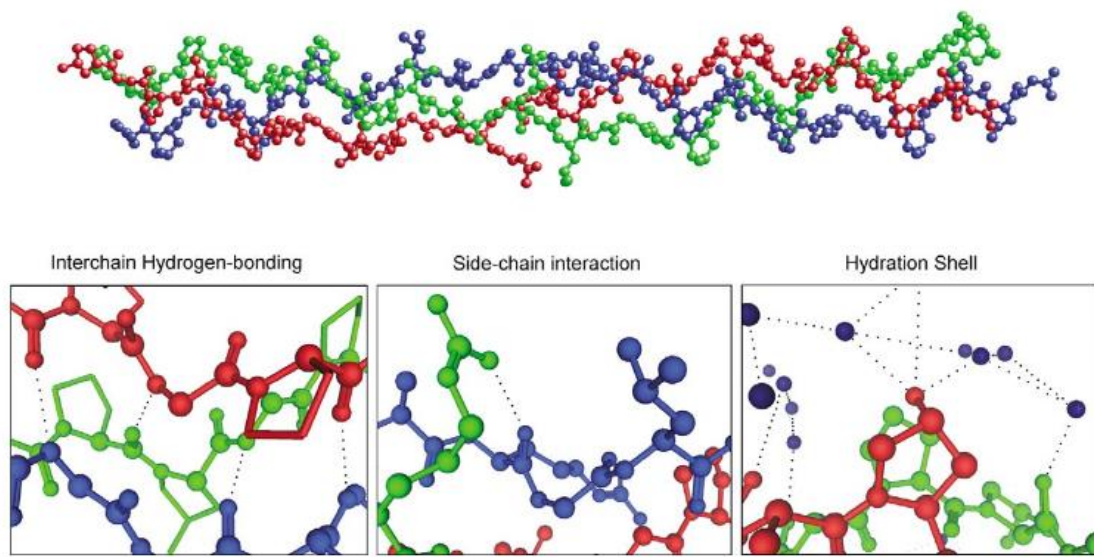


**Figure 2.2** – Molecular representation of the collagen triple helix, with prominent intramolecular interactions<sup>66</sup>.

Collagen has a long history of use in TE applications, going back several decades, and has featured notably in research for bone, skin, tendon, and cartilage repair. Lloyd et al.<sup>67</sup> used a controlled freezing rate to fabricate scaffolds of collagen and glycoaminoglycan with consistent porosity, and were seeded with keratinocytes and fibroblasts. The biological testing showed the scaffolds were effective as a host for cell growth and dermal TE application, and that the freezing process did not compromise the biological compatibility compared to a standard method of dehydration in ethanol. With the aim of cartilage repair, Matsiko et al.<sup>68</sup> used freeze-drying to develop collagen based scaffolds enhanced with Hyaluronic acid. Seeded with Mesenchymal Stem Cells (MSCs), the study showed strong ability to promote cell migration and chondrogenesis in experiments.

### 2.6.2 Elastin

Elastin is a highly crosslinked protein found in large quantities in vascular tissues, and as its name might indicate, is responsible for the elastic properties of such tissues. Elastin, unlike

collagen, is highly insoluble and therefore has a more limited applicability in biomaterial scaffolds. Elastin's beneficial characteristics are in its low interactivity with platelets, making it suitable for vascular grafts<sup>69</sup>.

### **2.6.3 Fibrin**

Fibrin is a polypeptide involved in the clotting of blood and is derived from fibrinogen. In the presence of thrombin, fibrin undergoes a structural change, bonding with other fibrin molecules to form long fibres in a fibrin clot. Fibrinogen is strongly biocompatible, undergoes regular biodegradation and contains the ECM protein fibronectin that has excellent cell adhesion properties. Due to its favourable cell compatibility and matrix-forming ability fibrin has been used to carry keratinocytes to chronic wounds ion the produce "Bioseed".

### **2.6.4 Hyaluronic Acid**

Hyaluronic acid (HA) is a glycosaminoglycan (GAG), a polysaccharide consisting of the co-polymer blocks, glucosamine and glucuronic acid. The polymer chain displays outward facing carboxylic acid and amino groups, making it easy to chemically functionalise. HA ranges in molecular weight from several thousand to several million and is present in most human tissues. Unlike many natural proteins, HA is completely water soluble, forming dense and viscous solutions, making it an excellent choice for hydrogel formulations. HA has an active role in biological tissues influencing biological processes such as differentiation, cell migration and ECM arrangement. HA has also been found to play a role in the repair of tissue by promoting mesenchymal and epithelial cell migration and differentiation, upregulating collagen deposition and angiogenesis.

### **2.6.5 Chondroitin Sulphate**

Like HA, chondroitin sulphate (CS) is a GAG and plays a significant role in wound healing<sup>70</sup>. CS is a major constituent of aggrecan, the most abundant GAG in articular cartilage. CS has been observed to regulate gene expression in articular cartilage, upregulating the production of anti-inflammatory pathways. CS is easily crosslinkable, forming a viscous gel I waster and like HA, makes an excellent component for hydrogel scaffolds. In addition to its cell adhesion and anti-inflammatory properties, CS has been shown to increase the bioactivity of chondrocytes, as shown by Van Susante, when CS was added to type I collagen scaffolds<sup>71</sup>.

### **2.6.6 Chitosan**

Chitosan is a non-human polysaccharide derived from the chitin shells of insects and is non-toxic to humans and stimulates minimal antigenicity. Despite chitosan's exogenous origins, it undergoes enzymatic degradation *in vivo* and can vary between several weeks to several months

before resorption, depending on how acylated it's copolymer units are<sup>72</sup>. This characteristic allows the tailoring of chitosan's degradation rate through chemical (de)acylation, with highly deacylated chitosan exhibiting a much faster degradation rate. Like other GAGs, chitosan has external amino groups which make it easy to functionalise.

### **2.7 The Use of Functionalised and Biosynthetic Scaffolds**

Synthetic polymers are fantastic for their versatility, especially in mechanical properties, however, they have issues with cellular adhesion, lacking the motifs that cell integrins adhere to in the extracellular matrix (ECM). Natural polymers, such as collagen or hyaluronic acid are commonly found in the ECM and possess protein structures that cells recognise and adhere to. While this is beneficial for cell growth, natural polymers often possess poor mechanical properties and are easily denatured by heat or chemical stimuli, making it difficult to process scaffolds of mechanical integrity, especially to the level that would be required in a musculoskeletal scaffold. By combining the properties of the two it may be possible to take the mechanical properties of synthetic polymers and the biological properties of natural polymers and fabricate an enhanced scaffold.

**Table 2.4 – Significant recent biosynthetic scaffold advances**

Materials	Relevance	Year
Polyurethane / Collagen <sup>73</sup>	Biosynthetic Electrospun PU / collagen fibres, seeded with smooth muscle cells	2014
Polylactic Acid / Collagen / Chitosan <sup>74</sup>	Freeze-dried and chemically crosslinked biosynthetic PLA / Chitosan / Collagen scaffolds, seeded	2014
PLGA / Collagen / Graphene Oxide <sup>75</sup>	Electrospun PLGA / Collagen / GO fibres, seeded with skeletal myoblasts	2015

Studies on the functionalisation of synthetic polymers with collagen have appeared in literature in recent years. Jia et al.<sup>73</sup> reported the electrospinning of biosynthetic PU / Collagen fibre scaffolds, fabricated through dissolving PU and Collagen type I in solutions of HFP, then spinning as a single solution. Scaffolds were produced in aligned and non-aligned morphologies, with both morphologies of the biosynthetic PU / Collagen scaffolds showing increased cell proliferation than the PU scaffolds. Also noted in the study was a higher protein

expression from smooth muscle cells seeded on aligned scaffolds. Yin et al.<sup>74</sup> reported the development of a PLA / Chitosan / Collagen crosslinked scaffold fabricated through freeze drying, with the proposed purpose of articular cartilage repair. The biosynthetic scaffolds reported were found to be suitable for cellular seeding through experimentation with chondrocytes, with mechanical properties within a reasonable range for use in articular cartilage. Shin et al.<sup>75</sup> reported the fabrication of PLGA / Collagen / Graphene oxide ECM biomimetic scaffolds. Scaffolds were fabricated using a solution of PLGA and Collagen in HFP, to which a dispersed Graphene solution was added; the solution was spun without additional chemical or physical crosslinking. The study noted the increased hydrophilicity and an enhanced early adhesion and proliferation in PLGA / Collagen / Graphene scaffolds vs PLGA / Collagen scaffolds.

Studies<sup>41</sup> on blends of synthetic polymer polylactic acid (PLA) and collagen have shown increased biocompatibility with fibroblastic cells in comparison to standard PLA (Fig. 3). The blends also displayed a lowered contact angle with deionised water, from 72° with PLA to 56° once blended with collagen. Scaffolds printed by FFF with PLA and subsequently grafted with collagen<sup>76</sup> have also displayed increased cellular adhesion in comparison to non-grafted scaffolds.

As a means to tailor the biological or mechanical function of PHBV scaffolds, blends, and composites with other natural or synthetic biopolymers<sup>77–81</sup>, and bioceramics<sup>25,82–84</sup> have been studied. In particular, collagen type-I<sup>44</sup> is one of the most commonly investigated materials for TE scaffolds and as a coating or component in composite TE scaffolds<sup>37,38,41</sup>.

PHBV is a hydrophobic polyester without many functional groups available for a covalent functionalisation<sup>85</sup>. In this regard, efforts have been made to incorporate biological motifs to render this material more attractive for cells and favour integration with surrounding tissues. To imbue scaffolds with these properties, collagen type-I is commonly combined with synthetic biocompatible polymers like poly-ε-caprolactone and poly-lactic acid, to improve cell growth and adhesion.



**Figure 2.3 –** 3T3 fibroblasts after 8 days. A) On glass as a control, B) on PLA and C) on PLA-collagen<sup>41</sup>

Likewise, blends of PHBV and collagen have been reported, with the incorporation of collagen resulting, in all cases, in superior cellular behaviour over pure PHBV scaffolds. Han et al.<sup>44</sup> examined the co-culturing of hair follicular epithelial cells with dermal sheath cells on electrospun scaffolds of PHBV, PHBV / Collagen, and PHBV / gelatin. PHBV / collagen blends not only showed the greatest extent of cell growth, but also the expression of extracellular materials, i.e., type I collagen, smooth muscle actin, and elastin. While a study by Prabhakaran<sup>84</sup> with similarly prepared electrospun scaffolds, compared PHBV and PHBV / collagen composites, in random and aligned orientations, as substrates for nerve regrowth. Composite scaffolds with a higher ratio of collagen content displayed higher levels of cell growth, and cells were observed to align with the orientation of composite fibres. However, no differences in the total cell proliferation were observed between different fibre orientations, indicating that the driver in cell growth was collagen content.

Biazar et al.<sup>86</sup>, fabricated nanofibre PHBV scaffolds using microwave plasma, afterwards submerged in a collagen solution at 50 °C, a method that may damage the side chain motifs to which cells bind. In a study of the use of somatic stem cells on PHBV-collagen electrospun membranes for skin defects<sup>47</sup>, Keshel et al. immobilised collagen via the plasma method onto nanofibrous PHBV scaffolds. Their approach found that the graft of collagen-coated nanofibrous PHBV scaffolds loaded with USSC cells increased cellular growth and improved the healing process of skin defects in rat models. In the studies where the PHBV and collagen were electrospun concurrently in fluorinated solvents (e.g., hexafluoroisopropanol or trifluoroethanol), there was no conclusive characterisation of the collagen. This leads to contention as an article<sup>87</sup> examining the electrospinning of collagen nanofibres showed the denaturing effect of highly teratogenic fluorinated solvents on collagen during the electrospinning process. This study and the lack of collagen characterisation in membranes spun from fluorinated solvents indicate benefit in the post-spinning conjugation of collagen of spun fibre scaffolds to preserve the triple helical structure. However, in the case of Han et al.<sup>44</sup>,

concurrently spun PHBV / collagen in fluorinated solvents still demonstrate superior cellular growth than PHBV / gelatin scaffolds prepared in the same manner.

### ***2.8 Collagen Functionalisation of Polymer scaffolds.***

There are multiple methods by which collagen or other similar proteins can be introduced into other scaffolds or used to jointly form a multi biomaterial scaffold. These include crosslinking of a physical, chemical, and enzymatic nature<sup>88</sup>. Physical crosslinking involves techniques such as dehydration, thermal treatment, UV, and gamma irradiation. Physical techniques do not require additional chemical reagents; however, they can interfere with the protein structure of the collagen. Chau et al.<sup>89</sup> used transglutaminase enzymes to crosslink bovine type I collagen, and found that it increased levels of cellular adhesion, migration, proliferation and growth, while decreasing the rate at which collagen degraded. The advantage of the biological method being the absence of toxic chemical reagents and a milder crosslinking process. Broadly, the predominant method for the conjugation of collagen and synthetic polymers is via chemical crosslinking. Of chemical crosslinking methods, carbodiimide chemistry (Figure 2.3 A) is commonly used. This relies on the use of carbodiimides (primarily N-(3-Dimethylaminopropyl)-N'-ethyl carbodiimide (EDC)) and N-hydroxy succinimide (NHS) to form amide bonds with the natural polymers by forming a labile ester with a carboxylic acid presenting molecule (typically the synthetic polymer) and displacing the NHS-ester group with an amine presenting molecule (in this case collagen). This chemistry is of special relevance to this project as the biocompatible thermoplastics of interest are of the polyester family, allowing for the use of carbodiimide techniques. This is a versatile technique, allowing for the adaptation of the chemistry to suit the molecules in question, for instance, it is entirely possible to functionalise collagen with the NHS ester and perform aminolysis (Figure 2.3 B<sup>36</sup>) on the polymer to form the amide. This is useful in the case of creating amide bonds with a hydrolysed polyester when the coating protein / molecule has available -NH<sub>2</sub> moieties but not -COOH. Another variation of the method is photo immobilisation (Figure 2.3 C), whereby a molecule is conjugated to a photolabile<sup>90,91</sup> group, capable of forming amide bonds with amine presenting molecules. Layer-by-layer<sup>92,93</sup> is a technique (Figure 2.3 D) by which the surface chemistry of polyesters is aminolysed with hexandiamine to present amino functional groups. These amine groups are subjected to acid washes to protonate the surface before the application of a collagen salt solution, which coats the surface of the polymer due to static interaction between negative charges on the collagen and the positive polymer surface.

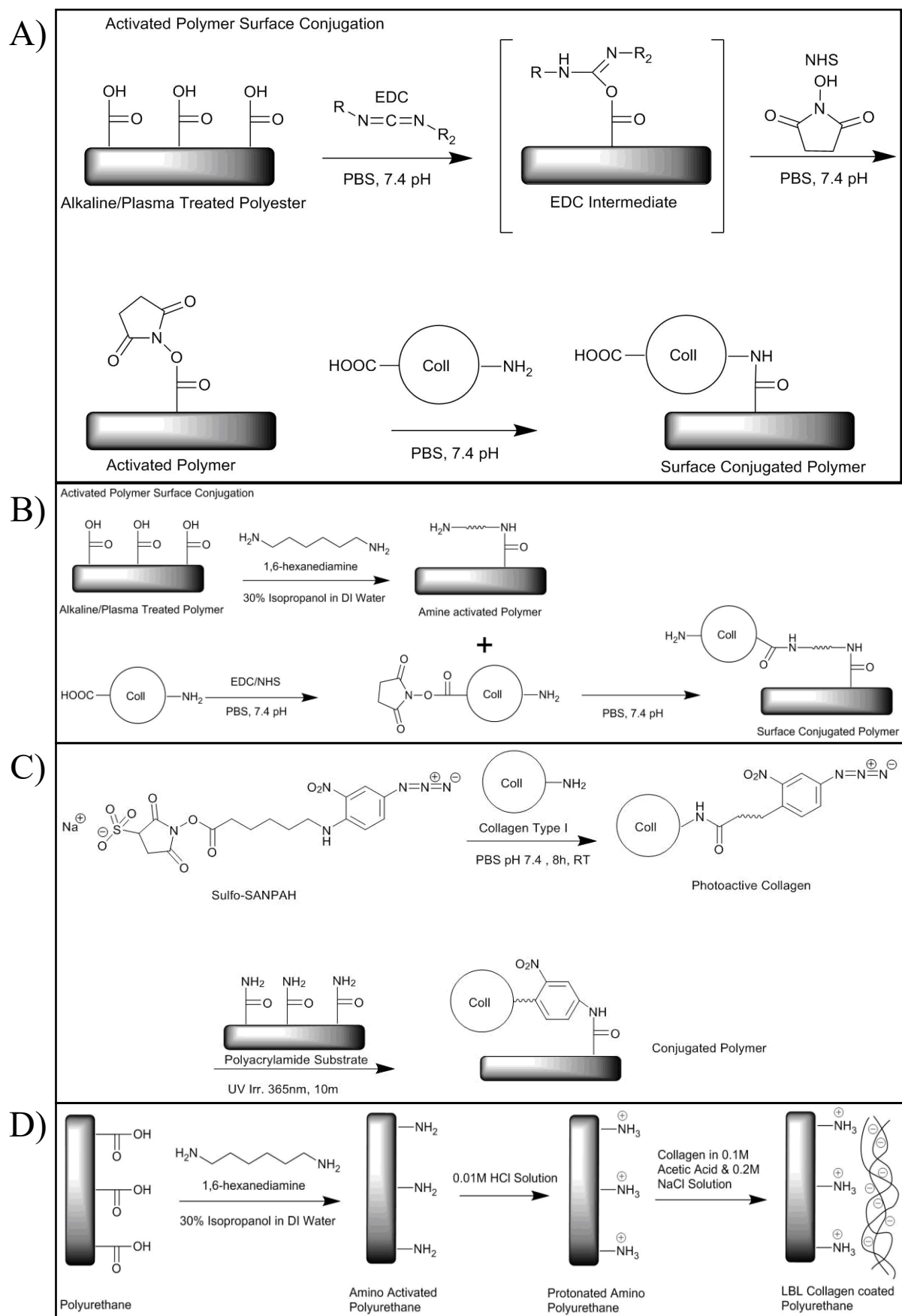


**Figure 2.4 –** A) Schematic drawing of Carbodiimide chemistry mechanism. B) Carbodiimide chemistry with aminolysis. C) Sulfo-NHS with a photoactive moiety, capable of conjugation by UV irradiation. D) Layer-by-Layer functionalisation.

## **2.9. Scaffold Fabrication Methods and Their Use in Musculoskeletal Applications**

As previously discussed, to create a scaffold for a particular application, multiple factors must be addressed, i.e. material biocompatibility, biodegradability, surface chemistry, mechanical properties, and porosity. To date the review has covered the materials and conjugation methods, which govern biocompatibility, degradability, surface chemistry, and mechanical properties. To achieve control in the geometry, porosity, and to a lesser extent, mechanical properties, a suitable manufacturing technique must be addressed. Focus has been given to methods which allow a versatile approach in design.

### **2.9.1 Additive Manufacturing for Tissue Engineering**

Scaffolds should preferably possess a highly porous interconnected framework and many traditional polymer manufacturing methods, such as injection moulding or compression moulding, produce dense parts or structures sealed at the edge. Additive manufacturing (AM) may present a viable alternative to traditional manufacturing processes in achieving the desired scaffold geometries with the additional benefit of custom manufacturing fit for individual patients. AM can fabricate high-resolution small parts from TE appropriate materials with complex internal geometry. Using AM gives a quick translation from scan data to CAD file to customisable products without costly retooling or the material waste that comes with reductive manufacturing.

### **2.9.2 Fused Filament Fabrication**

Several potential AM candidates may be suitable for the fabrication of biopolymer scaffolds, however, Fused Filament Fabrication (FFF), is the most viable candidate for this work. FFF (Figure 2.4) is probably the most well-known AM process, likely because of its low entry barrier for hobbyists. FFF devices are cheap, low-end models costing as little as £300 - £600 with standard desktop models costing around £2,000 to £3,000, higher end models advertised as having industrial manufacturing capabilities can cost over £15,000. Though FFF techniques are only compatible with thermoplastics, there are several biologically viable thermoplastic polymers available (such as PCL, PHBV, & PLA) making it suitable for the scope of this project.

FFF<sup>26</sup> works by partially melting thermoplastics and depositing material onto a build plate. Material is deposited in layers, building up the structure sequentially. A FFF printed structure is produced by creating a 3D structure in CAD software and exporting the file in .stl (stereolithography) format. The .stl file is then processed by software (e.g. Cura, Simplify 3D, Slic3r) into sliced models, representing the layers in which the model will be built up

corresponding to input parameters. The file type of these models was primarily .slc<sup>26</sup> in the past, with many new hardware-specific file types appearing with the proliferation of AM technology. The sliced model is then used to create a deposition path, producing a set of instructions for the machine in gcode. The FFF device then produces the physical part, following the path laid out in the gcode. As such, it would be possible to create a custom filament from pellets of PCL, PHBV or PLA via extrusion, which could then be processed in the manner above to create 3D porous scaffolds with control over the total size, porosity and geometry of the scaffold.

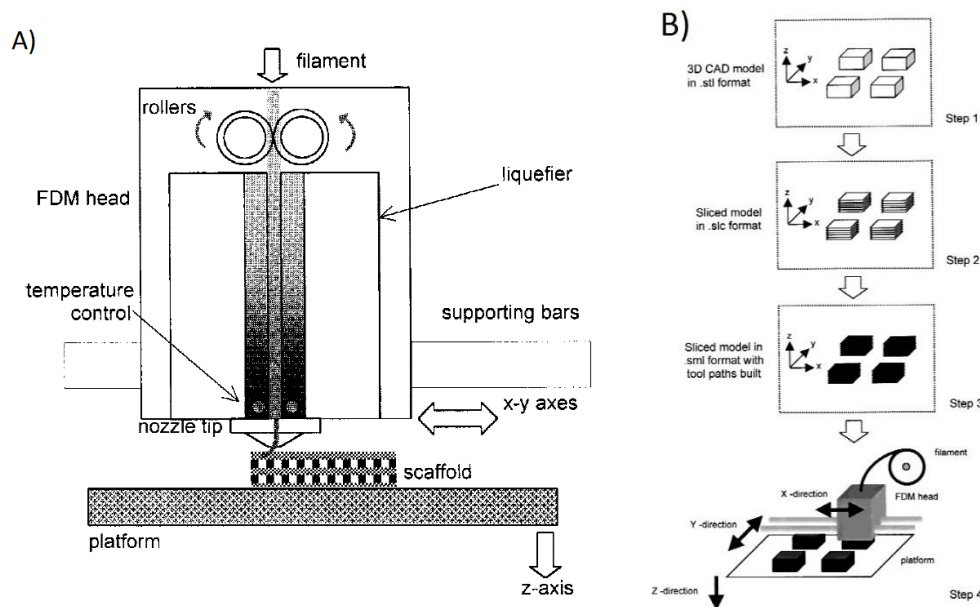


**Figure 2.5 – A)** FFF head apparatus, **B)** Steps taking CAD file to a physical model<sup>26</sup>.

PCL is commonly used in fused filament fabrication (FFF)<sup>26</sup>. The problem with PCL (and other hydrophobic scaffolds) is the low level of cellular adhesion to scaffold surfaces, however, by grafting a natural macromolecule such as type I collagen to PCL chains, it may be possible to increase the level of cellular viability. This would overcome the major flaw of polymer scaffolds while utilising the favourable physicochemical and mechanical properties, in addition to FFF compatibility allowing for complex porous internal geometries.

### 2.9.3 Electrospraying and Forcespraying

Nanofibres are of value for TE by mimicking the fibrillary structure of the extracellular matrix (ECM)<sup>94</sup>. Electrospraying is an established technique for the preparation of nanofibers with diameters ranging from tens of nanometres to several microns<sup>46</sup>. As previously stated, an ideal scaffold for TE should have an interconnected porous structure<sup>18</sup>; and porous microfiber scaffolds allow for the full integration of cells throughout the scaffold matrix making electrospraying an attractive option for fabricating TE scaffolds. Electrospraying uses electrostatic forces to produce fibres from a polymer solution, charging droplets of solution and

inducing electrostatic repulsion, causing the solution to disperse and fine polymer fibres to form. These fibres are typically collected onto a stationary plate or a rotating drum platform, the former collecting a non-aligned fibre mesh, the latter creating a mesh of aligned fibres (Figure 2.5). Electrospinning is highly versatile process, allowing the easy creation of scaffolds from a variety of biocompatible polymers. Electrospinning however does come with a detraction, it often involves the use of highly toxic or teratogenic solvents to create the dispersion, traces of which may remain in the scaffold post deposition

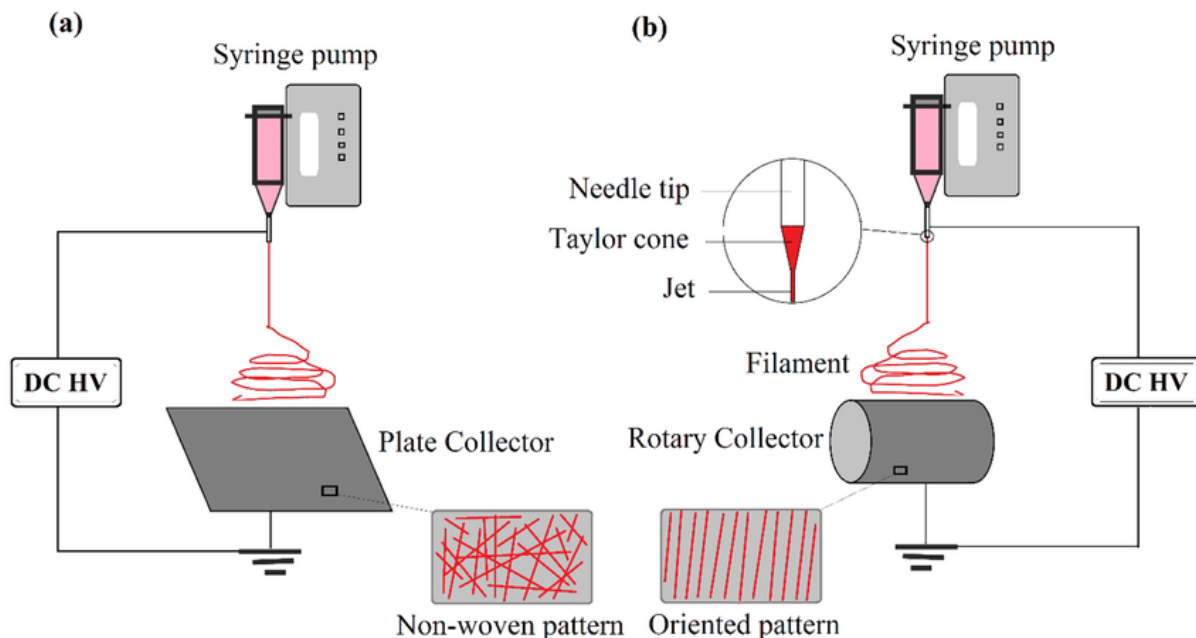


**Figure 2.6** – Schematic of an Electrospinning apparatus. (a) Production of non-woven pattern on plate collector, (b) formation of orientated pattern using a rotary collector<sup>95</sup>.

Forcespinning has presented itself as a viable, low-cost alternative to electrospinning. Forcespinning functions by ejecting polymer solution from spinnerets at high rotational speeds onto collecting frames (Figure 2.6), enabling the production of fibres from a wide range of materials and at higher rates than the electrospinning technique<sup>96</sup>. Moreover, as forcespinning uses centrifugal forces rather than electrical forces as in the electrospinning technique, processing fibres by forcespinning does not require a high voltage electric field or a conductive polymer solution<sup>96</sup>, and as such removes the restriction on use of materials with low dielectric constants<sup>97</sup>. As many materials can be forcespun into fibres with this method, this versatile method is a promising alternative to quickly produce the extracellular matrix (ECM) mimicking fibre membranes from biopolymers of interest for tissue engineering.

There are multiple factors involved in the creation of fibre scaffolds using Forcespinning methods; namely spinneret angular velocity, orifice radius, polymer viscoelasticity, surface

tension, evaporation rate, temperature, and the distance from the spinneret to the collector bars. Upson et al.<sup>98</sup> have reported the development of methods to produce forcespun PHBV membranes with fibre diameters between 0.5 and 3 µm. The study goes on to detail the optimisation of the parameters required to consistently produce PHBV fibre scaffolds. Using chloroform as a solvent, a PHBV polymer concentration of 25% w / v spun at 9000 r / min produced the highest quality fibres, and with a spinneret to collector distance of 39.2 cm, producing the equivalent of 11 km of fibre per minute, per needle. The rapid rate of production, mechanical properties (3 MPa average tensile strength), and biocompatibility of PHBV fibres, makes this an attractive method of large-scale production for ECM mimicking scaffolds.

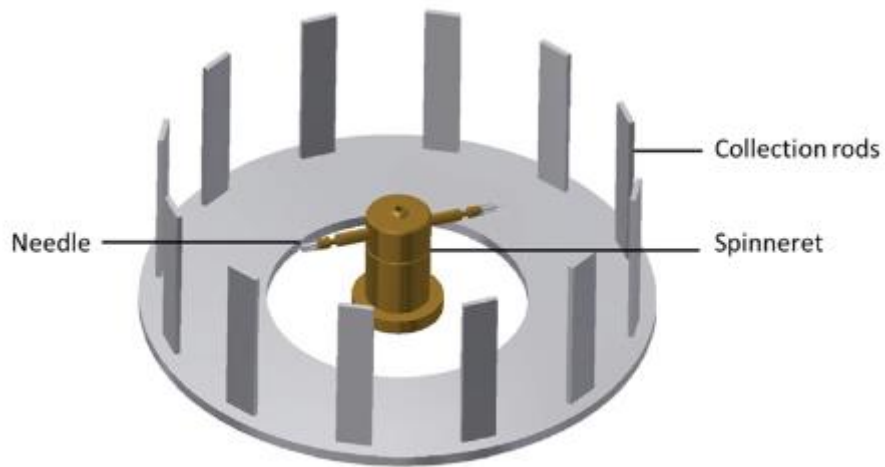


**Figure 2.7** – Schematic representation of the apparatus of a Force spinning system. Polymer solution is loaded into the centre spinneret and ejected through the needles onto the collection rods at high rotational speeds<sup>98</sup>.

### 3. Summary

Before progressing into the experimental components of the thesis, a moment must be taken to reconcile the subjects of the literature review with the experimental design and thematic narrative of the following chapters. As such, we ask the following questions:

- 1) Is it possible to take the beneficial properties of different materials and bring them together through physical/ chemical processing to create a product greater than the sum of its parts?
- 2) What is the optimal way to bring together synthetic and natural polymers to retain the desired properties of both?
- 3) Given the variety of manufacturing methods available, are specific processes suited to different outcomes? Can we reconcile these processes with their product applications?

## **Chapter 3: Methods and Materials**

### **3.1. Materials**

#### **3.1.1 General Reagents**

2-(N-Morpholino) ethanesulfonic acid hydrate (MES) powder, ≥99.5% (M8250), reagent grade Sodium Hydroxide (NaOH) pellets, ≥98% (S5881), and Tween 20 solution, cell culture tested (P2287), were purchased from Sigma Aldrich and used without further purification. Soluble Collagen Assay Sircol (Sirius Red) staining kit (S1000) was purchased from Biocolor.

#### **3.1.2 Scaffold Materials**

Poly (3-hydroxybutyric-co-3-hydroxyvaleric acid) (PHBV) pellets, 12% Valerate (403121), and medical grade Poly-ε-Caprolactone (PCL) pellets, 80,000 Da (440744), were purchased from Sigma Aldrich and used without further purification. Collagen Type I Pepsin-extracted 6 mg / mL was purchased from collagen Solutions Plc and used without further purification. Gelatin Powder, Type A from porcine skin (G1890), was purchased from Sigma Aldrich and used without further purification. Sodium Hyaluronate technical grade (300-500kDa) (600-02-22) and Sodium Hyaluronate technical grade (750-1000kDa) (600-02-24) were purchased from Contipro and used without further purification.

\*Note – In discussion on experimental design and the use of naturally produced polymer products, concerns around taking the products forward to clinical application, e.g. infection, consistency, immune response. Medical grade materials often differ in fundamental physical and chemical properties to those produced for lower purposes. In this project, the intention was to fabricate samples that generate results as close to that of a product that could be carried forward into clinical settings as possible. Hence, medical grade PCL and Collagen were used. The medical grade PCL sources was significantly higher in molecular weight and stiffness than other non-medical grades available. The medical grade collagen sourced was also differentiated in preparation and molecular weight to others on the market. To keep experimental outputs consistent, removing the potential of cellular response varying to different sources/ molecular weights of collagen, a single source of high-quality bovine sourced collagen was used. Communication with the company informed us the collagen was gamma ray sterilised, lowering the risk of infection that would come with other sources or from extracting the collagen from harvested cartilage tissues. Considering this, concerns over infection and consistency of the product were assuaged.

### **3.1.3 Solvents**

Dimethylformamide (DMF), anhydrous 99.8% (227056), Dichloromethane (DCM), anhydrous 99.8% (270997), Tetrahydrofuran (THF), anhydrous 99.9% (401757), 1,1,1,3,3,3-Hexafluoro-2-propanol (HFP), ≥99.9% (105228), Chloroform, 99.8% reagent grade (288306), Isopropanol, anhydrous 99.5% (278475), Ethanol (denatured) (02880), were purchased from Sigma Aldrich. Absolute ethanol, 99.8% (E/0650DF/17) was purchased from Fisher Scientific. All deionized water used in experiments was obtained using a Purite Suez Edi-60 with Suez PP8 and PT8 purification cartridges equipped.

### **3.1.4 Coupling Reagents**

N-(3-Dimethylaminopropyl)-N'-ethylcarbodiimide hydrochloride (EDC) powder (E7750), N-Hydroxysuccinimide (NHS) powder (130672), Dicyclohexylcarbodiimide (DCC) crystals (D80002), were purchased from Sigma Aldrich and used without further purification.

### **3.1.5 Cell Culture and Cytocompatibility Reagents**

Dulbecco's Phosphate Buffered Saline solution (without calcium chloride and magnesium chloride, sterile-filtered) (PBS) (D8537), Thiazolyl Blue Tetrazolium Bromide (MTT) (M5655), 4',6-diamidino-2-phenylindole dihydrochloride (DAPI) powder (D9542), Phalloidin, Tetramethylrhodamine B isothiocyanate (P1951), L-Glutamine solution (200 mM, sterile filtered) (G7513), Penicillin-Streptomycin solution (10,000 Penicillin units and 10 mg streptomycin per mL in 0.9% NaCl, sterile filtered) (P0781), and Trypsin-EDTA solution (0.5g porcine trypsin and 0.2g EDTA per litre of Hanks' Balanced Salt Solution) (T3924), were purchased from Sigma Aldrich (UK). Heat inactivated Fetal Bovine Serum (FBS) (10500) was purchased from Life Technologies. Dulbecco's Modified Eagle Medium (containing high glucose 4g / L, pyruvate) (DMEM) (11995073), and LIVE / DEAD Viability / Cytotoxicity Kit (containing green-fluorescent Calcein AM & red-fluorescent ethidium homodimer solutions) (L3224), were purchased from Thermo Scientific.

Normal Human Neonatal Dermal Fibroblasts (NHDF-Neo) (CC-2509), derived from the dermis of human neonatal foreskin or adult skin, were purchased from Lonza Bioscience. TC28a2 Human Chondrocyte Cell Line (SCC042), established by primary culture transfection of costal cartilage from a female 15-year-old donor, were purchased from Merck Millipore.

## **3.2 Methods**

### **3.2.1 Biosynthetic Materials Based on PCL and Collagen**

#### **3.2.1.1 PCL-g-Collagen Bulk Functionalisation**

Two grams of PCL pellets were solubilised in 100mL of 50:50 v / v DCM / DMF by stirring for 60-90 minutes. 1.25 mM (516 mg) DCC and 1.25 mM (288 mg) NHS were added to the solution and stirred for 16 hours. Dialysis was performed by transferring the reaction solution into a cellulose dialysis membrane (Medicell International, 12-14 kDa MwCO), which was immersed into a 10:1 volume of 50 / 50 v / v DCM / DMF. The dialysis solution was gently stirred for 24 hours (refreshed after 4 hours to maintain concentration gradient) to remove unreacted DCC and N,N'-Dicyclohexylurea by-products. 50 mL of 6 mg / mL collagen type I solution was neutralised using 1M NaOH solution and stirred for 2 hours at room temperature. The collagen solution was added dropwise, under agitation, to the activated PCL solution and pH levels were readjusted to pH 7.5 with 1M NaOH. Solution was stirred at room temperature for 16 hours, precipitating a clean white, highly malleable material. Material was washed thrice for 10 minutes in 30% v / v ethanol and deionised water before drying in a vacuum desiccator. Samples were stored at 4°C.

#### **3.2.1.2 PCL-s-Collagen Films Surface Functionalisation**

Two grams of PCL pellets were stirred in 100 mL chloroform until fully dissolved, after which the solution was evenly poured into two circular glass petri dishes of diameter 15 cm. The dishes were covered with perforated tin foil to allow solvent evaporation under light airflow in a fume hood overnight. The resulting films were washed with deionised water to remove residual solvent, then hydrolysed with 3M sodium hydroxide for 30 minutes, then further rinsed with deionised water. The films were cut to ~2 cm<sup>2</sup> squares and immersed in a 50 mL solution of 10 mM (191 mg) EDC and 10 mM (115 mg) NHS in 0.5M MES buffer (pH 6.5) and stirred gently for 4-6 hours, after which the solution was removed, and the films washed with deionised water. The films were immersed in a solution of 6 mg / mL collagen (pH 5.5-6.5) overnight at 4°C, after which the films were removed and washed with deionised water. Samples were dried in a vacuum desiccator and stored at 4°C.

#### **3.2.1.3 PCL / Collagen Biosynthetic Blend**

In a sealed jar, 2 g of PCL pellets were stirred in 100 mL chloroform until fully dissolved. Then, 17.5 mL of 6 mg / mL collagen solution was neutralised to pH 7 using 1M sodium hydroxide solution to a ratio of 5% w / w collagen / PCL was added. The mixture was stirred overnight at room temperature until fully mixed. The solution was cast into 15 cm diameter glass dishes and

the solvent allowed to evaporate under light airflow in a fume hood overnight. The resulting films were washed with deionised water to remove residual solvent before being dried in a vacuum desiccator, and stored at 4°C.

### ***3.2.1.4 PCL-g-Gelatin Films Surface Functionalisation***

One gram of gelatin type A, was dissolved in 50 mL of deionised water at 40°C. Upon dissolution, the pH of the gelatin solution was adjusted to pH 6 using 1M sodium hydroxide solution. PCL (films and scaffolds) were submerged in 3M sodium hydroxide solution for 15 minutes. Alkali treated PCL was washed with deionised water and added to a solution of 10 mM (191 mg) EDC and 10 mM (115 mg) NHS in 0.5 M MES buffer (pH 6) for 6 hours. Upon completion of PCL functionalisation with EDC / NHS, material was washed lightly with deionised water. Washed samples were then added to the gelatin solution and gently stirred overnight. PCL-Gelatin samples were removed from the solution and washed with deionised water before being dried in a vacuum desiccator and stored at 4°C.

### ***3.2.1.5 Surface Functionalisation of PCL with Hyaluronic Acid (PCL-g-HA) Films and Scaffolds***

Two hundred milligrams of sodium hyaluronate (hyaluronic acid) powder was dissolved by stirring at 30°C for 2 hours, to a concentration of 0.4% w / v in 50 mL 0.5M MES solution in deionised water. Upon full dissolution of the hyaluronic acid, 1.1 mM of EDC and NHS (126 mg and 210 mg) were added to the solution and allowed to stir at room temperature overnight, functionalising the hyaluronic acid. Add PCL (scaffolds or films) to a solution of 0.06 / mL 1,6-hexanediamine in isopropanol and gently stir for 120 minutes at 30°C. Upon completion, wash the PCL with excess quantities of deionised water to remove unreacted 1,6-hexanediamine. Washed samples were immediately added to the solution of functionalised hyaluronic acid in MES buffer and gently stirred overnight. Upon completion the PCL-g-HA samples were removed from the reaction solution and washed with excess deionised water. Samples were dried in a vacuum desiccator and stored at 4°C.

## ***3.2.2 Biosynthetic Materials Based on PHBV and Collagen***

### ***3.2.2.1 PCL / PHBV Blends Functionalised with Collagen***

Samples of PCL / PHBV (both scaffolds and films) were hydrolysed with 3M sodium hydroxide for 30 minutes before washing with deionised water. The hydrolysed scaffolds were then immersed in a 50 mL solution of 10 mM EDC and 10 mM NHS in 0.5M MES buffer (pH 6.5) and stirred gently for 4-6 hours, after which the solution was removed, and the scaffolds washed with deionised water. The scaffolds were immersed overnight at 4°C in a solution of 6 mg / mL

collagen (pH 5.5-6.5), after which the scaffolds were removed from the solution and washed with deionised water. Conjugated samples were dried in a vacuum desiccator and stored at 4°C.

### ***3.2.2.2 Surface Functionalisation of PHBV with Collagen***

Collagen Type I was immobilised onto the membrane surface using the following protocol. PHBV fibrous mats were immersed into 1M sodium hydroxide solution at room temperature for 3 minutes. The sodium hydroxide solution was removed, and the samples were gently washed with deionised water. Alkali treated membranes were submerged into a solution containing 10 mM (191 mg) of EDC and 10 mM (115 mg) of NHS in 0.5M MES buffer (pH 6) for 6 hours. Activated PHBV fibre membranes were submerged into a collagen solution (1 mg / mL, pH 6) overnight at 4°C. At reaction completion, the samples were gently washed three times with excess deionised water, before storage at 4°C.

Samples that were not immediately added to the functionalised hyaluronic acid solution were dried under vacuum in a desiccator and stored at 4°C.

## ***3.3 Materials Processing***

### ***3.3.1 Hot Compression Moulding***

Films of polymer were processed by placing 300 mg of polymer material between two glass microscope slides, on the surface of a hotplate, set at 85°C. A 3kg weight was placed on top of the slides for 60 seconds, after which the slides containing the molten polymer film were removed from heat and placed onto an ice pack for 120 seconds (flipping after 60 seconds). The resulting polymer films were measured to a thickness of between 0.9 mm and 1 mm.

### ***3.3.2 Filament Extrusion***

A Rondol 10 mm twin screw mini-extruder was used to produce filaments of PCL, PCL-g-Collagen, and PCL / PHBV blend. The extruded filament was pulled through a water bath by a Rondol belt Haul-off equipped with a laser measurement tool (the schematic of the process is shown in Figure 3.1., below). The extruder was operated at speeds of 40-60 rpm for filament production, with the haul-off operating at speeds of 1.20 m / minute – 1.50 m / minute. Filaments made of PCL, PCL-g-Collagen, and PCL-g-Gelatin between 1650-1750 µm were used for 3D printing. Filaments of PCL / PHBV between 1450-1800 µm were used for 3D printing. The filaments used to produce samples via 3D printing (log pile scaffolds or films) were processed by extrusion for one cycle, no re-pelletised materials were used in sample production.

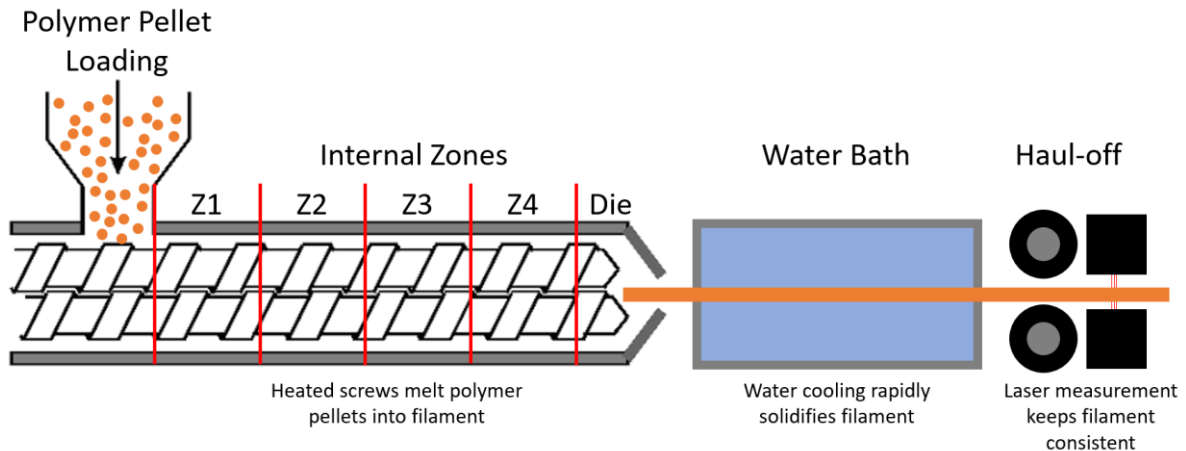


**Figure 3.1** – A schematic of the filament production process.

The final processing temperatures used in sample production for each material is shown below in Table 1. Process optimisation is detailed in Chapter 4 & 5 for individual materials.

**Table 3.1** – Extrusion temperature parameters for filament production.

Material	Zone 1	Zone 2	Zone 3	Zone 4	Die
PCL	110°C	145°C	140°C	140°C	95°C
PCL-Collagen	85°C	100°C	100°C	100°C	80°C
PCL-Gelatin	85°C	100°C	100°C	100°C	80°C
PCL / PHBV	100°C	150°C	150°C	145°C	135°C

### 3.3.3 3D Printing – Fused Filament Fabrication (FFF)

Scaffold geometries were designed using Autodesk Inventor Professional 2015 and exported as .STL files. Simplify3D slicing software was used to modify print settings and generate the .gcode files used to print the scaffolds.

A Flashforge Dreamer 3D printer, modified with a flexion extruder print-head and glass build plate was used to print scaffolds of PCL, PCL-g-Collagen and PCL / PHBV blends.

The final key parameters used to print samples are shown in Table 3.2, below. Parameter optimisation and further details are included in the Chapters 4 & 5 for individual materials.

**Table 3.2** – The key printing parameters used for individual biosynthetic material filament production.

Material	Nozzle Temperature	Bed Temperature	Print Speed
PCL	115°C	34°C	1200 mm / min
PCL-g-Collagen	85°C	30°C	400 mm / min
PCL-g-Gelatin	85°C	30°C	400 mm / min
PCL / PHBV blend	170°C	40°C	1200 mm / min

### **3.3.4 Laser Cutting of PCL and PCL / PHBV Scaffolds and Films**

An HPC<sup>99</sup> Laser model LS3020 using LaserCut software (V 5.3) was used to cut samples from 3D printed structures of both PCL and PCL / PHBV. For log pile structures, discs of 7 mm diameter by 2.4 mm height were cut from larger polymer scaffolds measuring 30 x 30 x 2.4 mm in size. Settings of Power 45 and Speed 30 were used and were proprietary to the accompanying software. To achieve a clean cut without charring or melting the scaffolds, the program was used twice in immediate succession. For flat disc samples, settings of: Speed 30 and Power 15 were used to cut samples.

### **3.3.5 Preparation PHBV Fibre Membranes and Films**

A FibeRio 1000M Forcespinning centrifugal spinning machine (Leeds University) was used to produce the PHBV fibre membrane samples. For each spin cycle, 1.6 ml of 25% w / v PHBV in chloroform solution was injected into a hollow fluid reservoir, which was tipped with two hypodermic needles (30 gauge with a shaft length of 12.5 mm). Spin cycles were run for 120 seconds at 9000 rpm. The collector was located radially to the spinneret and comprised a series of metallic bars at set 39.2 cm (OD) from the spinneret (Figure 3.2). Cardboard rectangular frames of dimensions 180 mm and 85 mm were affixed to the bars to facilitate the collection of flat areas of the fibrous web.

Films of PHBV were prepared by solvent casting. 5% w / v PHBV pellets in chloroform were added to 100 mL of chloroform and stirred until fully dissolved. The solution was cast into a 15 cm Ø diameter petri dish and the solvent removed overnight under gentle air flow.

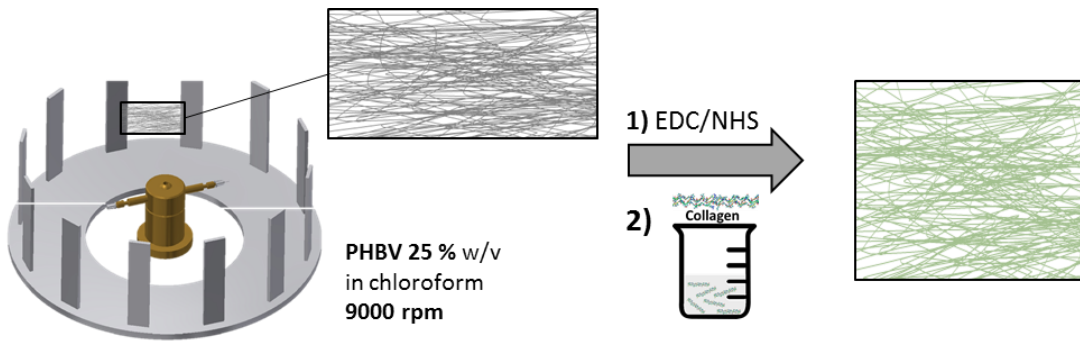


**Figure 3.2** – A schematic representation of the production of PHBV-g-Collagen fibre membranes<sup>100</sup>.

### 3.3.6 Spin Coating

Samples studied by spin coating were created by preparing solutions of material at 2% w / v in chloroform. 100 µL of each solution was pipetted onto a 10 mm glass cover slip and spun at 1000 rpm for 3 seconds followed by 10 seconds at 7000 rpm using a CSS-05 (PI-Kem) spin coating device.

## 3.4 Physicochemical Characterisation and Analysis

### 3.4.1 Scanning Electron Microscopy (SEM)

PCL and PCL / PHBV Based Films and Scaffolds: The surface morphology of scaffolds and films were imaged using scanning electron microscopy (Hitachi TM3030) using an accelerating voltage of 15 kV, working distance for 50x zoom – 3.9 – 10.1 mm. Samples were mounted on aluminium blocks using adhesive carbon tape. Hitachi TM3030 proprietary software was used to capture the images.

PHBV-Collagen Fibre Membrane Scaffolds: The surface morphology of forcespun PHBV fibres was analysed using environmental scanning electron microscopy ESEM (TESCAN VEGA LMU, Newcastle University) at an accelerating voltage of 15 kV at 600x and 800x magnifications, with a working distance of 4.7 – 9.7 mm.

### 3.4.2 Optical Microscopy and Fluorescence Analysis

Bright-field microscopy and fluorescent imaging were performed using a DMLB-Leica microscope, equipped with a mercury lamp, using Spot Advanced Software (Version 4.0.6).

### **3.4.3 Confocal Microscopy**

Confocal microscopy was performed using a Nikon AR1 inverted microscope, using Nikon NIS elements software (Version 5.2).

### **3.4.4 Image Processing and Analysis**

Image analysis not performed using proprietary software was completed using open-source software ImageJ (version 1.51k).

### **3.4.5 Sirius Red Staining**

Collagen content was qualitatively assessed using Sirius Red staining. Samples were incubated in 1 mL of Sirius Red for 30 minutes, allowing the stain to form a complex with any present collagen. Samples were removed from the dye and washed three times with chilled deionised water to remove all unbound stain. Samples were placed on a glass microscope slide and imaged using a DMLB-Leica Bright field light microscope.

### **3.4.6 Fourier Transform Infrared – Attenuated Total Refraction (ATR-FTIR)**

ATR-FTIR analysis was performed using a Spectrum Two PE, with Universal ATR attachment (Perkin Elmer), in a wavelength range of  $4000\text{ cm}^{-1}$  to  $550\text{ cm}^{-1}$ . Samples were dried under airflow before analysis. Polymer films, scaffolds and fibrous membranes were examined prior to and after collagen functionalisation by infrared spectroscopy. ATR-FTIR spectra of 36 scans at  $4\text{ cm}^{-1}$  resolutions were obtained by a Frontier PerkinElmer FT-IR spectrophotometer with a universal attenuated total reflectance (ATR) module in diamond.

### **3.4.7 Differential Scanning Calorimetry (DSC)**

Differential scanning calorimetry (DSC) was used to investigate changes in the polymer structure before and after collagen conjugation. Samples (4-8 mg, aluminium pans) were analysed using a Netzsch Polyma DSC, and analysed with Netzsch Proteus software. A heating scan from 0 to  $240^\circ\text{C}$  was conducted at a rate of  $10\text{ }^\circ\text{C minute}^{-1}$ , with the cooling segment of the cycle running at  $20^\circ\text{C minute}^{-1}$ , under a nitrogen atmosphere.

### **3.4.9 Contact Angle**

The sample surfaces static contact angles were investigated at room temperature using a Contact Angle CAM 200 KSV Instrument, equipped with Tetha software using the sessile drop method, dispensing  $5\text{ }\mu\text{l}$  water droplet (HPLC grade) directly on the sample surface. Contact angle measurements were analysed using automatic software and presented as the average of 100 measurements from three different points on each surface.

### **3.4.10 Degradation Studies**

The in vitro degradation study was performed using PBS solution at 37°C in a VWR Incu-line incubation oven. Samples were incubated in 5 mL flasks with 2.5 mL of PBS (pH 7.4). Samples were stored in a vacuum desiccator for 3 days before weighing and incubation. Samples were removed from the incubator at set time points, washed with DI water, and stored in a vacuum desiccator until fully dry, after which the weight was measured again on a KERN ABT 220-5DM analytical balance.

### **3.4.11 Mechanical Analysis**

Compressive: The compressive strength of printed logpile scaffolds (7 mm diameter x 2.4 mm height) was determined using a Shimadzu AGS X-10 equipped with a 1 kN load cell.

Dynamic Mechanical Analysis: The storage modulus of material films was examined using Dynamic Mechanical Analysis (DMA) on a Perkin Elmer 8000, using proprietary Perkin Elmer DMA software. Films were cut to 20 x 10 x 0.2 mm size for analysis. A temperature scan was performed from 25-100°C at a ramp rate of 2°C / minute, three-point bending was the method used to determine storage modulus, with a frequency of 1Hz and a displacement of 0.05 mm.

## **3.5 Biological Analysis**

### **3.5.1 Cell Culture and Expansion**

Neo-NHDF fibroblasts were grown at 37°C, 5% CO<sub>2</sub>, in Dulbecco's Modified Eagle Medium (DMEM, Sigma-Aldrich, UK), 4.5g / L glucose, supplemented with 10% foetal bovine serum (FBS) and a 1% antibiotic mix containing penicillin and streptomycin (100µ / mL). TC28a2 chondrocytes were grown at 37°C, 5% CO<sub>2</sub>, in F-12/DMEM (Thermofisher Scientific, UK), 4.5g / L glucose, supplemented with 10% foetal bovine serum (FBS) and a 1% antibiotic mix containing penicillin and streptomycin (100µ / mL). Fibroblasts being the major constituent cell type in skin, Neo-NHDF fibroblasts were selected for forcespun scaffolds with mechanical properties more in line with dermal tissue.

TC28a2 cells were seeded at 50,000 cells in T-175 flasks and 20,000 for T-75. NHDF-Neo fibroblasts were seeded at a concentration of 100,000 cells for T-175 and 40,000 for T-75. Cells were passaged at ~80% confluence. Old cell media is aspirated, and adhered cells are washed using 10mL of PBS to remove remaining media. Trypsin-EDTA (1.5 mL for T-75, 3 mL for T-175) solution is added to the flask and incubated at 37°C, 5% CO<sub>2</sub>, for 3 minutes. After the incubation period, the flask is vigorously agitated without splashing the internal contents, after which the cells are checked for detachment by brightfield microscopy. The contents of the flask are diluted to 10 mL total fluid content by the addition of DMEM, after which the contents of

the flask are transferred to a 50mL falcon tube. The cells suspension is centrifuged for 5 minutes at 1200 RPM. After centrifugation, the cell media / trypsin mix is aspirated, with care not to disturb the condensed cell pellet, and the cells are suspended in fresh warm DMEM. Cell culture flasks are pre-filled with warm DMEM (15 mL T-75, 25 mL T-175), before cells are aliquoted by pipette. Chondrocytes being the constituent cells of articular cartilage, TC28a2 cells were selected for use in scaffolds aiming to mimic the properties of articular cartilage.

### **3.5.2 Cell Counting using Haemocytometer**

During the passage, cells counted using a manual haemocytometer. Two samples of 10 µL are taken from the cell suspension after trypsin treatment and before centrifugation. Cells are counted by taking an average count of the cells observed in eight individual 1x1 mm grids on the haemocytometer.

$$\text{Measured Cell Density} = \frac{\text{Average cells per small square}}{\text{Volume of a small square}}$$

$$\text{Volume of square} = W \times H \times D = 1 \times 1 \times 0.1 = 0.0001 \text{ mL}$$

### **3.5.3 Cell Freezing and Defrosting**

Cryovials in storage are removed from storage in liquid nitrogen and gently stirred in a water bath at 37°C until the internal suspension has fully defrosted. The suspension of cells in freezing media is carefully pipetted into 40 mL of warm DMEM, which is lightly agitated to fully disperse the cells in the solution. The suspension is centrifuged at 1200 RPM for 5 minutes, after which the DMEM / freezing media solution is aspirated, without disturbing the cell pellet. The pellet is re-suspended in fresh warm DMEM before pipetting into a cell culture flask.

### **3.5.4 Technique for Cell Seeding onto Scaffolds**

#### PHBV-Collagen Fibre Scaffolds and Neo-NHDF Fibroblasts:

Force spun samples were secured in well inserts with a 10 mm internal diameter (Cellcrown 24, Scaffdex), positioned in 12 well plates (Tissue culture treated, 3526, Costar) and sterilised with a UV lamp at 254 nm for 30 minutes, at a distance of 5 cm from the point of emmission. DMEM was placed into each well up to the level of the scaffold surface, pre-wetting the material for 30 minutes before cell seeding. A suspension of 40000, cells in 100 µL DMEM was seeded onto the surface of each scaffold, incubated at 37°C, 5% CO<sub>2</sub>, for 30 minutes, then the wells were topped up with DMEM to a volume of 1500 µL.

## TC28a2 Chondrocytes Culture onto PCL and PCL / PHBV based Scaffolds:

Prior to seeding, 1 mL of 2% agarose gel solution is syringed into each well of a 24 well plate and allowed to cool, to avoid cell adhesion to the tissue culture plastic and encourage favourable migration to the scaffolds. The plates and samples are sterilised under UV light at 254 nm for 30 minutes. The samples are placed into the wells on top of the solid agarose gel and a suspension of 20,000 cells in 50  $\mu$ L is pipetted onto the top of the scaffolds. The plates are incubated at 37°C, 5% CO<sub>2</sub>, for 30 minutes to allow for cell adhesion, after which the wells are topped up with 1 mL of F12 / DMEM.

### ***3.5.5 Cytoskeletal and Nucleus Staining***

Cell morphology was observed using cytoskeleton and nuclear staining. At relevant time points, media was removed from well containing seeded scaffolds, and scaffolds were washed with PBS. 4% Paraformaldehyde solution warmed to 37°C is added to the well and left for 15 minutes at room temperature or overnight in the fridge to fix the cells.

After culture, samples were fixed using 4% paraformaldehyde for 15 minutes at room temperature, after which samples were washed with PBS / tween (0.1%) three times. 1500  $\mu$ L of Rhodamine-Phalloidin solution (prepared to 1:1000 dilution in PBS) was added to each sample for 30 minutes at room temperature, after which the solution was removed, and samples were thrice washed with deionised water. DAPI (1 mg / mL in PBS) was added to each well for 30 minutes at room temperature, samples were then washed with PBS before mounting on microscope slides. Images were obtained with a Nikon AR1 inverted microscope using Nikon NIS elements software. Emission filter 490 nm for DAPI, and 594 nm for Phalloidin stain.

### ***3.5.6 Metabolic Activity Analysis by Presto Blue Assay***

Metabolic activity was assessed by Presto Blue assay (Life technologies, Thermo Fisher Scientific, USA). Cell culture media was removed from samples and replaced with 1500  $\mu$ L of 1:9 v / v Presto Blue to DMEM. Treated samples were incubated at 37°C, 5% CO<sub>2</sub>, for two hours after which the solution was removed and 200  $\mu$ L from each sample placed into a 96 well plate with opaque white walls. Experimental timepoints were examined from 24 hours post seeding to 21 days at longest. Fluorescence readings were measured by a BioTek ELx800 microplate reader using Gen5 software (Version 3.02), at 570 nm and 630 nm. The values at 630 nm were taken as reference and subtracted from the values at 570 nm. Presto Blue samples were calibrated by seeding known quantities of the cell line under examination onto well plates, allowing to adhere, then running the assay under conditions described above. The results

produced a calibration curve, against which experimental results were compared. Sample number = 3.

### ***3.5.7 Analysis of Cell Viability by LIVE / DEAD Assay***

Cell viability was assessed with LIVE / DEAD staining (LIVE / DEAD® Imaging Kit, Life Technologies, Thermo Fisher Scientific, USA) at Days 1 and 3. Samples were washed with PBS and stained with 1.5 mL solution of 1 µL calcein AM and 2 µL Ethidium homodimer-1 per mL in PBS. After 30 minutes of incubation at room temperature, the scaffolds were mounted on glass slides and imaged with DLMB-Lecia microscope, using Spot Advanced software (Version 4.0.6). Rhodamine and FITC filters were used to detect Ethidium homodimer-1 (ex 570 nm, em 602 nm) and calcein AM (ex 488 nm, em 515 nm) respectively. Sample number = 2 per sample type.

### ***3.5.8 Statistical Analysis***

Analytical tests were performed in triplicate to attain statistical validity. Statistical analysis was determined using Prism 7 software (GraphPad). Statistical difference between groups was denoted using the \* symbol, signifying a threshold of  $p < 0.05$  (\*). Where differences were assessed between two groups, a standard t-test was used. Where 3 or more groups were used, Anova one-way tests were used as significance. Tukey post-hoc was used to compare paired group means among samples of equal size.

## **Chapter 4: Evaluation of Conjugation Methods for 3D Structures**

### ***4.1 Introduction***

This chapter details the methods by which methods of creating biosynthetic materials of PCL and Collagen were examined. The experimental process was used to refine the methodology by which the biosynthetic polymers are created, examine their efficacy for processing into scaffolds, and steer the course of production for further biological testing. Multiple approaches were taken in the creation of PCL-Collagen biosynthetic materials: 1) “Bulk” conjugation involving carbodiimide coupling chemistry with both PCL and collagen in solution, 2) surface conjugation using carbodiimide chemistry to graft collagen to the surface of PCL structures, and 3) blending of both polymers in solution without covalent coupling.

These materials were processed by a variety of methods, including heat moulding, spin coating, extrusion, and Fused Filament Fabrication. Physicochemical examination at different stages of the processing pathways was used to determine the suitability of both the biosynthetic material and the process to generate biosynthetic scaffolds suitable to carry through to the biological testing stage. Optimisation of the filament extrusion and 3D printing parameters were achieved to a high level of repeatability and fidelity, through extensive process iteration.

### ***4.2 Synthesis of Biosynthetic Materials Based on PCL and Collagen***

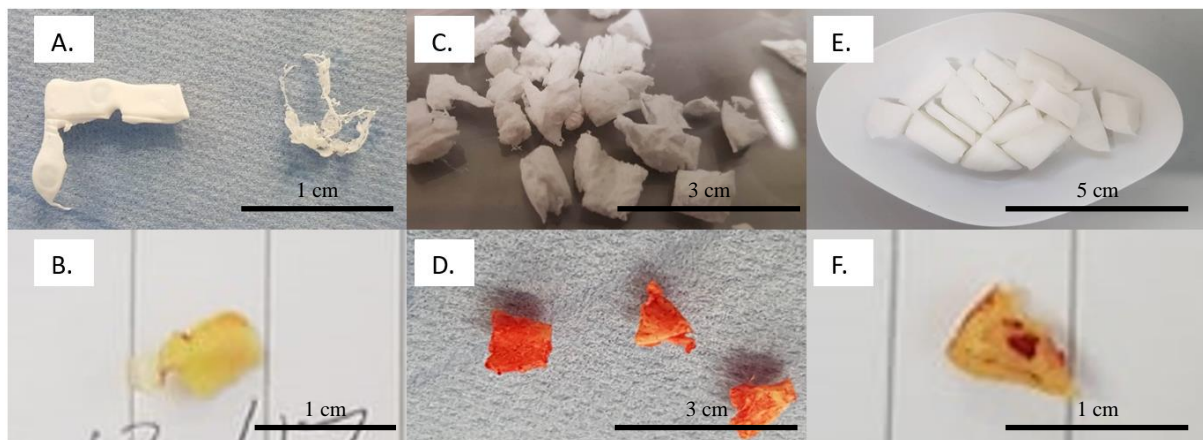
#### ***4.2.1 PCL-g-Collagen Bulk Material***

The development of a synthetic approach to creating biosynthetic materials was studied using the Polycaprolactone (PCL) and collagen type I, as bulk conjugation (PCL-g-Collagen) via carbodiimide chemistry. The initial synthesis process (based on Protocol 1, Table 4.1) comprised five stages of optimisation: (1) dialysis volumes for efficient removal of unreacted carbodiimide, (2) time for dialysis of conjugated material, (3) washing steps of remaining organic solvents, (4) time required for removing solvent residues, and finally (5) optimisation of PCL and Collagen material amounts for obtaining a higher reaction yield. The process began with the initial Protocol 1 and developed to Protocol 3 (Table 4.1). Note that collagen content is related to the quantity of collagen used in the production process, and not the collagen content in the final product.

**Table 4.1 – Synthesis protocols for PCL-g-Collagen**

<b>Conditions</b>	<b>Protocol 1</b>	<b>Protocol 2</b>	<b>Protocol 3</b>
dialysis volumes (mL)	4000	4000	2000
time dialysis (hours)	48	48	24
washing steps (No)	1	3	3
Washing time (min)	90	90	30
PCL:Collagen ratios	2g:120 mg (1:60 w / w ratio)	2g:300 mg (1:150 w / w ratio)	3.5g:300 mg (1:86 w / w ratio)

The PCL-g-Collagen materials obtained by the different protocols were primarily assessed in terms of collagen content by Sirius Red staining and ATR-FTIR for chemical analysis, to establish the reaction yield. In Figure 4.1. can be observed the collagen distribution (collagen is stained in red by Sirius red assay) for the three protocols. The collagen yield was determined as the mass of resulting PCL-collagen produced. The level of collagen integration in the product was visually assessed by Sirius Red staining. Following the analysis, it was obtained that PCL-g-Collagen material Yield produced by Protocol 2 was lowest, with the highest level of collagen integration, while the lowest values were found for protocol 1. This can be seen appreciated in Figure 4.1 C and D, which presented the highest overall level of Collagen integration. Therefore, this protocol was selected as the synthesis method for producing bulk biosynthetic PCL-g-Collagen material to be processed as 3D constructs in next project stages.



	Protocol 1	Protocol 2	Protocol 3
Collagen Input	120 mg	300 mg	300 mg
PCL Quantity	2 g	2 g	3.5 g
PCL-g-Collagen Yield	1.73 g	1.60 g	3.77 g

**Figure 4.1 – PCL-g-Collagen synthesis process development.** The protocols describe key stages in development. Images A&B relate to Protocol 1, C & D relate to Protocol 2, E & F are related to Protocol 3. Sirius Red collagen stain was used to produce the red colouring on images B, D & F. Collagen content is in referral to the quantity of collagen used in the production process, not the final product.

#### **4.2.2 PCL and Collagen Blend Material (PCL / Collagen Blends)**

A blend of PCL and collagen has been explored as another method of creating biosynthetic materials without the need of chemical conjugation. Figure 4.2 A, B & C show the product of attempts to blend PCL in a chloroform solution with an aqueous phase collagen solution. As can be seen in image A, despite being stirred vigorously for 16 hours, there is strong phase separation in the final product after the solvent was removed. As a consequence of this phase separation, collagen distribution throughout areas of the film is not homogenous, observing collagen material accumulations in random areas of the blend (Figure 4.2, images B & C) particularly in areas around the edge of the film.

Figure 4.2 D shows the product of the surface conjugation process. The surface conjugated materials, PCL-s-Collagen, showed a more even distribution of collagen along the surface of the films than the PCL / Collagen Blend samples.

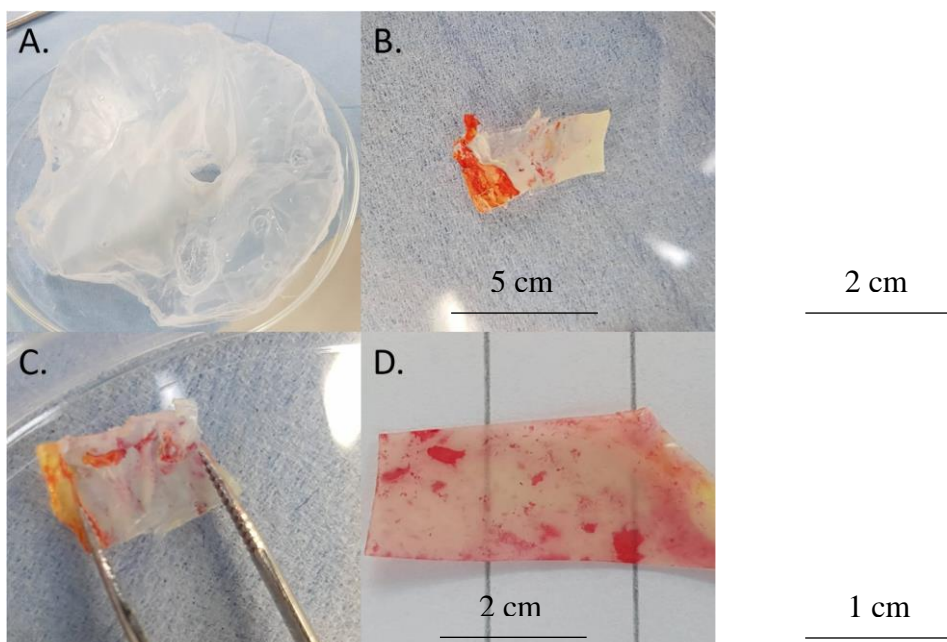


**Figure 4.2 –** **A.** Image of PCL / Collagen Blend after solvent removal, washing and drying. **B.** A Sirius Red stained section from the thick area of the blend film. **C.** A Sirius Red stained section from the edge of the film where phase separation was observed. **D.** Image of PCL-s-Collagen film after Sirius red staining.

#### **4.2.3 Chemical Analysis by ATR-FTIR**

The ATR-FTIR spectra for PCL-g-Collagen and PCL / Collagen Blends are shown in Figure 4.3. In both conditions, blend and bulk PCL-g-collagen materials, it is possible to observe the presence of the typical collagen bands amide I and II. For blend films, the intensity of Amide I & II ( $1671\text{ cm}^{-1}$  &  $1559\text{ cm}^{-1}$ ) peaks vary significantly depending on where in the blend film the analysis is performed. The Blend material spectra indicated that higher intensities of the Amide peaks ( $1638\text{ cm}^{-1}$  &  $1568\text{ cm}^{-1}$ ) were present in thinner areas of the film, while lower intensity levels of collagen amide bands were detected in thicker areas of the film. Moreover,

those areas in which a strong phase separation was observed, with colloidal segments of a primarily Collagen film, resulted in peaks with low PCL typical ester signals  $\sim$ 1725 cm $^{-1}$  and 1230 cm $^{-1}$  and intense Amide signals at 1671 cm $^{-1}$  & 1559 cm $^{-1}$ . However, when contrasting PCL-Collagen blends and bulk conjugated material, PCL-g-Collagen spectra showed lower variability in the peak intensity signals for the Amide I & II within batches, indicating a more homogeneous material, however, variation in amide I & II signal intensity was still observed. The other characteristic Collagen peaks, Amide III and pyrrolidine peaks ( $\sim$ 1450 cm $^{-1}$  and 1235 cm $^{-1}$  respectively) are obscured by overlapping PCL peaks in both the PCL-g-collagen and PCL / Blend samples.

A comparison between select spectra of PCL-Collagen modified by different chemical methods and an unmodified PCL base material is shown in Figure 4.3. Broadly, both PCL-Collagen modified material showed the characteristic Amide I & II bands, although the strongest intensity in PCL / Collagen Blend samples was detected. Moreover, associated -OH and -NH stretching bands at 3450 cm $^{-1}$  were detected in all PCL-Collagen samples, with a higher proportional intensity detected in PCL-g-Collagen samples, indicating a higher quantity of collagen in the material, or possibly water retention within the material pellets. PCL-g-Collagen and PCL / Collagen Blend samples both exhibited similar levels of -OH & -NH signals. However, PCL / Collagen blend samples evidenced a lower intensity of PCL characteristic bands, including the -C=O ester peak at 1720 cm $^{-1}$  and the C-H signal bands in the range of 800-1400 cm $^{-1}$ , suggesting a higher collagen content in the samples.

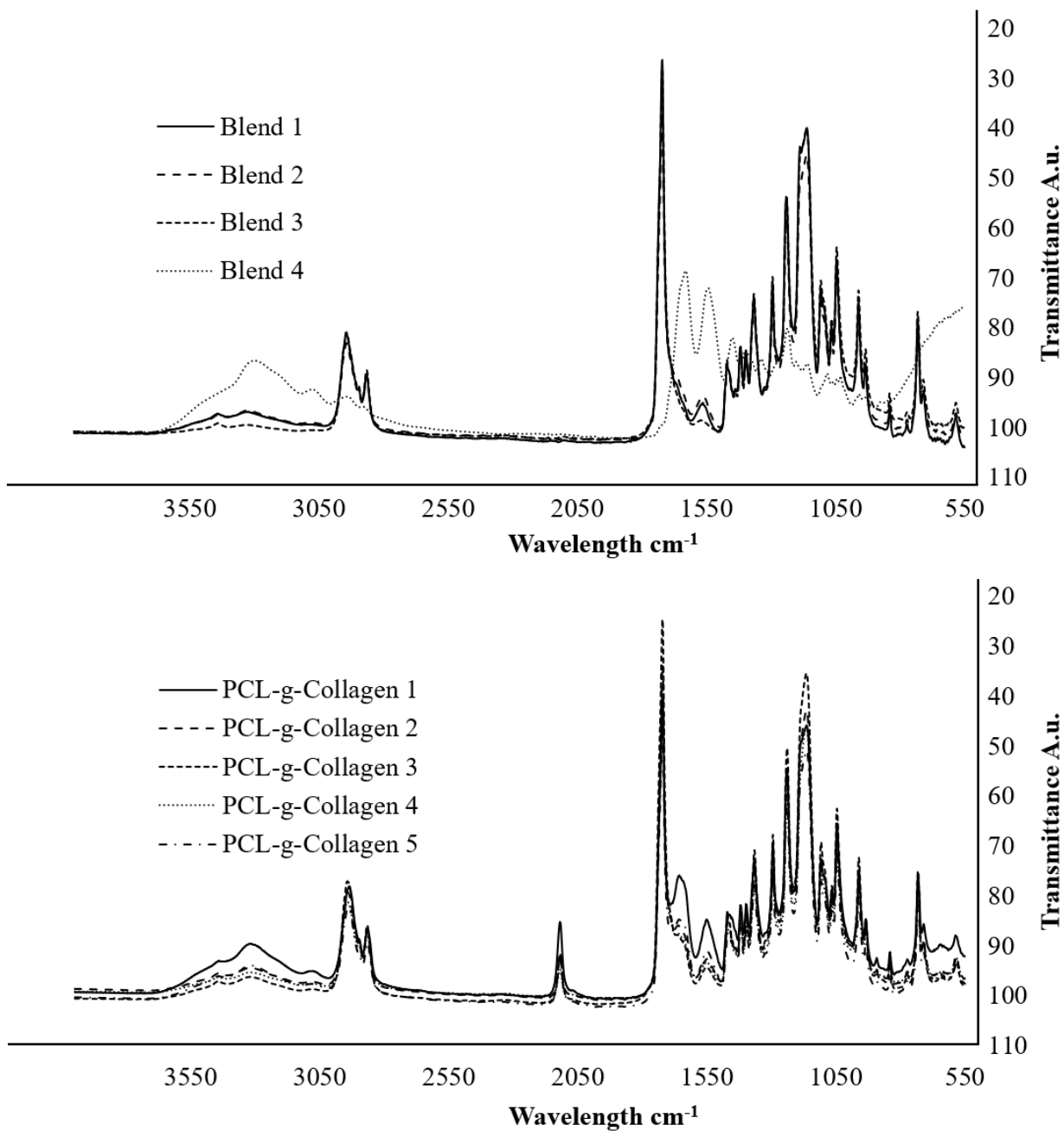


**Figure 4.3 – Top.** PCL / Collagen blend ATR-FTIR signals. Collagen characteristic Amide I & II peaks are present at  $1671 \text{ cm}^{-1}$  &  $1559 \text{ cm}^{-1}$  respectively for blended areas and  $1625 \text{ cm}^{-1}$  &  $1561 \text{ cm}^{-1}$  in collagen films. **Bottom.** ATR-FTIR analysis of PCL-g-Collagen. Characteristic Amide I & II peaks are shown at  $1638 \text{ cm}^{-1}$  &  $1568 \text{ cm}^{-1}$  respectively.

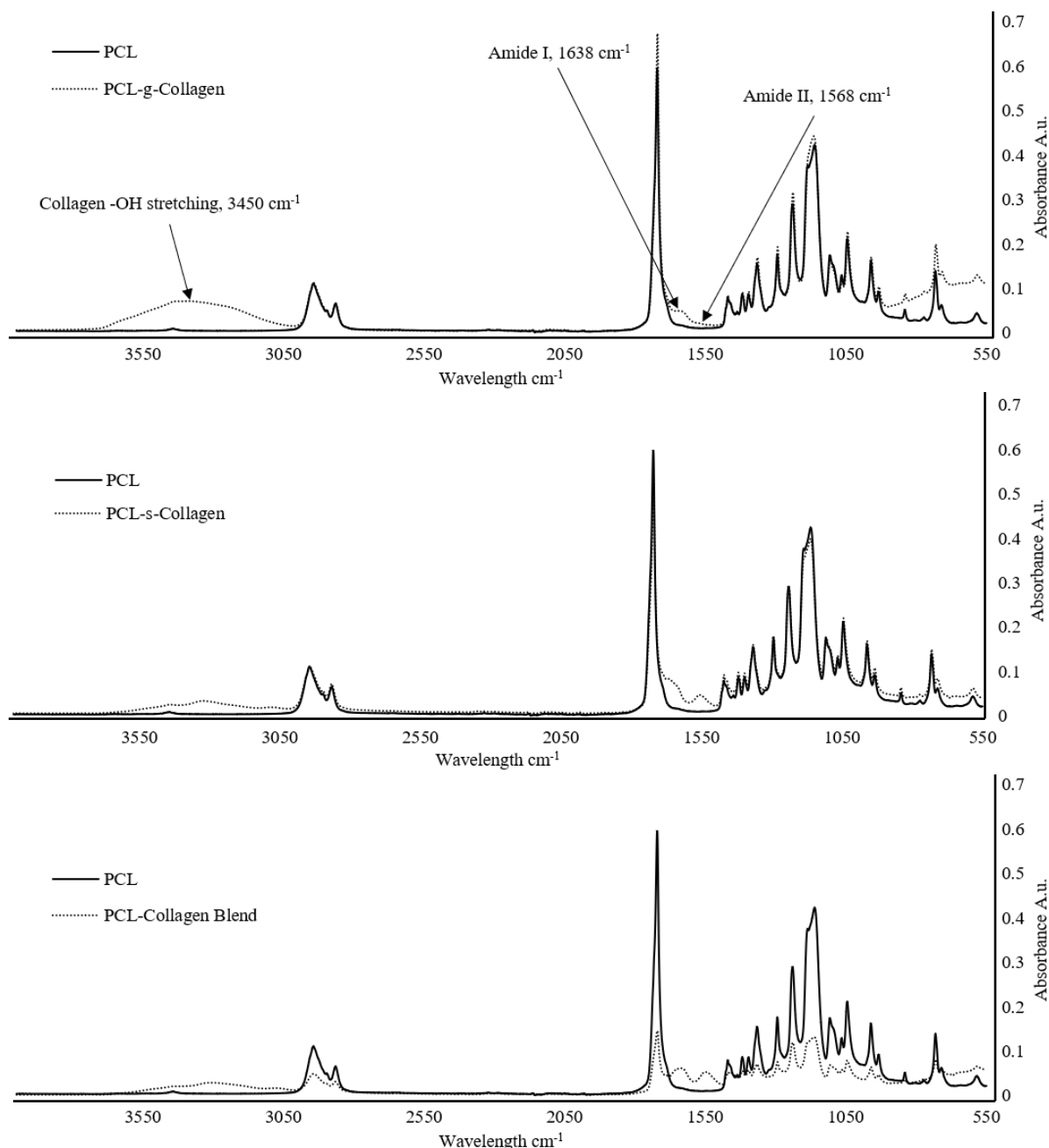


**Figure 4.4** – Comparisons of ATR-FTIR of different PCL-Collagen samples with unmodified PCL samples, read in absorbance. **Top.** PCL-g-Collagen and PCL. **Middle.** Surface modified PCL films (PCL-s-Collagen) and PCL. **Bottom.** PCL / Collagen blend films with PCL.

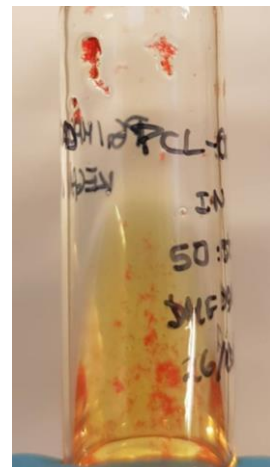
### **4.3 Material Processing Development and Analysis**

#### **4.3.1 Assessment of collagen content and wettability changes onto Spin Coated thin-films**

The collagen content and the contact angle was studied in flat 2D samples processed by spin-coating. To ability to solubilise modified PCL-g-Collagen for further processing was determined by using different solvents (as seen in Table 4.2) at different concentrations, including 1,1,1,3,3,3- Hexafluoro-2-propanol (HFP) and Tetrahydrofuran (THF). The solvents were selected based on solubilising strength, and what can dissolve PCL from literature<sup>32</sup>. 100uL droplets of PCL-g-Collagen solution were placed on a glass disc and spun at rotational speeds of 1000 rpm for 3 seconds, followed by 7000 rpm for 10 seconds.

**Table 4.2 – Attempts to solubilise PCL-Collagen materials in common solvents and those used in Electro / Force spinning methods.**

Material	Solvent	Mass (mg)	Concent ration (w / v)	Soluble?
PCL-g-Collagen	DMF / DCM 1mL	30	3%	No
PCL-g-Collagen	DMF / DCM 3mL	30	1%	No
PCL-g-Collagen	Chloroform 5mL	27	0.54%	No
PCL-g-Collagen	THF	13	1.3%	No
PCL-g-Collagen	HFP	10	1.0%	No
PCL-Collagen Blend	Chloroform 1mL	16	1.6%	No



Collagen Staining by Sirus Red Assay: Following colorimetric staining with Sirius red assay, there are no red coloured areas observed suggesting the absence of structural collagen molecules in the spun sample. It was observed that in PCL-g-Collagen samples, the presence of red-stained solid residues remaining in the solvent, indicating that the PCL-g-Collagen conjugated molecule cannot fully solubilise.

Contact Angle: The wettability characteristics of spin coated films of PCL and PCL-g-collagen were measured by determining the contact angle as detailed in Chapter 3, Section 3.3.6.. PCL-g-collagen films gave a value of  $89.2^\circ$  ( $SD \pm 2.7^\circ$ ), PCL films gave a value of  $80.0^\circ$  ( $SD \pm 1.4^\circ$ ), and the glass slide control sample gave a value of  $60.6^\circ$  ( $SD \pm 5.6^\circ$ ). Statistical analysis shows that a significant difference in angle was present between each sample, indicating that the introduction of collagen by conjugation significantly reduces the hydrophobicity of PCL. Results displayed in Figure 4.5.

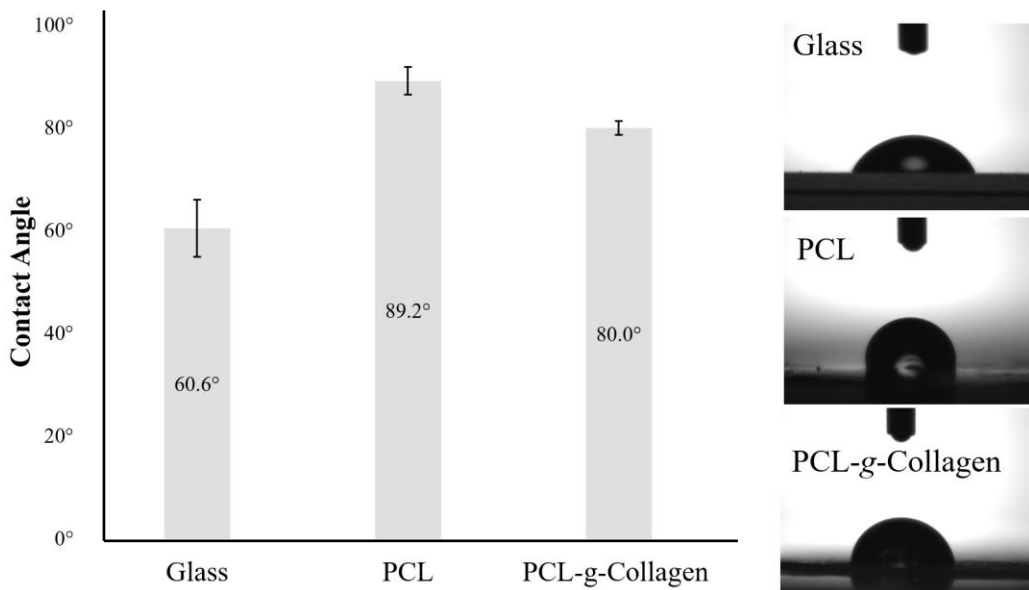


**Figure 4.5** – Analysis of the contact angle of de-ionised water on PCL, PCL-g-Collagen, and a Glass control sample. Images on the right of the figure directly correspond to the analysis performed.

#### 4.3.2 PCL and Collagen Modified Samples Processed by Hot Moulding

Pellets of PCL and PCL-g-Collagen were moulded under pressure as described in Chapter 3, Section 3.3.1.. After the initial heating phase at 85°C, the still semi-molten samples were removed from the hotplate and embossed by pressing a 1 x 1 cm ridged mould, with the goal of inducing surface features to the polymers, providing detail for microscopy.

Collagen Staining by Sirius Red Assay: Figure 4.6 depicts these embossed 1x1 cm cuttings from the materials, after staining with Sirius Red. Red staining appeared on the PCL-g-Collagen sample, indicating that after heating for 60 seconds under a 5kg load, the material could be moulded without losing internal structural collagen. Figure 4.6 shows a comparison of Sirius Red stained PCL-g-Collagen pellets and a film of the same material stained after moulding. Here it can be seen that while not all collagen is lost in the short heating / moulding process, a significant quantity is, with the finished film having a far smaller area of red staining than the pellets prepared by synthesis.

Morphological Analysis by SEM: Figure 4.6 also displays SEM images of the same embossed samples. The disparity in the surface texture of PCL and PCL-g-Collagen samples indicates a change in physical properties, an effect induced by the conjugation process. The microscopy images of PCL-g-Collagen samples display a rougher, more fibrous surface texture, characterised by tears and cracks in the surface of the sample. By comparison, embossed PCL

samples displayed a smoother surface texture without tears and cracks, despite being processed in an identical manner.

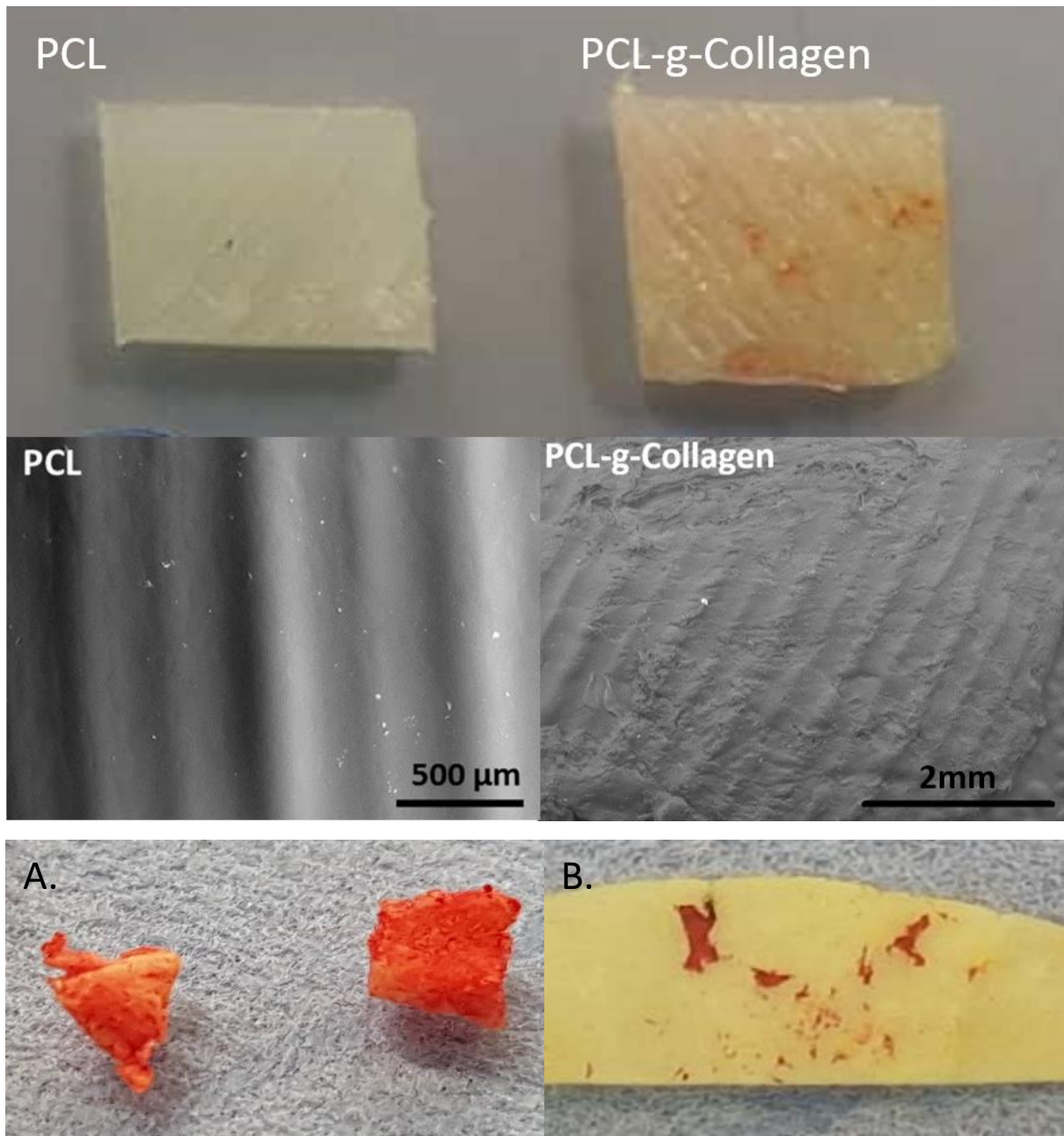


**Figure 4.6 – Top.** Moulded and embossed 1x1 cm cuts of PCL and PCL-g-Collagen stained with Sirius Red. **Middle.** SEM images of the samples displayed in the top row. **Bottom.** **A.** Pellets of PCL-g-Collagen stained with Sirius Red. **B.** Films of PCL-g-Collagen after hot moulding, showing that Collagen-containing biosynthetic materials can be thermally processed and retain structural collagen.

#### 4.3.3 Extrusion of PCL and Collagen Modified Samples

While optimising the parameters of filament production using PCL pellets with the Haul-Off, it was determined that a minimum rate of 1.2 meters / minute must be maintained for the Haul-Off to function, which in turn necessitated an extrusion screw speed of ~70 RPM to maintain a consistent 1.75 mm ( $\pm 0.05$  mm) filament of PCL. The use of a laser measurement tool in the

filament production process, allowed for the manufacture of PCL filaments that within the range of 1.65-1.80 mm in diameter, fitting within the tolerance of the FFF printhead's feeding port. The initial and final process temperatures can be observed in Table 4.3, with a decrease from an operating temperature of 140°C to 100°C through gradual optimisation. Though successful in producing a filament, operation at lower temperatures with PCL requires a decrease in the speed of the twin screws to avoid levels of torque that pass the extruders tolerance. This is due to the slow melting rate of PCL and resulted in a method by which PCL was processed at lower speeds (~ 40-50 RPM), remaining in the extruder barrel for a longer duration, exposed to heat.

**Table 4.3** – Optimised extruder temperature settings used to produce PCL filaments.

	<b>Zone1</b>	<b>Zone2</b>	<b>Zone3</b>	<b>Zone4</b>	<b>Die</b>
Original	110°C	145°C	140°C	140°C	95°C
New	85°C	100°C	100°C	100°C	80°C

To test the efficacy of the new extrusion temperature and speed parameters, PCL pellets were conjugated with collagen using surface conjugation techniques, then processed at both temperature settings. Figure 4.7 shows the effect of Sirius Red staining on the pellet feedstock and the filament product produced from each material. While successful in the production of consistently shaped filaments; cross-sectional staining of conjugated PCL filaments indicate that the extrusion process denatured most of, if not all, of the structural collagen present in the material. Sirius Red staining does not bind to non-structural or denatured collagen, and a complete lack of bound red dye in the product was evidence of complete collagen denaturing<sup>101</sup>. Moreover, this is confirmed by ATR-FTIR analysis of the filaments, in which the absence of the two characteristic Collagen Amide peaks suggest that the conjugated collagen was lost during the extrusion process.

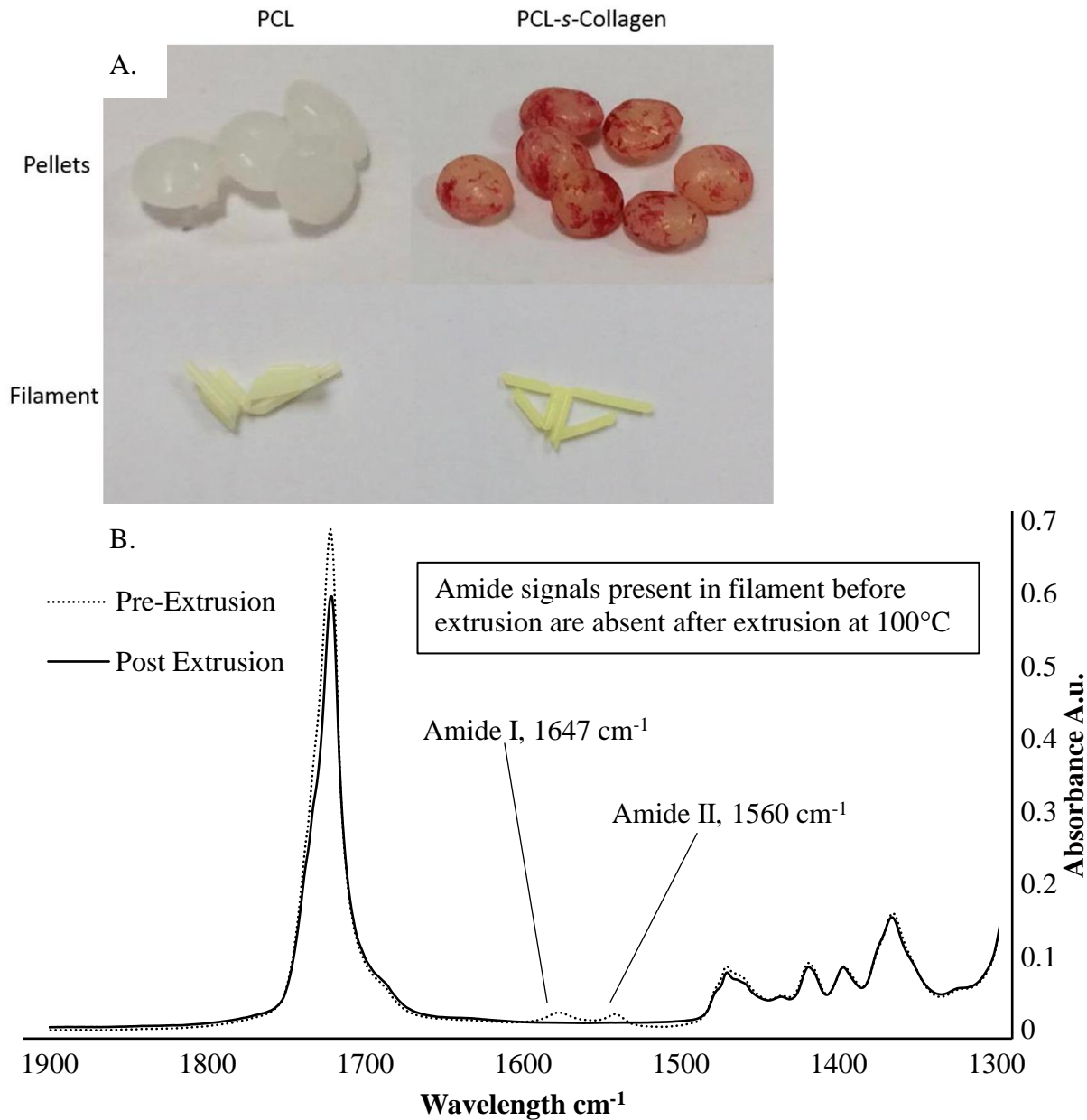


**Figure 4.7 – A.** Stained pellets of PCL and PCL-s-Collagen and stained filaments produced by the low temperature extrusion method. **B.** ATR-FTIR analysis of Sirius Red staining of surface conjugated PCL pellets before and after extrusion. ATR-FTIR spectra of the PCL-s-Collagen pellets before extrusion compared with the spectra of the pellets after extrusion, showing a lack of Amide peaks, indicating a lack of Collagen. This data was gathered by Thomas Kelly and Kegan McColgan-Bannon.

An additional experiment was performed for further understanding of how long the pellets remain in the extruder barrel during filament production. For this, 90g of PCL pellets were separated into three 30g portions, one 30g portion was dyed with green food colouring. The first portion was fed through the extruder at a typical production speed. When the filament stopped extruding, the dyed portion was added to the extruder. Therefore, the produced filament at this point was stained green, and when the filaments started shrinking in diameter (indicating the polymer in the extruder was running out) the third 30g portion was added. Interestingly, it was observed that the green colouring was present on the entirety of the next 30g of filament,

rather than having a small, dyed section at the start of the next filament. This finding suggested that material does not always pass fully through the extruder and that the polymer is spending more time in contact with heated zones than anticipated.

#### **4.3.4 Processing PCL and Collagen Modified Samples by Fused Filament Fabrication (FFF) Printing**

The printing process was optimised to print PCL scaffolds as shown in Table 4.4.. The iterative optimisation aimed to decrease the printing temperature closer to PCL melting temperatures and to preserve some of the structural collagen molecule by reaching 85°C. The temperature as previously established in the hot moulding process as allowing for the manipulation of PCL-g-Collagen while not completely denaturing the internal structural collagen.

**Table 4.4** – The optimisation of printing parameters used to establish a low-temperature method of printing PCL based scaffolds.

<b>Experiment</b>	<b>Nozzle Temperature (°C)</b>	<b>Print Speed (mm / min)</b>	<b>Extrusion Multiplier</b>	<b>First layer width</b>	<b>First layer speed</b>	<b>Success?</b>
1	140	1400	1.2	125%	100%	Yes
2	130	1400	1.2	125%	100%	Yes
3	115	1400	1.2	125%	100%	Yes
4	105	1400	1.2	125%	100%	Yes
5	95	1400	1.2	125%	100%	No
6	95	1200	1.2	125%	100%	No
7	95	800	1	125%	100%	No
8	95	400	1	100%	60%	Yes
<b>9</b>	<b>85</b>	<b>400</b>	<b>1</b>	<b>100%</b>	<b>60%</b>	<b>Yes</b>
10	75	400	1	100%	60%	No
11	75	300	1	100%	50%	No

Due to the mild variation in the diameter of custom produced PCL filaments, an extrusion multiplier of 1.2x was used in initial process iterations to compensate for thinner segments of filament. The first layer width of 125% and a print temperature of 140°C allowed for the rapid print speed of 1400 mm / minute. These settings were able to produce successful prints, at the temperature was incrementally brought down to 105°C. To successfully print at temperatures below 105°C, reductions in print speed, first layer width, first layer print speed, and extrusion

multiplier were required to allow the PCL filament to pass through the hot end without clogging. A print temperature of 85°C was eventually achieved by reducing the print speed to 400 mm / min, extrusion multiplier to 1x, first layer width to 100%, and first-layer speed to 60%. Attempts to print at temperatures below 85°C were not successful, even with further reductions in print speed and first layer speed. It should be noted that the use of an adhesive spray is vital to producing successful prints at temperatures below 105°C.

With the establishment of optimised printing conditions, PCL filament was used to print scaffolds as porous blocks of 30 x 30 x 2.4 mm using the parameters described in Chapter 3, Section 3.3.3., with 0.6 mm strut width, height, and pore width. From the porous blocks, scaffold discs of 7 mm diameter and 2.4 mm height, were laser cut to provide the samples shown in Figure 4.8. Brightfield microscopy imaging was used to take measurements from printed PCL scaffolds. Image analysis using 10 measurements per criteria showed an average strut width of 624 µm (SD ± 7.4 µm), pore width of 568 µm (SD ± 9.5 µm), and an average pore height of 578 µm (SD ± 9.4 µm), all of which are significantly (P<0.05) different from the design parameter of 600 µm.

Despite having a functional set of parameters for printing PCL at 85°C, filaments of PCL-*s*-Collagen (conjugated after extrusion) were not printable at this temperature, however, were still printable at 130°C. Analysis of the filament and printed scaffolds using ATR-FTIR (no Amide I or Amide II peaks) and Sirius Red (no red staining) showed no indication of collagen remaining in the polymer after the printing process.

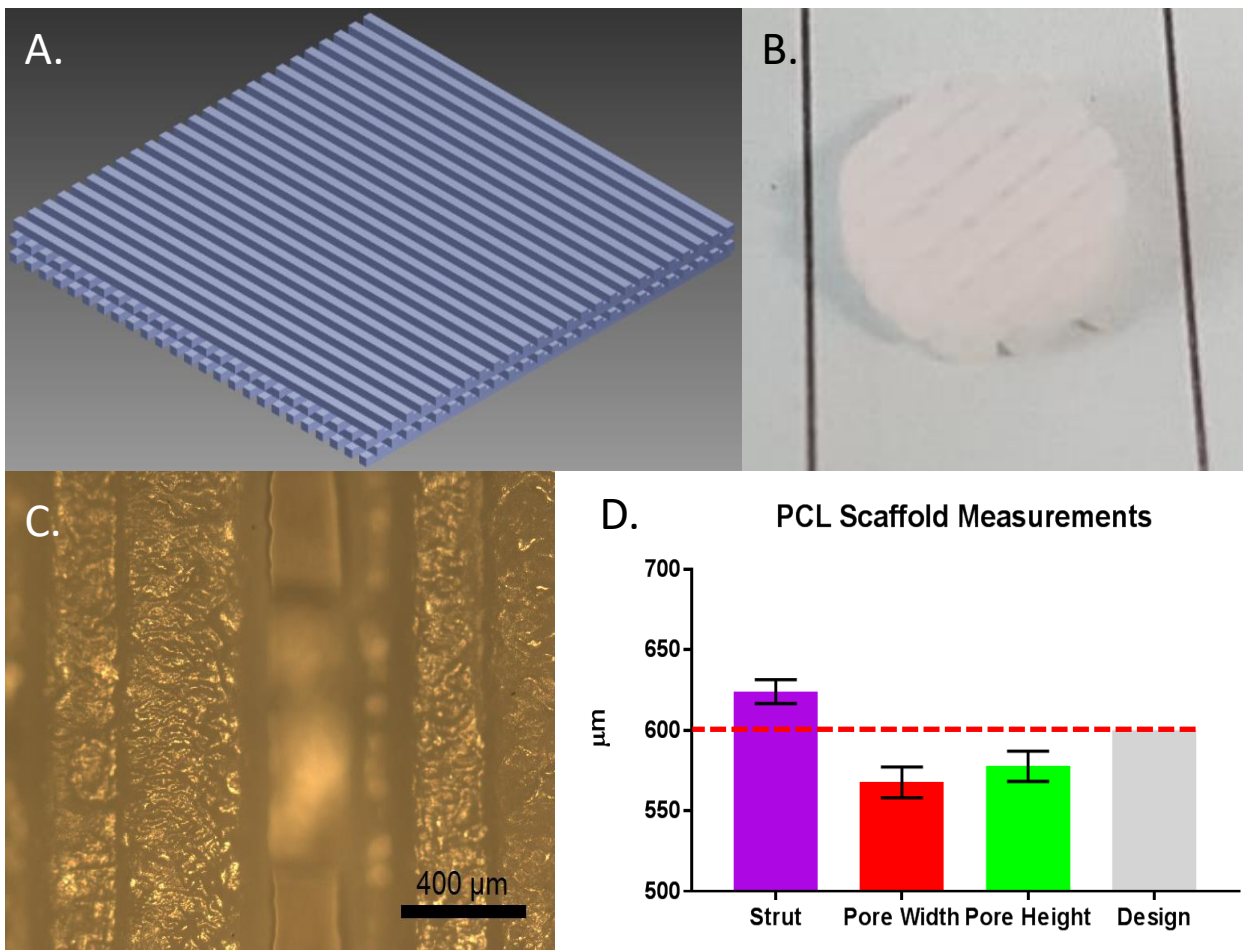


**Figure 4.8 – A.** CAD design of the 3D log pile structure used to create the scaffolds examined in the study. **B.** Laser cut 7 mm diameter scaffolds (ruled lines 10 mm apart). **C.** Brightfield imaging of PCL scaffold sample in B. **D.** Statistical analysis of the struts and pores of sample B.

#### 4.3.5 Hydrolytic Degradation Studies of PCL-Collagen films and Scaffolds

Two 12-week hydrolytic degradation studies at physiological conditions (in PBS at 37°C) were conducted on the three different PCL-Collagen materials processed by the heat moulding method described in Chapter 3, Section 3.3.1.: PCL-g-Collagen, PCL / Collagen Blend and PCL (Figure 4.9 A). In general, it was observed no significant ( $P < 0.05$ ) difference between the average % mass measured before and after incubation over 12 weeks, indicating a negligible material mass loss during this time. It should be noted that at week 12, the samples did display differences between each other in terms of % mass change, with PCL / Collagen blends appearing to lose mass while PCL-g-collagen increasing it, and PCL showing no changes.

The second study shows the hydrolytic degradation of all the different materials used at each stage of production. As previously shown, no significant difference in materials % mass changes was detected, indicating that no significant degradation over 12 weeks of incubation.

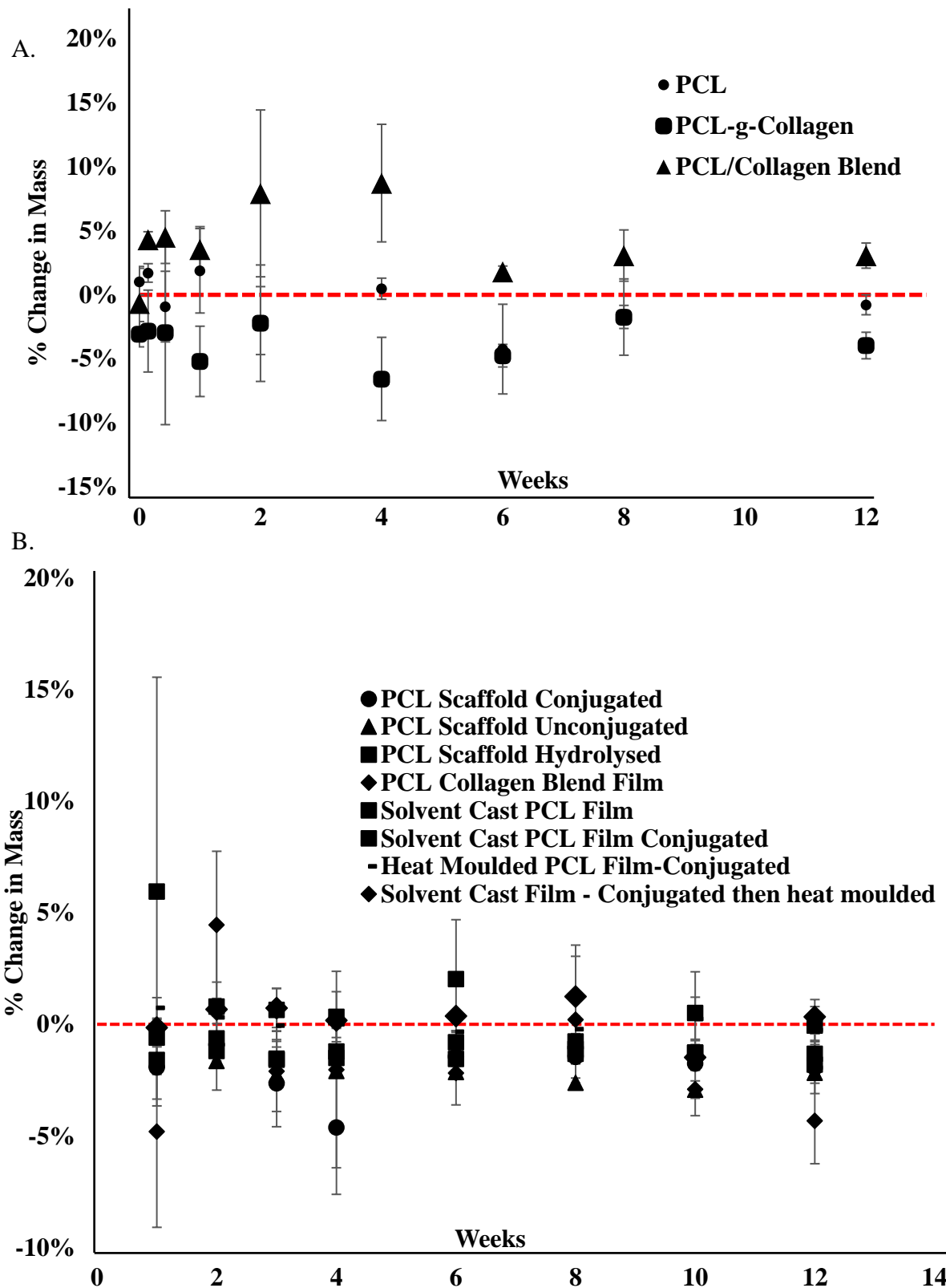


**Figure 4.9 – A.** Graph depicts the first degradation study on PCL-Collagen materials, charting % change in mass over the course of 12 weeks. **B.** The second chart shows a larger degradation study covering other end products and intermediaries involved in the PCL-Collagen material development project. Samples from both studies were found not to display any significant change in mass during the 12-week study.

## 4.3 Discussion

### 4.3.1 PCL-Collagen Synthesis and Analysis

To create 3D printed PCL-Collagen scaffolds via Fused Filament Fabrication (FFF), five routes to final product fabrication were devised; the methods are outlined below in Table 4.6.. The study aimed to compare fabrication methods, assessing efficacy by characterising the physicochemical properties of the synthesised materials, filaments, and scaffolds.

**Table 4.5** – Breakdown of the different production routes fabricating PCL scaffolds conjugated with Collagen.

Material	Method	Reference
PCL	Unmodified PCL Pellets extruded into a 1.75 mm filament. Extrude Filament into a scaffold by FFF.	Chapter 3, Section 3.3.3. and 3.3.2.
PCL-g-Collagen	Use chemical coupling to conjugate collagen in solution to solubilised PCL pellets. Pelletise material and extrude into filament. Extrude Filament into a scaffold by FFF.	Chapter 3, Section 3.2.1.1.
PCL-s-Collagen	Cast sheets of PCL. Use coupling chemistry to attach collagen to the surface of the PCL sheets. Pelletise material and extrude into filament. Extrude Filament into a scaffold by FFF.	Chapter 3, Section 3.2.1.2.
PCL / Collagen Blend	Solubilise PCL pellets, mix with Collagen solution. Cast mixed material into sheets. Pelletise material and extrude into filament. Extrude Filament into a scaffold by FFF.	Chapter 3, Section 3.2.1.3.
PCL scaffold-s- collagen	Print from pure PCL filament. Use coupling chemistry to attach collagen to the surface of the PCL scaffolds.	Chapter 3, Sections 3.3.3. and 3.2.1.2.

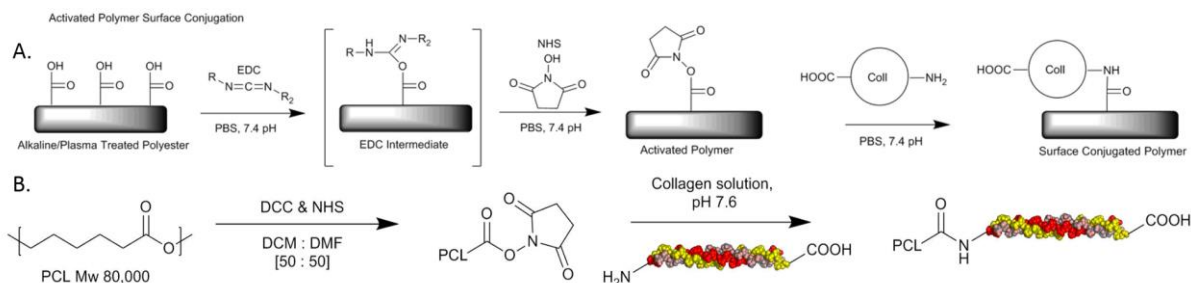


**Figure 4.10** – The two primary chemical conjugation techniques used in material synthesis. **A.** Method A is a surface chemical conjugation using aqueous phase carbodiimide coupling chemistry with EDC / NHS. This will produce samples with the “s” notation, e.g. PCL-s-collagen. **B.** Method B is the carbodiimide coupling method used to conjugate PCL and collagen in a solubilised organic phase using DCC / NHS. This process is used to synthesise PCL-g-Collagen.

Initial experiments were undertaken to optimise the yield and collagen content of PCL-g-collagen. The overarching experimental process remained structurally identical, however, the duration of time used for dialysis, solvent volume in dialysis, the quantity of PCL, and quantity of collagen used in the process were varied. Of the 7 total batches assessed, a method using 300 mg of collagen, 2g of PCL, yielding 1.6g of high-quality material was used as the template method for production for PCL-g-Collagen. This decision was based on the qualitative assessment of total collagen content with Sirius Red staining, seen in the end material. The material was observed to possess the highest quantity and most homogeneous distribution of collagen among tested samples, as observed in Figure 4.1. It is also the material observed in Table 4.2 in the solubility testing section.

Before assessment by more analytical means, factors such as process duration, cost, and consistency of product can be used to draw comparisons between the fabrication routes. While undeniably producing the PCL-Collagen material with the highest quantity of Collagen integration and a comparatively higher isotropic distribution of collagen in PCL, the PCL-g-Collagen synthetic process required significantly more resources than other the other methods examined. The PCL-g-Collagen process took approximately 10 lab days and required the use of significant quantities of harmful solvents (2.5 litres of each DCM & DMF, 200 mL pure ethanol) and 150 mL of 6 mg / mL Collagen solution to produce 1.5-3.5 grams of material. In contrast, the PCL / Collagen Blend fabrication process required 200 mL of chloroform, 200 mL pure ethanol, and 17.5 mL of 6 mg / mL collagen solution, the whole process is completed in 1.5 lab days. The PCL-s-Collagen fabrication process was even less resource-intensive, with 20 mL 3M NaOH solution, and 50mL of MES buffer with conjugation reagents being all that is required, the total process finishing in 1.5 lab days. When considering the ease and cost of

production, the surface conjugation method was superior to the full conjugation and blending methods.

#### ***4.3.2 Chemical Analysis by ATR-FTIR of Produced PCL and Collagen Materials***

The twin amide peaks, characteristic of collagen, were easily observable in all PCL-Collagen materials and were absent in pure PCL. ATR-FTIR analysis of PCL / Collagen blend films showed a high level of signal variability in each film, a result backed up by Sirius Red staining and visual observation. This variability is most likely attributed to phase separation between aqueous soluble Collagen and organic soluble PCL. Despite being stirred for over 16 hours in chloroform the two materials remained immiscible, separating primarily into distinct material micelles when dried to remove residual solvents. Upon testing with ATR-FTIR, the PCL / Collagen blend films showed mostly pure signals of either PCL or Collagen in their respective micelles, however, it was also observed through staining that trace amounts of either material could be found in the colloidal spheres of the other.

When comparing films of PCL-g-Collagen and PCL / Collagen blend there was a large discrepancy in signal strength internally within sample groups, and when comparing one sample material to another. PCL-g-Collagen was observed to have more internally consistent Amide I and II signal strengths than the PCL / Collagen Blend samples, this phenomenon is directly attributable to the phase separation observed in the PCL / Collagen Blend films contrasted with the homogeneous PCL-g-Collagen material. When selecting a material to go forward within the experimental process it was clear that PCL-g-Collagen was a better choice in terms of homogeneity. Samples of PCL-s-Collagen were also tested by ATR-FTIR and shown to have consistent levels of collagen apparent in all areas of the surface of the films. Though PCL-s-Collagen did not appear to have the same level of signal intensity as present in PCL-g-collagen, it was superior in terms of consistent collagen presence to that of PCL / Collagen Blend.

The other characteristic Collagen peaks, Amide III and pyrrolidine peaks ( $\sim 1450\text{ cm}^{-1}$  and  $1235\text{ cm}^{-1}$  respectively) are obscured in both the PCL-g-Collagen and PCL / Blend samples. It is possible to determine the ratio of structural collagen remaining in the samples vs. denatured collagen by taking a ratio of the height of amide III and the pyrrolidine peaks, however, with obfuscation from PCL signals in the spectra this is not possible.

#### ***4.3.3 Assessing the Solubility Properties of PCL-Collagen Biosynthetic Materials***

Early in the material development investigation, contemporaneous attempts were made to solubilise the PCL-Collagen materials for potential use in electrospinning / force spinning to generate scaffolds. Proving the concept was initially attempted by solubilising the material and

spin coating it onto glass samples. Initial attempts appeared to produce a thin coating on the glass discs, however, upon staining with Sirius Red, no collagen was detected in the samples. Despite the lack of red staining, the assessment of wettability properties (Section 4.3.5) showed a significant decrease in contact angle between the films of PCL and PCL-g-collagen, this would indicate that there is change in chemical composition that is not reflected by the Sirius red staining, perhaps indicating that there is no structural motif for the stain to bind to, or an extremely low level of structural collagen present in the spin coated films.

This is an interesting result to compare with the method of electrospinning PCL and Collagen, using separate solutions of PCL and Collagen in strongly fluorinated solvents, researched by Zhang et al.<sup>102</sup> in their 2005 paper characterising non-conjugated PCL-Collagen spun scaffolds, in which both PCL and Collagen were soluble in fluorinated solvents separately. In comparison, after conjugation, PCL-g-collagen has become less soluble due to chemical crosslinking between the synthetic and natural polymers. The typical analytical techniques for assessment of molecular weight, Gel Permeation Chromatography and Mass Spectrometry. These techniques require the full solubilisation of the material in either a DMF or Chloroform, depending on how the system is set up. As established in Section 4.3.1., solubilisation of the material was not completely possible with these solvents, and so it was not possible to analyse the materials in this manner to test this theory. The evidence of solid red residues remaining in the solubilisation medium, while residues non-staining polymer appear on the glass slides after spin coating indicate that two classes of material existed in the solids after synthesis: PCL and PCL-Collagen.

#### ***4.3.4 Creation of PCL and PCL-Collagen Films by Hot Moulding***

To measure the change in wettability induced by the conjugation of Collagen to PCL, and after the establishment of non-viability in solubilising the materials to produce spun films, an effort was made to develop a method of melt processing the materials into flat films that retained the structural collagen in the samples. After moulding and Sirius red staining, structural collagen was proved present in the PCL-g-Collagen samples. This indicates that after heating for 60 seconds under a 5kg load, the material was capable of the manipulation characteristic of thermoplastics, without the complete denaturing of its internal structural Collagen. The SEM images of embossed PCL-g-Collagen after moulding show a rougher and more cracked surface by comparison to the smooth surface of embossed PCL (Figure 4.6). It is possible that due to the crosslinking effects of the carbodiimide coupling, the molecular mass of the polymer has increased, altering its physical properties to a less elastic form.

If correct, this increase in molecular weight may also be responsible for the lack of solubility observed in Section 4.3.1., where solvents that PCL has been known to solvate in, are ineffectual for PCL-g-collagen.

Using this method of moulding under heat, films of different PCL-collagen (some shown in the bottom of Figure 4.6, A & B) combinations were manufactured and the hydrolytic degradation was assessed. It was observed that the mixing that occurs during melting providing a more isotropic film. This was beneficial in the case of PCL / Collagen blend as the homogenising reduced areas of Collagen concentration, which may be susceptible to rapid mass loss during the study due to collagen's hydrophilic nature. The results of the experiments in hot moulding PCL-Collagen served to give guidelines for the temperature tolerance and duration of exposure that the PCL-Collagen materials could withstand, which provided a starting point for developing the processing parameters used in Extrusion and FFF printing processes.

#### ***4.3.5 Assessment of the Wettability Characteristics of PCL and PCL-Collagen by Contact Angle***

Analysis of the surface wettability of PCL and PCL-g-Collagen films demonstrated an increase in hydrophilicity of spin coated films of PCL-g-Collagen. This is the expected observation due to the increase in the hydrophilic composition of the material with the inclusion of Collagen. The significant change in contact angle from 89.2° in unconjugated PCL to 80.0° in PCL-g-Collagen films strongly indicates a preferable surface for cellular adhesion<sup>103,104</sup> which is in line with available literature<sup>105</sup>. While a reasonable indicator of enhancing cellular adhesion, wettability is only one factor governing the process, with roughness and surface chemistry also being major determinants<sup>106</sup>.

Therefore, it is demonstrated that the incorporation of Collagen to PCL in this manner has a dual effect: 1. Enhancing the cellular adhesion potential of PCL, and 2. Retaining the beneficial properties of structural collagen even through a heat moulding process.

#### ***4.3.6 Creation of PCL and PCL-Collagen Filaments by Extrusion***

Printing custom materials by FFF requires the production of printer compatible filaments. To meet this requirement, a twin-screw extruder was used to produce a filament from polymer pellets. The pellets are fed into a barrel with two rotating screws, which push the material through four controlled heated zones, forming a homogenous pool of molten material in the die reservoir. The subsequent material being fed through the screws then pushes the molten material through a 3 mm circular die.

Upon exiting the die, the filament is pulled through a cold-water bath, solidifying the filament to a degree in which it can be placed into the Haul-off without inducing deformation of the

cylindrical shape. The Haul-Off operates by using two pinch rollers covered with rubber track to pull the filament from the extruder, through the water bath, at a set rate in meters / minute. The Haul-Off is equipped with a laser measurement tool which gives live feedback on the width of the filament being produced, allowing for the live maintenance of filament diameter through adjusting the speed of the Haul-off pinch rollers or the extruder's twin screws.

It is important to note several technical constraints that played an important role in the development of the parameters that allowed for the successful printing of filaments. Firstly, the Haul-off equipment must be run at a rate above 1m / minute; running below this rate will cause the device to display errors, initiating an emergency stop. Secondly, the twin screws of the extruder have a torque tolerance of 12 Nm, which when exceeded, initiates an emergency stop. Lastly, the discrepancy between the 3 mm circular die of the extruder and the required filament diameter of 1.75 mm, which in addition to the flow effect of molten polymer exiting the extruder, requires experimental tuning of the Haul-off and extruder settings to make a consistent filament.

By using a setting of 1.2m / minute on the Haul-off, coupled with a twin-screw speed of 70 RPM it was possible to maintain a consistent diameter of 1.75 mm ( $\pm 0.05$  mm) when producing pure PCL filament. Initial extrusion protocol settings stated a die temperature of 135°C, which while functional in filament production, led to an overly liquid state in the PCL filament, in turn creating diameter variations in the product. To mitigate this effect, the die temperature was lowered to 95°C, to allow the polymer time to resolidify after processing through the 140°C heated zones, leading to a more stable filament diameter. It should be noted that the heated zones of the extruder barrel must be kept at a consistently higher temperature than the die to maintain the speed of the extrusion. The speed of twin screws must be kept at 70 RPM to operate with the required Haul-off speed of > 1m / minute, or the filament becomes too thin in diameter. Lowering the heated zone temperatures while maintaining 70 RPM leads to a torque overload in the extruder due to the rate at which PCL pellets melt, initiating an emergency stop to production.

In Hot Moulding experiments, the structural collagen in PCL-g-Collagen was demonstrated to remain present after the pressurised heat moulding process. Attempts were made to modify the process parameters of the Extruder to replicate earlier results for filament production. This required the extrusion temperature to be as low as possible while still melting the PCL while keeping the speed as fast as possible without overloading the twin screws. Trials were conducted using both higher temperatures / extrusion speeds and lower temperatures / speeds to attempt to produce a PCL-collagen filament that retained its structural collagen. The attempts

proved unsuccessful in producing filaments containing collagen biomolecules, or of consistent diameter. It is unclear whether the absence of structural collagen molecules is a consequence of the protein degradation caused by high temperatures of the extruder or due to the duration and long-exposition to heat, or a combination of both. Using higher extrusion speeds to produce a proof-of-concept PCL-Collagen based filament without concern for consistent diameter also proved unsuccessful, despite the assumption that the total time spent in the extruder was low. This was assessed through an experiment in which dyed PCL pellets were processed through the extruder. Dyed materials were still appearing in the filament after subsequent aliquots of undyed pellets were processed, indicating the material does not pass through the extruder linearly. It was extrapolated that this effect was taking place when processing PCL-Collagen pellets, with the material spending longer in contact with the heated chambers than would be indicated by the rate of filament production. Therefore, making the processing of pre-conjugated PCL by extrusion unsuitable for further processing by 3D printing to make a biosynthetic scaffold of PCL-collagen.

These experiments in material production and process optimisation showed that it is highly challenging to produce a PCL-Collagen filament with an extruder. Attempts to produce PCL-Collagen at high and low temperatures / speeds with surface conjugated materials were unsuccessful. ~50g of material pellets are required to attempt a production run of filament. At this point in the study, between 15 and 20g of PCL-g-Collagen pellets were produced in total, with an expensive production rate of 2 to 3g of PCL-g-collagen pellets in 2 weeks and several hundred pounds in material costs. Therefore, the decision was made not to attempt to process these via extrusion given the low production rate, yield, and expensive process. As such, using a surface conjugation technique to produce PCL-Collagen at a stage after the extrusion process was deemed the more viable option for the project.

Despite the inability to process conjugated PCL-Collagen into a filament, it should be acknowledged that a high level of optimisation and repeatability in results was derived for the PCL filament. Experimentation with hopper feeding speeds, extruder zone temperatures, extrusion rates, and haul-off speeds resulted in a filament that was consistently 1.7mm diameter (+/- .05mm), which allowed for exceptionally consistent PCL prints. It should be noted that the optimisation of these protocols (in combination with the extrusion work in Chapter 5) was the result of months of experimentation, consternation, and destroyed polymers.

#### **4.3.7 Printing of PCL and PCL-Collagen Scaffolds; Optimisation and Results**

Most standard FFF printers are designed to process two polymers; PLA and ABS. Soft filaments, such as PCL, are challenging to print due to limitations of the printhead design. Metallic pinch rollers chafe soft filaments, causing material residue to embed on the pinch rollers, a build-up of which results in a reduction of traction when pulling the filament into the heated nozzle. This loss of traction can cause the filament to be fed into the heated nozzle at an inconsistent rate, which can cause gaps in the print. If gaps are large enough or occur often enough, layers do not get deposited, and when the machine adjusts to build the next layer, there is nothing to build upon and the part fails. The mechanical stress of being pushed into a heated nozzle can cause a soft filament to bend severely. Standard printheads often have small gaps between components, which soft filaments are prone to get stuck in when bent, often causing a jam in the print head and subsequent print failure.

The first experiments to print scaffolds with custom made PCL filament was attempted with a standard Flashforge Dreamer (MakerBot Replicator 2 clone). The issues detailed above became readily apparent through the frequency with which build failures occurred and through the disassembly of the printheads when investigating the problem. Considering these limitations to achieve consistent viable prints with PCL, a Flashforge Dreamer was modified with a Flexion Extruder Dual-Head (Figure 4.11). The Flexion print head possesses several design features specifically designed for printing soft filaments that are not present in standard FFF printheads.

**Self-cleaning Pinch Rollers:** A metal wire brush continually cleans the inner tracks of the pinch rollers, preventing polymer residue build-up, and avoiding filament slippage.

**Adjustable Pinch Settings:** The space between the pinch rollers is adjustable with four tightness settings, allowing for the firm grip of soft or thinner filaments. This is useful when using filaments produced by the Extruder / Haul-off as they have greater diameter variability than commercial filaments, thus, drops in diameter width will not result in the feed stopping.

**Integrated Feed System:** Two precision cut PTFE tubes create a seamless path from the filament feed port of the printhead to the heated nozzle, preventing the apparatus clogging due to flexible material being pushed into small gaps.

In addition to the Flexion print head, the printer's stock heated build plate was replaced with a smooth glass plate. The Dreamer comes with a coarse polymer covering on the build plate, which causes strong adhesion to soft polymer prints, resulting in tears and deformation when attempting to remove the print from the plate, even after extended periods of cooling.

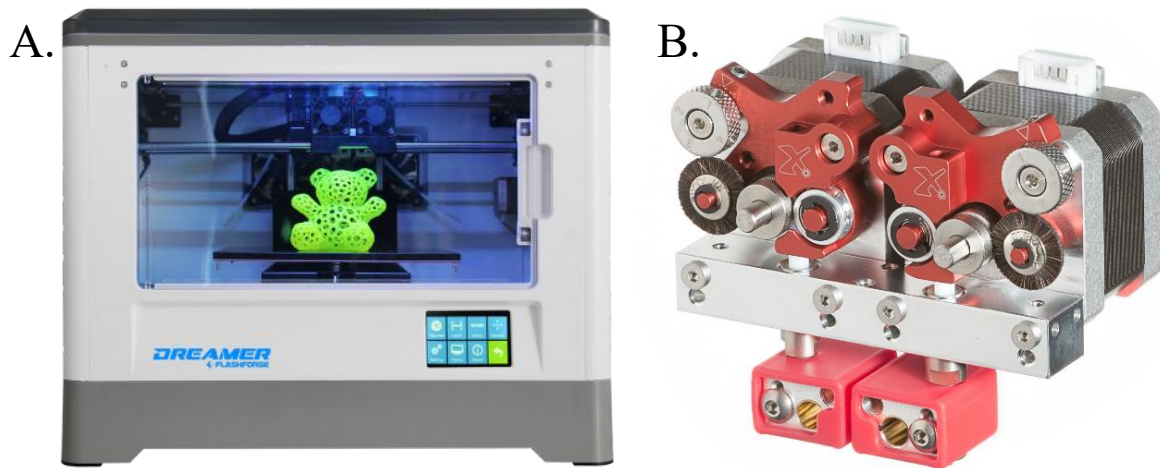


**Figure 4.11 – A.** Flashforge Dreamer, a clone of MakerBot's Replicator X2, equipped with twin printheads and a heated build plate. **B.** The Flexion extruder dual nozzle printhead used to modify the Flashforge Dreamer for the printing of soft filaments.

A set of printing parameters were derived previously within the group, optimised to work with a commercial 1.75 mm PCL filament (30-40k molecular weight) on an unmodified Flashforge Dreamer. Starting with a nozzle temperature of 140°C and a print speed of 1400 mm / minute, the process was optimised to work at a lower temperature. To print a PCL-Collagen scaffold with a pre-conjugated filament; the lowest temperature achieved was 85°C. This temperature reduction came with other constraints. Like with the filament production via Extrusion, it was observed that PCL slowly became liquid enough to process when heated. The lower the nozzle temperature, the slower the PCL softened, and the print speed had to be reduced from 1400 mm / min to 400 mm / min, greatly increasing the time in which the filament is in contact with the hot end. Experiments using extruded filament, then surface conjugated with collagen with the lower temperature processing parameters proved unsuccessful in creating consistent builds. When later analysed by ATR-FTIR, no structural collagen was observed in the product. Raising the print temperature to a higher level, accommodating the faster print speeds resulted in a successful print regarding the geometry of the part, however, there was no sign of structural collagen in the product. Using the higher temperature / speed route samples of both PCL-s-Collagen and PCL-s-Gelatin were produced, but both products stained negative for their respective bio-additives.

With the establishment of parameters that allowed for the consistent printing of PCL parts, experiments were conducted to ascertain the consistency of the printed parts. Despite having functional print parameters at 85°C, print temperatures of 115-120°C and bed temperatures of 35°C were used to produce pure PCL scaffolds as this allowed for the use of a higher print

speed. Using geometric designs influenced by literature reviews on the effect of scaffold porosity<sup>18</sup>, scaffold blocks were printed and analysed. As seen in Figure 4.8, scaffold discs were cut from these larger blocks for measurement. Despite the design of 600 µm struts and pores, when observed from above the width of the struts was consistently greater than the designed specifications and the width of the pores consistently narrower than the design. This discrepancy is attributable to material flow after deposition, which fits with the nozzle temperature being double PCL's<sup>32</sup> melting temperature. While an important observation, the difference was consistently between 3-5%, which was deemed low enough that the process parameters were not altered for future builds. Given that PCL filaments were processed by an extruder with a 3mm exit die, and made to a tight tolerance by adjusting the rate at which the haul-off pulled filament out of the extruder, these results should be seen as a strong endorsement of the consistency achieved from the optimised parameters.

These experiments helped steer the course of the rest of the study regarding the route of production for PCL-Collagen scaffolds. Despite the ability to print at a lower temperature working consistently with filaments of PCL, PCL-s-Collagen filaments displayed difficulties in attaining the same print results. When successfully printed, PCL-Collagen filaments did not retain structural collagen when tested with staining and ATR-FTIR. With the difficulties in retaining structural collagen through the FFF printing process, it was deemed more prudent to proceed with a performing conjugation on samples that had already been printed and laser cut.

#### ***4.3.8 Assessing the Decomposition of PCL and PCL-Collagen through Hydrolytic Degradation***

Assessment of the degradation properties of PCL, PCL-Collagen variants, and process relevant derivatives was carried out in two stages. The initial study examined PCL, PCL-g-collagen and PCL / Collagen Blend prepared as consistent films by the hot moulding process. The second study took a more comprehensive approach, aiming to assess the key intermediaries in each PCL-Collagen production path.

The results of the initial study showed no significant difference ( $P > 0.05$ ) in the % difference in mass displayed by PCL-g-Collagen and PCL films at different time points, with a small reduction in mass noted for PCL / Collagen blend samples. The non-significant ( $P > 0.05$ ) difference in % mass change was noted between weeks 0-8 of the study, by the end of the study, samples appeared to have differentiated, with PCL-g-collagen gaining mass, PCL remaining constant, and PCL / Collagen Blends losing mass. The results are attributed to PCL / Collagen blend samples losing collagen to the degradation medium as it was not chemically bonded. PCL-g-Collagen retaining mass due to the absorption and binding of structural water to the

internal collagen. Pure PCL samples exhibit the same properties as in literature, with no significant change in mass over 12 weeks<sup>32</sup>.

The second study compared scaffold products at the point of printing, mid conjugation after hydrolysis, and conjugated with Collagen. Also examined were non-moulded PCL / Collagen Blend films, and solvent cast PCL films (conjugated and not), to identify points at which thermal or chemical processing could introduce a change in the degradation properties of the materials. PCL / Collagen blends showed no statistical significance independently of the thermal treatment. Therefore, the surface conjugated method was selected as the functionalisation method for the remainder of the study made this investigation unnecessary, as it preserves and exposes the collagen molecules superficially for longer incubation times.

In summary, in the assessment of material degradation, no significance was garnered outside of potential considerations in the processing of PCL / Collagen blends, however, this material synthesis route was unlikely to be considered for use in the remainder of the study. The results observed are in line with those detailed in literature for the degradation of PCL<sup>32</sup>, and the study eliminated potential issues with degradation as a factor to consider with choosing the production route to PCL-Collagen scaffolds.

#### **4.4 Chapter Conclusion**

The primary aim of this section of the study was to gather the data necessary to determine the best route to production for PCL-Collagen scaffolds while characterising material properties and assessing their viability across several processing methods. Throughout the study, it became clear that it would not be possible to process pre-conjugated PCL-Collagen materials into a filament by extrusion or into a scaffold by 3D printing while maintaining the beneficial properties of structural Collagen.

In Table 4.7, below, is presented a comparison of the performance of the different materials production and analytical categories. Here it can be seen that PCL possesses strong advantages in processing and degradation but did not possess the advantageous properties of collagen. PCL-g-Collagen despite scoring highly in consistency and properties, was unable to be processed consistently in extrusion or printing. Proxy analyses were used to show the likely favourable biological properties through wettability studies, and ATR-FTIR analysis, indicating a similar amount of collagen present in PCL-s-Collagen and PCL-g-Collagen. In which case, the ease of processing with PCL and advantages of PCL-g-collagen are combined in PCL-s-collagen.

Another consideration for the choice of material was the ease of manufacture. When considering the other experimental conditions, there was little difference observed between

samples of PCL-g-Collagen and PCL-s-Collagen, steering a decision towards the material manufacturing method that was more time and material efficient. PCL-g-Collagen required a significantly higher number of days in the lab to manufacture in addition to several hundreds of pounds of toxic solvents and collagen to obtain between 1.5 – 4g of material, with an average cost of ~£70 per gram to produce in materials. A slow, inefficient, and expensive process. Comparatively, PCL-s-Collagen required one day, no organic solvents, and only a small quantity of buffer salts and conjugation reagents to produce; all of which are less toxic than those required to produce PCL-g-collagen. In addition to which, the process can be applied to PCL scaffolds after extrusion & printing, which avoids the thermal damage to collagen incurred in these processes. The context of these results combined with the similar degradation properties, difficulty in thermally processing PCL-Collagen under various conditions, and the large time / monetary expense in producing PCL-g-Collagen, drove the decision to use surface conjugation to add collagen to the PCL scaffolds.

**Table 4.7** – Summary of material performance in key processes / analyses. Key: Green = Successful experiment with viable result to carry forward, Yellow = Usable method, but with issues; Red = Poor/non-viable result or unable to run experiment due to material properties; Grey = Experiment not reported. Ranking 1-4, 1 = best result of comparable materials, 4 = worst result.

	PCL	PCL-g-Collagen	PCL-s-Collagen	PCL / Collagen Blend
Production	1 – No cost, no processing.	4 – Complex, time consuming and expensive method.	3 – Relatively simple surface conjugation, moderate/low cost.	2 – Simple mixing in chloroform, low cost.
Collagen	4 – No collagen content.	1 – Homogenous with a high collagen content. Internal distribution, bonded to PCL.	2 – Homogenous and high content on surface, bonded to PCL. No internal collagen.	3 – Variable Collagen content and material properties. No bonding to PCL leaving collagen soluble to aqueous environments.
Solubility	1 – Readily soluble in a range of standard solvents.	3 – Not soluble.	N/A – not tested. Can be applied after solubility stages.	2 – Collagen partially soluble in chloroform during synthesis, small quantities of collagen interspersed in PCL film product. Forms aqueous micelles in product due to solubility problems. Leaves inconsistent product.
Moulding	1 – Easy with low risk of product destruction.	2 – Can be heat moulded at 85°C for 60-90 seconds without losing all structural collagen content. Homogenous product.	3 – Possible without losing all structural collagen, however, it is preferable to surface conjugate after hot moulding.	4 – Can be heat moulded with loss of collagen. Less homogenous due to phase separation in synthesis stage.
Wettability	2 – Standard PCL wettability characteristics, more hydrophobic than PCL-Collagen variants.	1 – Lower contact angle, more hydrophobic than PCL. Results likely to apply to PCL-s-Collagen and PCL / Collagen Blend in a broad manner.	N/A – Not tested.	N/A – Not tested.
Extrusion	1 – Possible to manufacture consistently once process optimised.	N/A – Not tested based on PCL-s-collagen experiments showing the destruction of structural collagen during extrusion.	2 – Possible to process into a consistent filament, however, structural collagen destroyed. Recommend conjugating after processing.	N/A – Not tested.
Printing	1 – Possible over a range of parameters.	N/A – Not possible to test.	2 – Like extrusion, structural collagen destroyed during process.	N/A – Not possible to test.
Degradation	1= No significant loss.	1= No significant loss.	1= No significant loss.	2 – Possible marginal mass loss.

# Chapter 5: PCL / PHBV-Collagen Materials Development and Scaffold Production

## 5.1. Introduction

This chapter describes the process by which Scaffolds of PCL blended with PHBV and surface conjugated with collagen were developed. The chapter begins with the testing and rationale behind the selection of blend ratio used to create the scaffolds. This is followed by the physicochemical and mechanical characterisation of PCL / PHBV-Collagen scaffolds. The chapter closes with a discussion on the process of tuning the scaffold fabrication. The process by which the scaffolds were created is shown below in Figure 5.1.

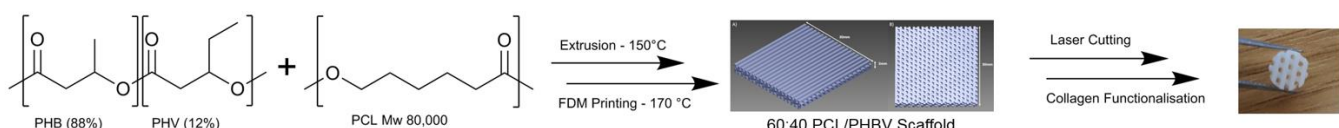


**Figure 5.1 – PCL / PHBV-Collagen scaffolds fabrication process.** Polymer pellets get blended by the extruder, which produces a printable filament from the mix. After printing, the material is laser cut to requirement before being conjugated with Collagen via surface functionalisation chemistry.

## 5.2. PCL / PHBV blend at different ratios: blend selection analysis

To determine a ratio of PCL to PHBV for use in the scaffolds, analyses were performed on films of melted PCL and PHBV polymer pellets, with an average thickness of 1.25 mm.

### 5.2.1. Contact Angle

The contact angle Figure 5.2. A for blend ratios (PCL:PHBV, w:w) was measured as: 100:0, 70.8° (SD ± 4.2°), 80:20 67.3° (SD ± 5.8°), 60:40 68.3° (SD ± 2.6°), 40:60 67.5° (SD ± 2.3°), 20:80 68.6° (SD ± 3.2°), 0:100 66.8° (SD ± 1.5°). Statistical analysis of the samples ( $P > 0.05$ ) found there to be no significant difference in the contact angle readings between blend samples.

### 5.2.2. Tensile Strength

The tensile strength Figure 5.3. B of blend ratios (PCL / PHBV w / w) was measured as: 100/0, 11.9 MPa (SD ± 1.6 MPa), 80/20 11.5 MPa (SD ± 0.7 MPa), 60/40 12.2 MPa (SD ± 2.0 MPa), 40/60 1.6 MPa (SD ± 1.2 MPa), 20/80 1.3 MPa (SD ± 0.4 MPa), 0/100 1.1 (SD ± 0.3 MPa). Statistical analysis shows there is a significantly higher ( $P > 0.05$ ) tensile strength in samples with a majority PCL content over those with a majority PHBV content. Within sample groups with a majority PCL or PHBV content in the blend ratio, there is no significant difference ( $P < 0.05$ ) in the tensile strength between samples.

### **5.2.3. Tensile Modulus**

The tensile modulus Figure 5.4. C for blend ratios (PCL / PHBV w / w) was measured as: 100/0, 70.5 MPa ( $SD \pm 15.5$  MPa), 80/20 102.1 MPa ( $SD \pm 6.4$  MPa), 60/40 183.7 MPa ( $SD \pm 34.2$  MPa), 40/60 199.8 MPa ( $SD \pm 11.6$  MPa), 20/80 229.9 MPa ( $SD \pm 5.2$  MPa), 0/100 249.3 ( $SD \pm 24.6$  MPa). Statistical analysis shows that samples of 100/0 PCL / PHBV had a significantly lower ( $P > 0.05$ ) modulus than samples containing any % content of PHBV.

### **5.2.4. ATR-FTIR Characterisation of PCL / PHBV Blends**

Figure 5.3. shows the FTIR characterisation of the PCL / PHBV blends at different w / w ratios. Characteristic alkyl -C-H twin shoulder peaks of PHBV are observed in samples at  $2974\text{ cm}^{-1}$  and  $2935\text{ cm}^{-1}$ , a split caused by the PHB and PHV co-units. The characteristic single alkyl -C-H peak of PCL is observed at  $2945\text{ cm}^{-1}$ . The peaks vary intensity in proportion to the quantity of PCL and PHBV in the blends.

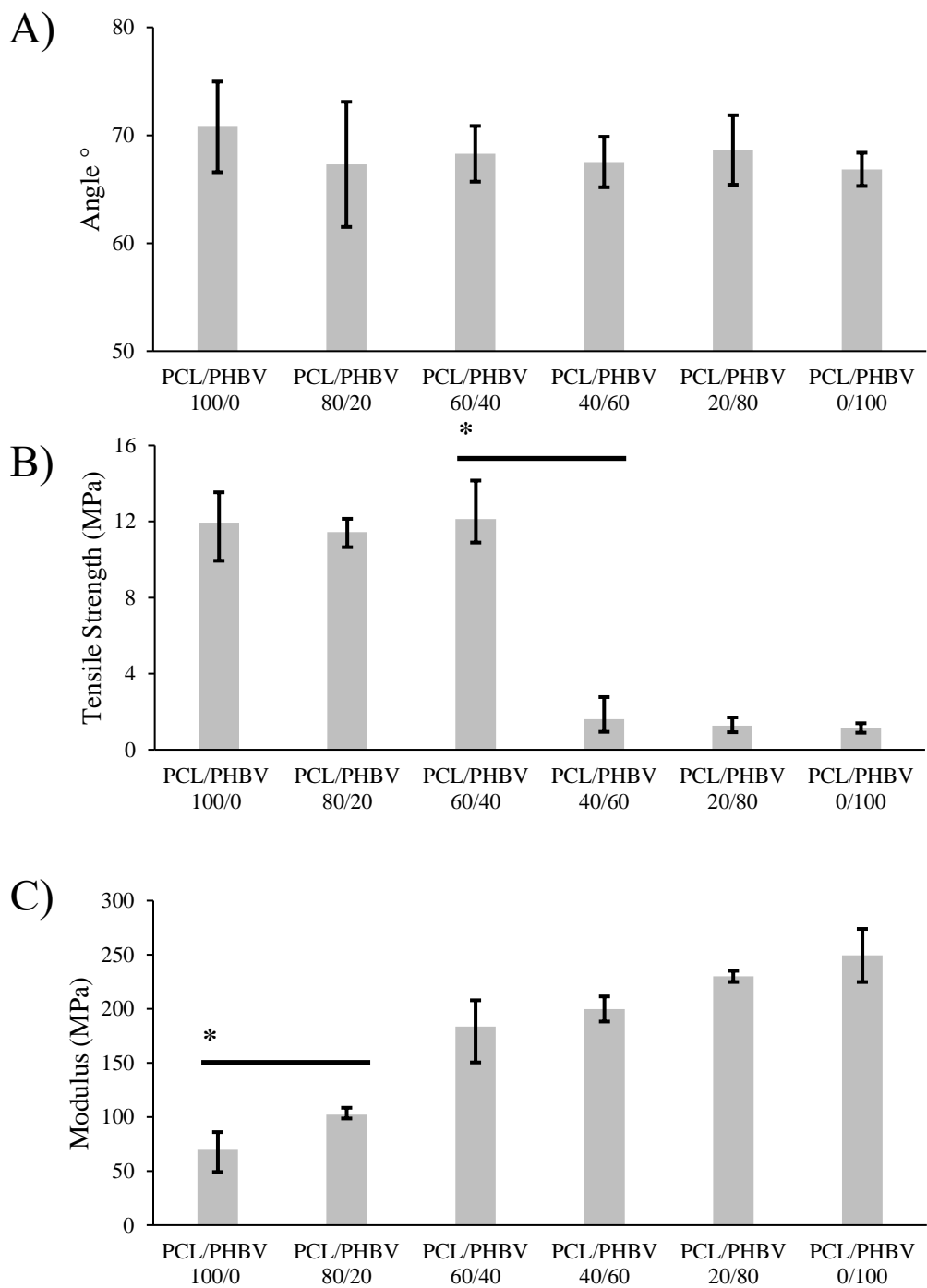


**Figure 5.2 – A.** Wettability of PCL / PHBV samples measured with contact angle. **B.** Tensile strength measurement of films of PCL / PHBV at different ratios. **C.** Tensile modulus measurement of PCL / PHBV blend ratios. This data was gathered by Yunuo Lin and Kegan McColgan-Bannon.

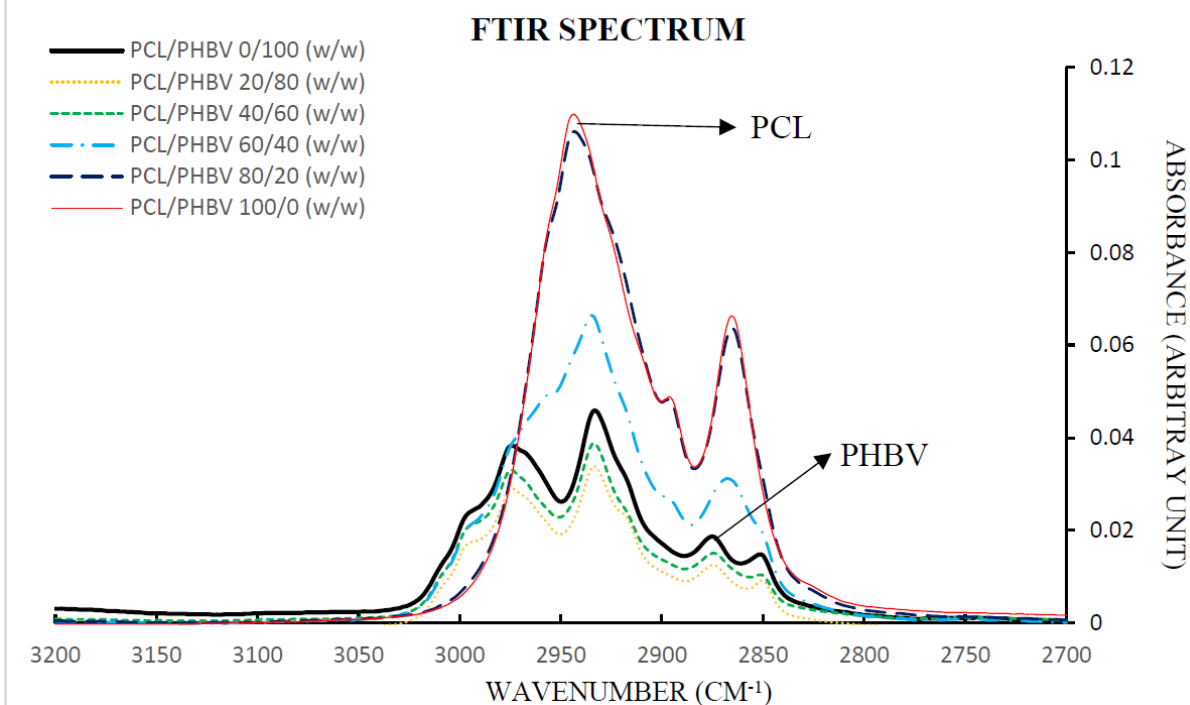


**Figure 5.3** – ATR-FTIR analysis of blend ratios allow the distinguishing of blend ratios from the ratio of peaks in the 2800–3050 cm<sup>-1</sup> range. This data was gathered by Yunuo Lin and Kegan McColgan-Bannon.

### 5.3. PCL / PHBV and PCL / PHBV-Collagen films: physical-chemical properties

#### 5.3.1. Contact Angle

Based on previous results, the blend ratio of PCL:PHBV 60:40 was selected as the base material for use in scaffolds and will hereby be referred to as PCL / PHBV. For initial testing, films of PCL / PHBV were heat moulded as described in Chapter 3, Section 3.3.1. and conjugated with collagen. The contact angle Figure 5.3 for these films was measured as: PCL / PHBV 72.7° (SD ± 7.9°), PCL / PHBV-Collagen 37.9° (SD ± 9.9°). Statistical analysis shows that there is a significant reduction ( $P < 0.05$ ) in contact angle to the PCL / PHBV blend upon collagen conjugation.

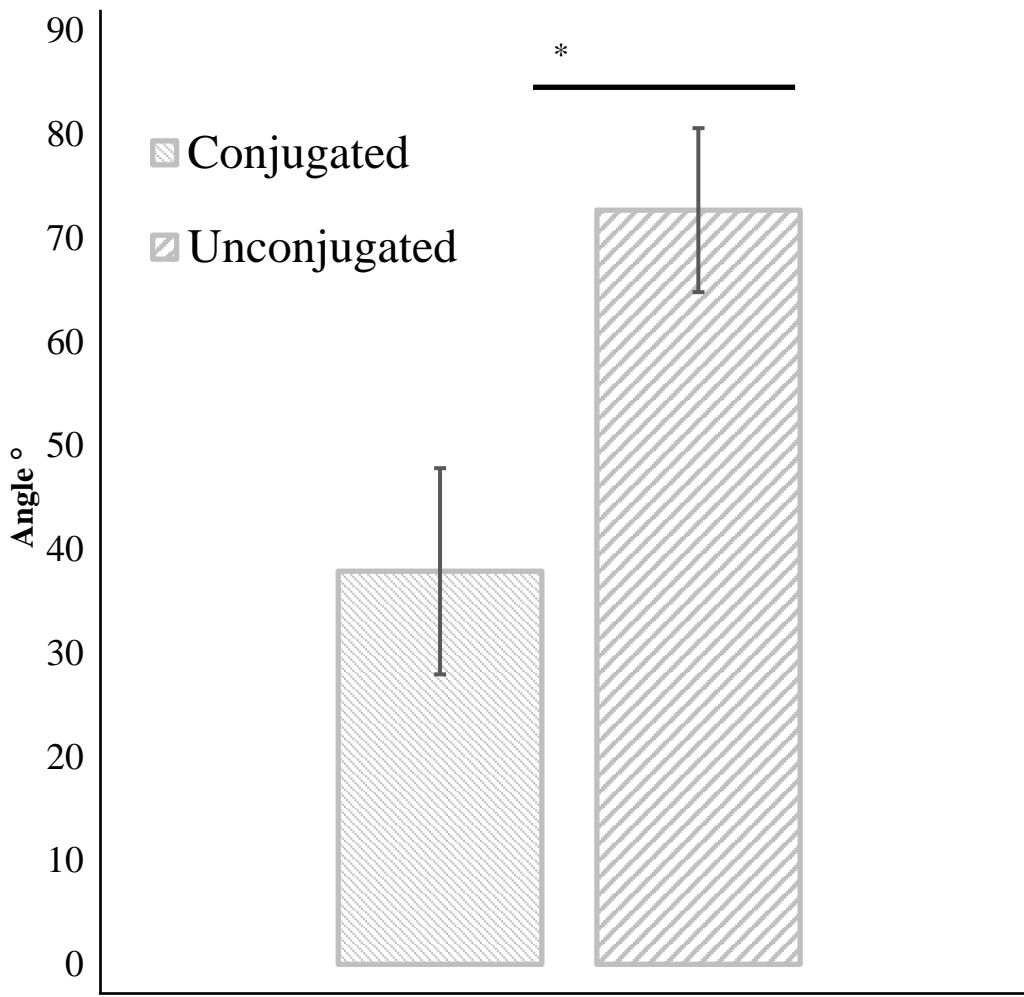


**Figure 5.4** – Measured contact angle for films of PCL / PHBV conjugated with collagen and unconjugated. The bar left represents the conjugated films with a value of  $37.9^\circ$  ( $SD \pm 9.9^\circ$ ). On the right is the measurement for unconjugated films with a value of  $72.7^\circ$  ( $SD \pm 7.9^\circ$ ). A significant reduction ( $P < 0.05$ , \*) in the angle was observed when films were conjugated.

### 5.3.2. ATR-FTIR chemical analysis

ATR-FTIR analysis of PCL / PHBV and PCL / PHBV-Collagen films are shown in Figure 5.5. The characteristic collagen Amide I peaks at  $1658\text{ cm}^{-1}$  and Amide II peaks at  $1544\text{ cm}^{-1}$  are observed in PCL / PHBV-Collagen films, while PCL / PHBV films (shown below in comparison) did not display these. A large -OH & -NH stretching band at  $3400\text{ cm}^{-1}$  was observed in PCL / PHBV-Collagen samples but not in PCL / PHBV samples.

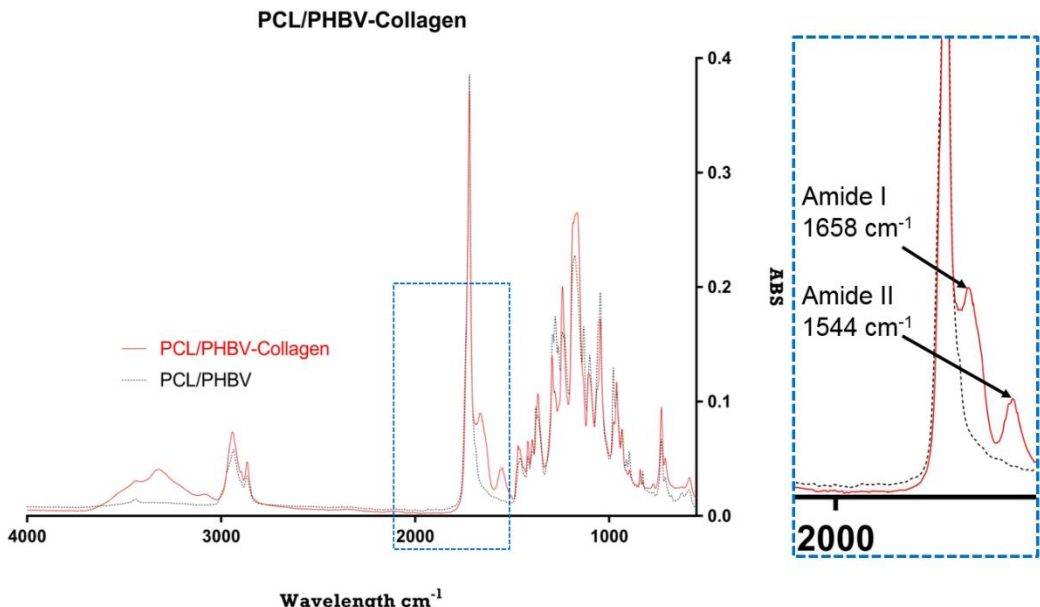


**Figure 5.5 – ATR-FTIR analysis of conjugated and unconjugated PCL / PHBV films. The presence of collagen was identified in conjugated samples by the presence of the characteristic Amide I & II peaks.**

#### 5.4. Manufacturing of PCL / PHBV and PCL / PHBV-Collagen scaffolds by FFF printing

##### 5.4.1. Filament Extrusion

With the use of a laser measurement tool integrated into the Haul-Off, a filament of diameter 1.7 mm ( $\pm 0.1$  mm) was successfully produced. It should be noted that the filament produced was cyclically variable in diameter. This effect made it difficult to harvest longer sections of PCL / PHBV filament with a consistent diameter, leading to lower production rate than that of the pure PCL filaments from Chapter 4. The result was the production of shorter usable sections of filament, which impacted the ability to print larger scaffold blocks. The most effective temperature inputs are shown in Table 5.6..

##### 5.4.2. FFF Printing

Dimensions of 30 x 30 x 3 mm blocks of interconnected porous scaffolds (Figure 5.6) were printed using the conditions shown in Table 5.6., with the purpose of creating smaller scaffold discs from the main block for mechanical and biological testing. From the printed blocks, scaffold discs were cut with a laser cutting tool. The surface morphology of conjugated and unconjugated scaffolds was examined by SEM (Figure 5.6.) taking measurements using ImagJ. The observed strut width averaged 0.68 mm (SD  $\pm 0.06$  mm), with a range of 0.63-0.71 mm. Pore width was an average of 0.90 mm (SD  $\pm 0.03$  mm), with a range of 0.85-0.99 mm.

**Table 5.6 – Optimised extrusion temperature protocol and FFF parameters.**

<b>Extrusion</b>	Zone 1 - 100°C	Zone 2 - 150°C	Zone 3 - 150°C	Zone 4 - 145°C	Die - 135°C
<b>Printing</b>	Nozzle - 170°C	Build Plate - 40°C		Print Speed 1200 mm / minute	

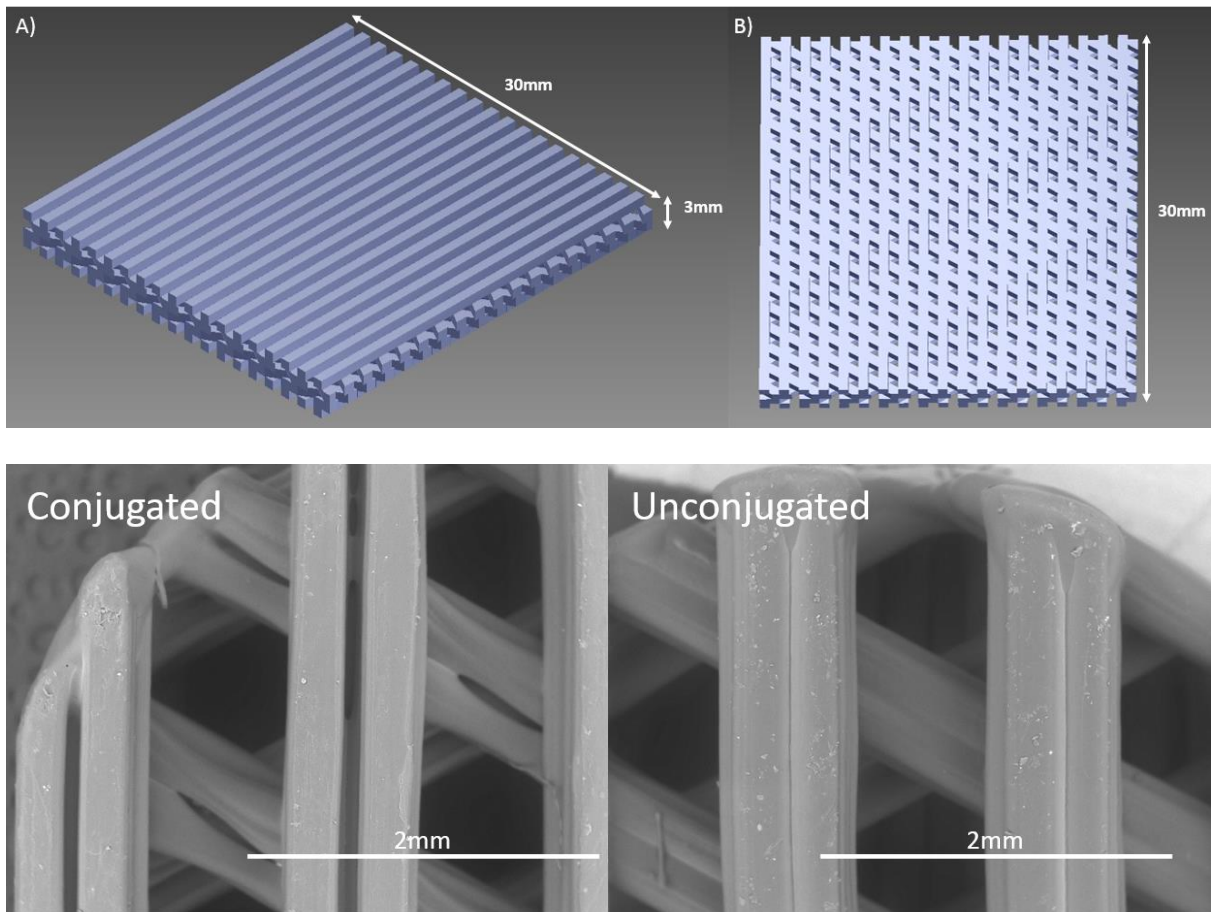


**Figure 5.6** – Top. Original CAD designs for the scaffold geometry, showing the 30 x 30 x 3 mm porous blocks. Bottom. SEM images of conjugated and unconjugated PCL/PHBV scaffolds.

#### 5.4.3. Compressive Modulus

Figure 5.7. shows the measured values for the compressive modulus which were taken from the linear elastic region of the stress / strain curve. The relative moduli of scaffolds were measured as: PCL 0.89 MPa (SD  $\pm$  0.11 MPa), PCL / PHBV 0.89 MPa (SD  $\pm$  0.06 MPa), PCL / PHBV-Collagen 0.84 MPa (SD  $\pm$  0.30 MPa), PCL / PHBV (Hydrolysed) 0.86 MPa (SD  $\pm$  0.21). Statistical analysis shows that there is no significant difference in the compressive modulus of samples.

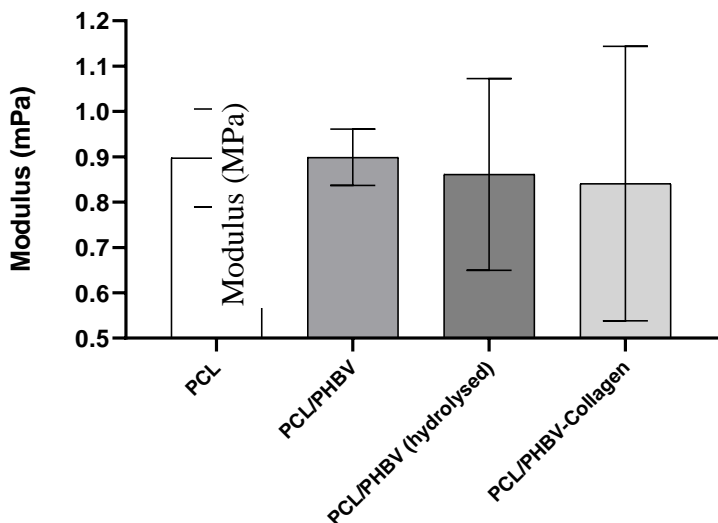


**Figure 5.7** – The relative compressive modulus of printed scaffolds of PCL, PCL / PHBV, PCL / PHBV (hydrolysed), and PCL / PHBV-Collagen.

#### 5.4.5. Degradation Studies

A hydrolytic degradation study Figure 5.8 of PCL / PHBV scaffolds was carried out over the course of 12 weeks. The samples examined were PCL / PHBV, PCL / PHBV-Collagen and PCL / PHBV (hydrolysed), to show the effect of chemical processing on degradation rate, post printing. Statistical analysis of the results showed that the average change in mass by % was not significant over the course of the study.

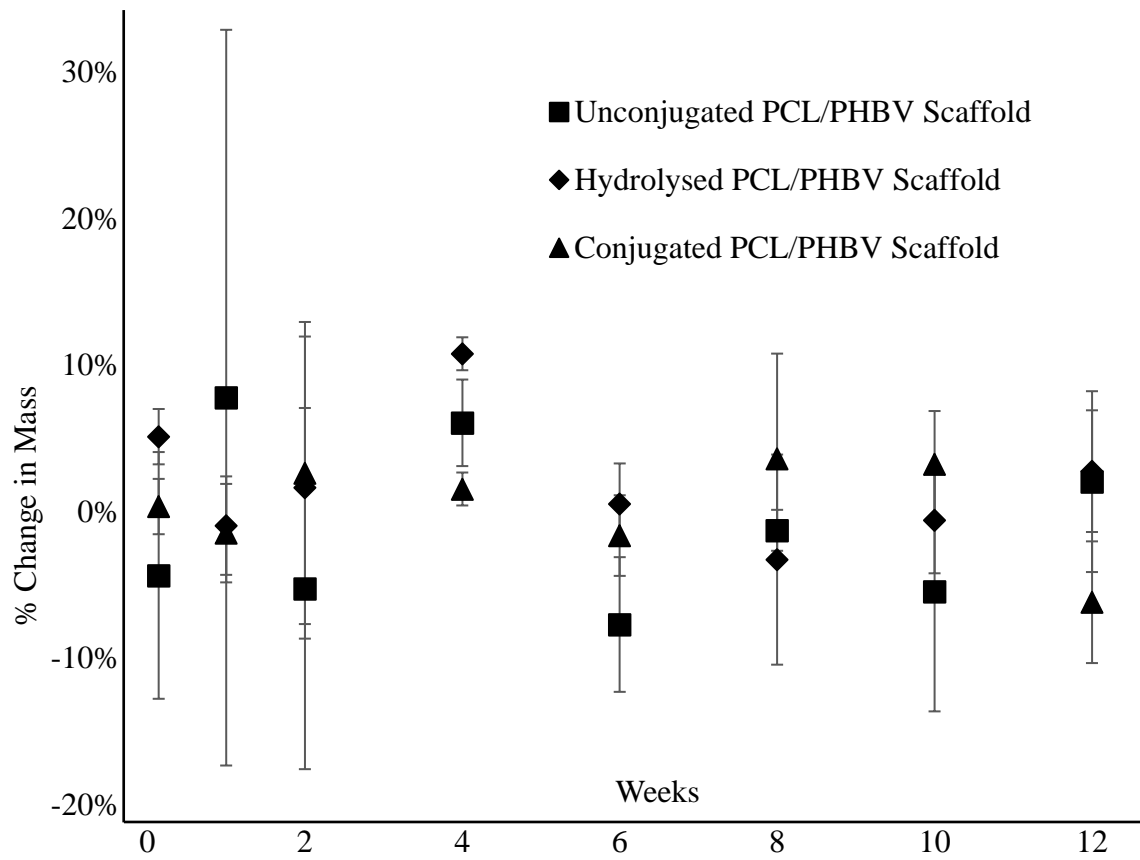


**Figure 5.8 – Hydrolytic degradation study of PCL/ PHBV scaffolds.**

### 5.5. Discussion

#### 5.5.1. PCL / PHBV Material Analysis

During the investigation of the PCL-Collagen material scaffolds, a branching study was initiated into the efficacy of creating scaffolds from blended PCL / PHBV polymer. This study details the manufacture and characterisation of FFF printed scaffolds made from PCL and PHBV blended at a ratio of 60 / 40 w / w and conjugated with collagen.

There was no significant difference between the contact angles of the different blend ratios, including between pure PCL and pure PHBV. Given that wettability is used as a proxy for potential to have enhanced cellular adhesion properties, these results indicate that the ratio of polymer content in the base material before conjugation would not play a role in the cellular adhesion properties of the final scaffold.

The tensile strength measurement of the blend films showed a stark divide in the results. Blends with a majority of PHBV content (PCL / PHBV: 0 / 100, 20 / 80, 40 / 60) exhibited much weaker tensile properties in the region of 1-2 mPa, whereas majority PCL blends exhibited values in the 10-12 mPa range, results which are consistent with the literature values for PCL<sup>32</sup>.

Given that a degree of flexibility and mimicry of mechanical properties was a pre-requisite goal

in the development of scaffolds for osteochondral regeneration, a majority PCL ratio was more favourable in mechanical properties. Modelled tensile strength values for articular cartilage fall into the range of 0.8-25 MPa according to Little et al.<sup>107</sup>, into which both blend ratios fall comfortably. Though both majority polymer blends fit the profile for tensile strength, the majority PHBV blends lie at the extremity of the range, whereas PCL majority blends are in the centre of the range.

When characterising the tensile modulus of the polymer blends, a more gradual trend in properties between the materials was observed, with a growth in modulus MPa from pure PCL at 70 MPa ( $\pm 15.5$  MPa) to pure PHBV at 250 MPa ( $\pm 24.6$  MPa). The increase in modulus exhibited by blends with a higher PHBV content, coupled with the tensile properties of the PCL majority blends, suggested that the optimal blend would be a PCL majority with a higher content of PHBV, and thus the blend ratio of PCL / PHBV 60 / 40 was decided on, as PCL dominant blends have a tensile strength closer to the centre of the range for articular cartilage. From this point will only be referred to as PCL / PHBV.

It should be noted that the changing ratios had a different pattern when contrasting tensile strength and modulus. The tensile strength properties aligned closely with the properties of the majority polymer, exhibiting a significantly higher value when a majority PCL was used. This would indicate that to achieve a better degree of flexibility, a majority PCL blend should be used. Whereas, the modulus appeared to increase more steadily with the addition of PHBV. It would be interesting to examine this relationship in more detail.

The materials were additionally characterised by ATR-FTIR, with characteristic alkyl -C-H peaks, the signal intensity of which corresponded to the weight ratio of the polymers in the blend, as seen in Figure 5.3.

### **5.5.1. PCL / PHBV-Collagen Discussion**

Drawing on the results of the contemporaneous PCL-Collagen study (Chapter 4, Section 4.4), the most effective route of integrating collagen into the scaffolds was via surface conjugation, and as such was used as the only conjugation method for this study.

### **5.5.2. Wettability**

The change in wettability between conjugated and non-conjugated materials was assessed through measuring the contact angle of the material films. A significant reduction in contact angle was observed in PCL / PHBV films upon collagen conjugation, indicating that the integration of collagen on the material surface produces an environment more conducive to

cellular adhesion and growth, as described in this study by Dowling et al.<sup>106</sup>. These results are congruent with those observed in the PCL-Collagen study.

#### **5.5.3. ATR-FTIR**

ATR-FTIR analysis was used to assess the success of Collagen integration to PCL / PHBV. Figure 5.5 shows the absorbance signal of conjugated and non-conjugated PCL / PHBV films. The overlay shows the characteristic amide I & II peaks of collagen at 1658 cm<sup>-1</sup> and 1544 cm<sup>-1</sup>, only present in the conjugated samples, in addition to a large increase in -OH and -NH stretching bands around 3400 cm<sup>-1</sup>, indicating the conjugation was successful.

#### **5.5.4. Extrusion**

As PHBV has different mechanical and physical properties to PCL, notably a higher melting point of 150 - 170°C<sup>108</sup>, the previous parameters for PCL extrusion were not fit for use and more optimisation was required. It was found that despite a quoted melting point of 150°C and above, the polymer pellets melted at extruder temperatures of 150°C, however, using a die temperature of lower than 135°C resulted in a filament with unmelted lumps that would break easily upon placement in the Haul-Off. It should be noted that when using heated zone temperatures of >150°C, the filament became too liquid to process, which is likely due to the blend being primarily PCL, which has a melting point of 60°C. Literature on the processing of PCL / PHBV blends by extrusion and FFF, have limited extrusion temperatures to 150°C<sup>109</sup>.

It should be noted that the creation of a blended PCL / PHBV filament was considerably more challenging than that of pure PCL. Though the polymers appeared miscible in the filament as it left the extruder die, upon applying a pulling force from the Haul-off, the filament would elongate in cycles. This resulted in filaments that would oscillate between too thick and too thin, >2.5 mm at largest and <0.5 mm at thinnest, with diameters outside of 1.5-1.8 mm unusable in FFF 3D printers. It should be noted that the oscillation effect in filament diameter would appear worse at the beginning of the extrusion process, reducing in severity as the extrusion went on, but only if consistent speeds were maintained. If the extruder speed increased or decreased sharply, the filament diameter would start to vary more heavily. This is possibly due to the increased tensile modulus brought on by the increasing % mass of PHBV, as seen in Figure 5.2 C, or due to a differential in the rate of melting between PCL and PHBV in the extruder.

There was no technical solution or optimisation that completely mitigated this effect, despite experimenting with a range of extruder speeds and temperatures (constrained to heats of ≤150°C). The result was a process whereby the extruder was operated at a consistent rate and

gradually tweaked until the filaments fell within a usable range. This method allowed the production of sections of usable filament typically shorter than 1 meter in length, which dictated the total size of builds possible with this material in addition to creating a significant quantity of waste. Considering PHBV pellets were c. £7500 / kg, this was a costly process to implement. Perhaps if PHBV were more abundant, the process could have been further optimised, however, as materials could not be reused once thermally processed, the filament with diameters closest to 1.7 mm were selected and proceed to printing. I suspect the observed effect was due to the difference in melting point between PCL and PHBV, large, unmelted pellets moving at a different rate through the extruder and causing heterogeneous flow in the melt pool of the die. Though it was possible to harvest enough usable filament to conduct experiments, the variability in the filament width was greater than that of regular PCL, resulting in downstream variance in the PCL/PHBV scaffolds.

**Table 5.8** – Printing protocols used for the best quality prints of other custom materials.

Material	Nozzle Temperature (°C)	Bed Temperature	Print Speed (mm / minute)
PCL-Gelatin	130	30	1000
PCL-Collagen	130	30	1000
PCL / PHBV 50:50	170	40	1400-2000
PCL / PHBV 60:40	170	40	1400-2000

### 5.5.5. FFF Printing of Scaffolds

Like with extrusion process, the physical properties of PHBV were significantly different to that of PCL, and the printing process was optimised to reflect this. To compensate for the higher melting point of the PHBV content in the blend filament, the nozzle temperature was adjusted to 170°C, at which point the material flowed in a semi-liquid state that did not cause blockages. The bed temperature was also adjusted to 40°C, as scaffolds of PCL / PHBV would unadhered themselves from the build plate at 35°C. A lower printing speed of 1200 mm / minute was also necessitated, as higher speeds would cause nozzle blockage, which is likely due to the higher modulus of PHBV.

When examined in SEM, PCL / PHBV scaffolds exhibited greater visual variance than their PCL counterparts. Whereas PCL scaffolds appeared to possess one singular strut, a product of the post printing material flow, PCL / PHBV scaffolds appeared to form two distinct struts in following with the tooling path. I suspect two factors contribute to this observation: First, a lower level of material flow due to the harder, higher melting point, PHBV material content. Second, greater variance in filament width produced can lead to less material flowing through the nozzle at points.

### **5.5.6. Compression Testing**

The relative compressive modulus of PCL, PCL / PHBV, PCL / PHBV-hydrolysed, and PCL / PHBV-Collagen were examined to determine if the addition of PHBV, and chemical processing stages have any effect on the compressive modulus of scaffolds. Statistical analysis between samples indicates that there was no significant difference ( $p > 0.05$ ), however, it should be noted that the effect of hydrolysis, and collagen conjugation both appeared to introduce greater variance within sample groups. The results indicated that there was little evidence of detrimental effect to the compressive modulus through blending, hydrolysing or collagen integration. The conjugation and hydrolysed scaffolds were of particular interest in this area as the materials were subjected to hydrolysis with 3 M sodium hydroxide solution to enhance the surface chemistry for the carbodiimide conjugation process. Though not directly analogous in terms of the absolute blend ratios examined, a study by Kosorn et al.<sup>109</sup> on PCL / PHBV blend scaffolds measured the compressive strength of scaffolds at different blend ratios: PCL / PHBV, 100 / 0, 75 / 25, 50 / 50, and 25 / 75. 0 / 100 was not measured. The study shows blend ratios gain in compressive strength with the addition of higher ratios of PHBV, with a large increase in MPa when moving from a 50 / 50 to a 25 / 75 ratio. For the experiment detailed in this thesis ratios of 100 / 0 and 60 / 40 were used, which when considering a majority PCL content, are most closely comparable to Kosorn's blends of 100 / 0 and 75 / 25. Where Kosorn shows a difference in the absolute compressive strength values between the two blend ratios, this study does not. This could be due to the additional processing step employed by Kosorn, using a rotary ball mill to mix the two polymer pellets prior to extrusion, more effectively mixing the two materials. It has been observed in literature that loading with bioceramics in composite scaffolds of PHBV has been observed to increase the stiffness of the material with progressively higher loading<sup>110,111</sup>. Studies conducted by Beck et al.<sup>112</sup> noted that the expected compressive modulus range of human articular cartilage was 0.25-1 MPa, indicating the compressive modulus of the scaffolds was appropriate for the application.

### **5.5.7. Hydrolytic Degradation**

Analysis of the mean change in mass at timepoints throughout the study indicated there was little significant deviation from the original weight. It should be noted that at week 4 in the study, there appeared to be a significant increase in the mass, however, there was an uncharacteristically low variance in the samples measured at this timepoint, which was not observed at any other timepoint. When comparing the different sample groups at individual time points, no significant change in mass was observed at any time point beside week 4, which again I attribute to uncharacteristically small standard deviations.

### **5.5.8. Summary**

This study set out to assess the viability of blending PHBV with PCL to enhance the mechanical and biological properties of the material and study the materials suitability to be processed into 3D scaffolds for further tissue growth. In this work, PCL and PHBV polymer pellets were successfully blended at different ratios and further processed into 3D porous scaffolds by FFF. The studies determined that the integration of PHBV to PCL was unlikely to perform worse than pure PCL scaffolds in terms of mechanical properties or potential for biocompatibility. The compressive and tensile strength of PCL / PHBV 60 / 40 appeared to be unchanged from that of pure PCL, however, the tensile modulus appeared to be stronger in the PCL / PHBV 60 / 40 blend compared to blends with a higher PCL content. Wettability of the unconjugated materials did not appear to change between blend ratios, however, there was a significant % reduction of contact angle when collagen was integrated to PCL / PHBV. No observable changes were detected for the degradation properties of PCL / PHBV scaffolds, there was no stability introduced by the chemical process of collagen conjugation or from the introduction of PHBV to PCL. The main difference between PCL and PCL / PHBV scaffolds was in the ease and rate of manufacture, in which PCL filaments and scaffolds were more consistently produced. In addition, the introduction of PHBV incurred significant costs to the material production.

## **Chapter 6: Biological Performance of 3D Printed PCL and PCL / PHBV Scaffolds Functionalised with Collagen**

### ***6.1. Introduction***

This chapter describes the results of biological tests performed on 3D printed logpile scaffolds of PCL and PCL / PHBV conjugated with collagen. Cytocompatibility is assessed by LIVE / DEAD assays, cell morphology and actin deposition are assessed by DAPI and Phalloidin staining, and cell metabolism is assessed by Presto Blue. The results of these assays are described and followed by a comparative discussion.

### ***6.2. 3D printed porous PCL-scaffolds functionalised with Collagen***

#### ***6.2.1. Cell viability by LIVE / DEAD assay***

The first experiment on scaffolds, using TC28a2 chondrocyte cells, allowed for the collection of data at Day 5 & 8 of the study for the LIVE / DEAD assay (Figure 6.1). After 5 days of scaffolds incubation, most of the cells appeared dead (as stained red) on both conjugated and unconjugated (control) samples. However, at day 8, it is possible to observe the presence of small clusters of living cells (stained in green) on both scaffold samples, although the evidence of many dead cells. On day 5 on the glass sample, and day 8 on the scaffold samples, it was observed that the chondrocyte morphology appeared rounded.

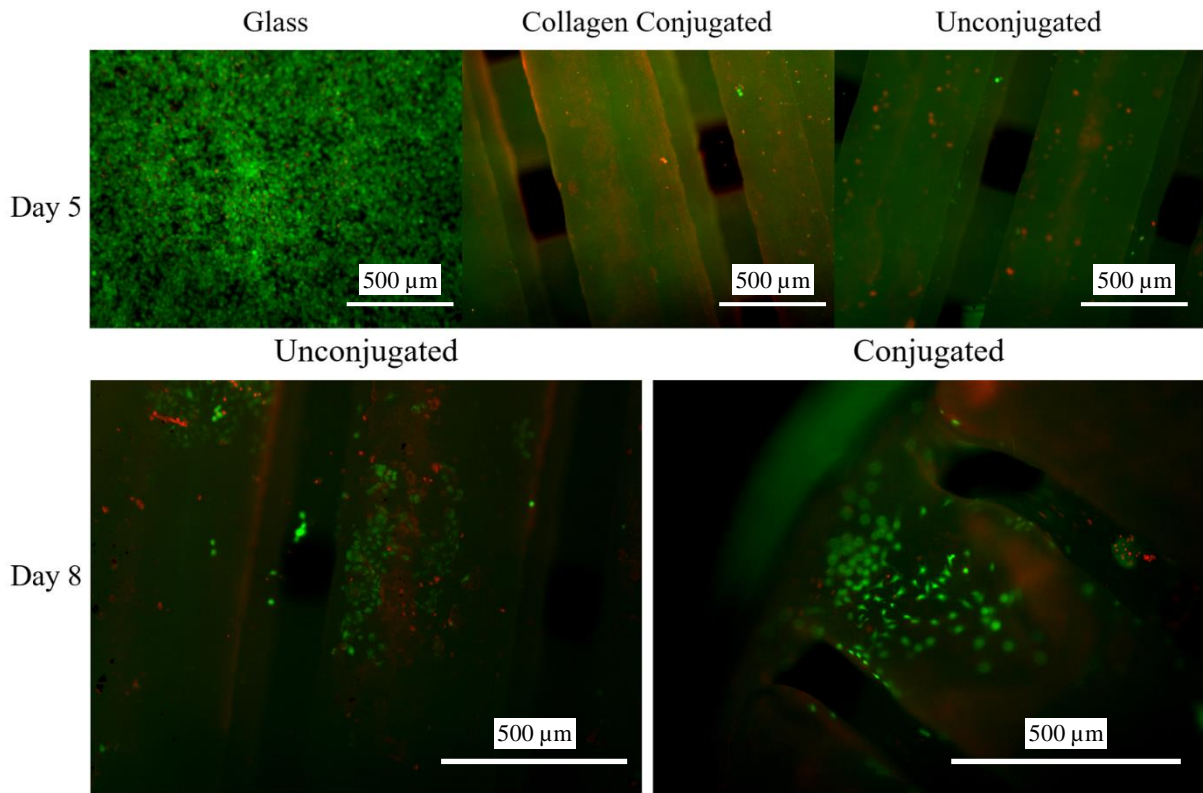


**Figure 6.1** – Images from the LIVE / DEAD assay performed on samples at day 5 and 8 of the first PCL-Collagen cell experiment.

A second assay, aiming to repeat the conditions of the first, with PCL-Collagen scaffolds was prepared to reattempt gathering results for the scaffolds. Figure 6.2 shows the LIVE / DEAD assay results of the experiment at Day 1. It can be observed that on PCL scaffolds conjugated with collagen, small clusters of live cells have adhered, while there is little evidence of dead cells. The unconjugated samples had no evidence of hosting live cells but had many dead cells evident.

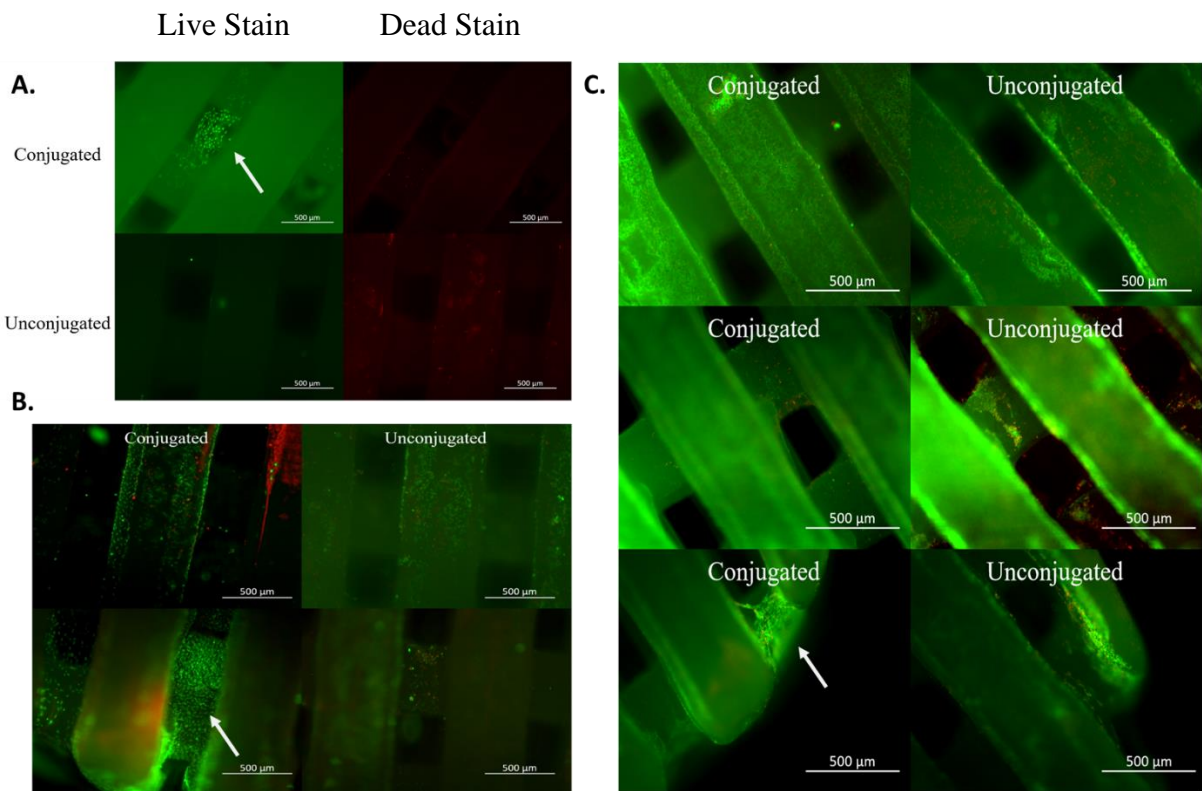


**Figure 6.2 – A.** LIVE / DEAD assay performed on PCL-Collagen scaffolds on Day 1, **B.** at Day 7, and **C.** at Day 14 of the second biological experiment. The column on the left (green) shows the presence of live cells. The column on the right (red) shows dead cells.

Figure 6.2 B shows samples imaged on Day 7 of the experiment with strong cell growth on both conjugated and unconjugated scaffolds, with a denser clustering of cells visible on the conjugated scaffolds. Figure 6.2 C shows images of scaffolds after a LIVE / DEAD assay on Day 14 of the study. While both scaffolds possessed dense levels of living cells, the unconjugated scaffolds displayed more dead cells. At the edges of the scaffold, the chondrocytes can be observed to be suspended between the printed struts of the scaffold, supported in a 3D structure between struts, indicating the production of an extracellular matrix, which was not observed on the scaffolds imaged at earlier time points. It was also observed on these scaffolds that the morphology of the chondrocytes was circular, non-fibroblastic.

### 6.3. 3D printed PCL films functionalised with Collagen

Filaments of PCL were printed into 30 x 30 x 2.4 mm dense cuboidal structures, from which 9 mm discs were laser cut. The samples were seeded with 20,000 Neo-NHDF fibroblasts and analysed over 7 days, assessing viability through cytotoxicity and metabolic activity. The morphological study samples were, likewise, performed on printed discs, but during a different experiment, and as such were seeded with Tc28a2 chondrocytes. The cell line was changed

with the intention of assessing scaffolds for compatibility with cartilage forming cells, to move towards assessing the proposed use of the scaffolds in osteochondral environments.

#### **6.3.1. Neo-NHDF fibroblasts viability by LIVE / DEAD assay**

Figure 6.3 shows the results of a LIVE / DEAD assay used on the seeded samples at Day 1 & 3 of the study. Comparison of conjugated and unconjugated samples at Day 1 and 3 both show significantly higher levels of live cells on conjugated samples, in addition, there were lower indications of dead cells (red staining) on the conjugated samples. It can also be observed that cells seeded onto conjugated samples exhibit a more fibroblastic morphology than those seeded on unconjugated samples on Day 1 and 3.

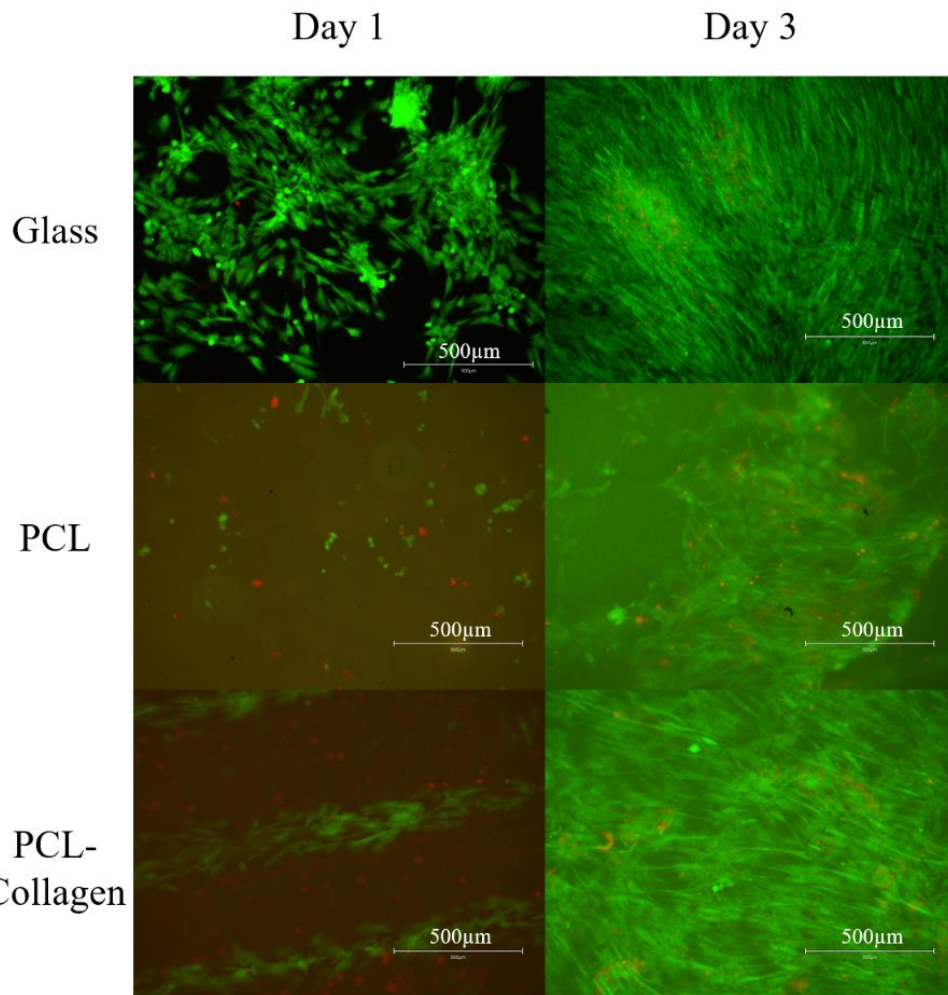


**Figure 6.3** – Figure displays cytotoxicity and cell viability analysis, and cell morphology of Neo-NHDF cells cultured 3D printed PCL discs with and without collagen conjugation, and with a glass control. Magnification 10x.

#### **6.3.2. Neo-NHDF fibroblasts Metabolic Activity**

Figure 6.4 displays the results of the Presto Blue metabolic activity assay measured in fluorescence. On Day 1 the metabolic activity output of conjugated samples was significantly higher ( $P < 0.05$ ) than the unconjugated or control samples. On day 3, conjugated PCL samples

registered significantly higher ( $P < 0.05$ ) metabolic activity than unconjugated samples but not significantly higher ( $P > 0.05$ ) than the glass control samples. On day 7, there was no significant difference ( $P > 0.05$ ) in activity measured between conjugated and unconjugated samples, however, the glass control sample registered significantly higher ( $P > 0.05$ ) metabolic activity than other samples.

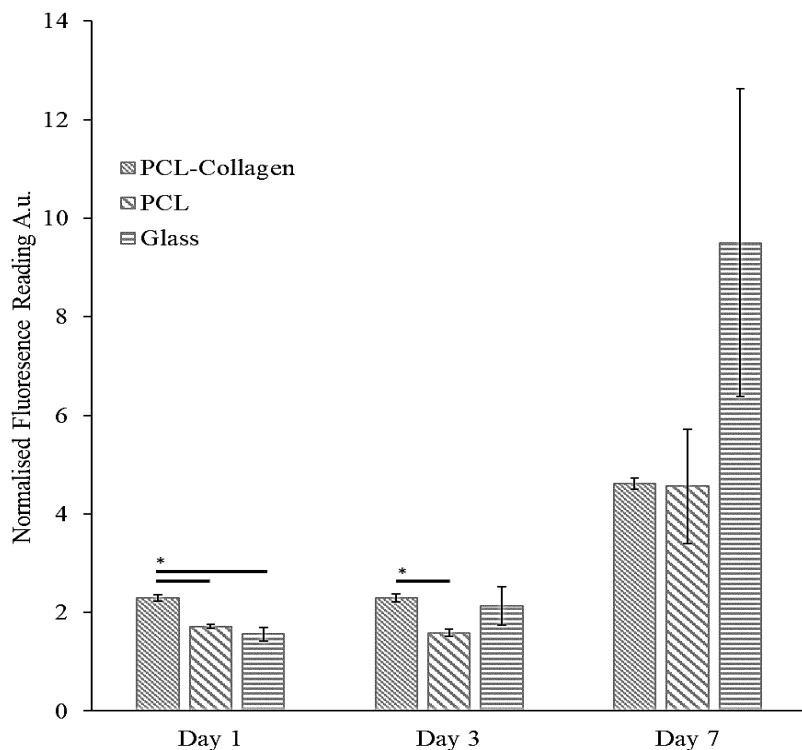


**Figure 6.4** – The relative fluorescent output of metabolised Presto Blue reagent, this is representative of cellular metabolic activity on scaffolds of PCL, PCL-Collagen, and Glass control samples (\* =  $P < 0.05$ ).

### 6.3.3. Cell Morphology of Tc28a2 chondrocytes

Figure 6.5 shows a compressed z-stack image taken of DAPI / Vinculin treated cells on 9 mm laser cut discs of PCL and PCL-Collagen. On Day 1 of growth, strong actin deposition can be observed on both sample types. Days 3 and 7 show a higher density of cell growth, however, little difference in cell morphology or density can be observed between the sample types.

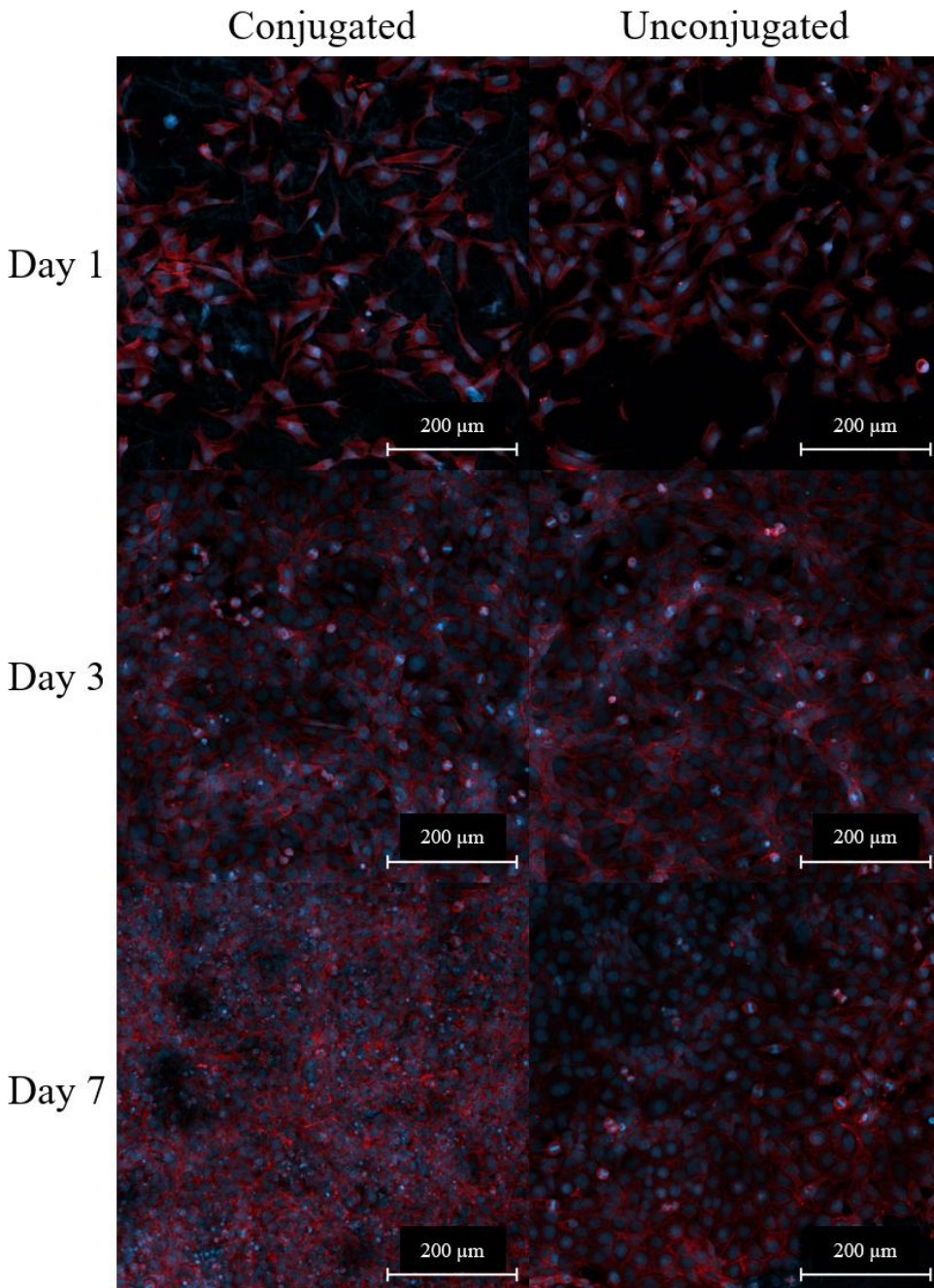


**Figure 6.5** – Confocal microscope images showing the morphology of TC28a2 cells seeded on PCL and PCL-Collagen scaffolds on Days 1, 3, and 7 (red- phalloidin, and blue – DAPI, 10x magnification).

#### 6.4. 3D printed PCL / PHBV-scaffolds functionalised with Collagen

##### 6.4.1. TC28a2 chondrocytes viability by LIVE / DEAD assay

Figure 6.6 shows images taken after a LIVE / DEAD assay was performed on PCL / PHBV and PCL / PHBV-Collagen scaffolds at Day 1 in the study. As can be seen from the images, the cells formed dense clusters within the scaffold pores and are growing sparsely on top of the scaffolds. There is little discernible difference in the ratio of Live to Dead cells between the two samples.

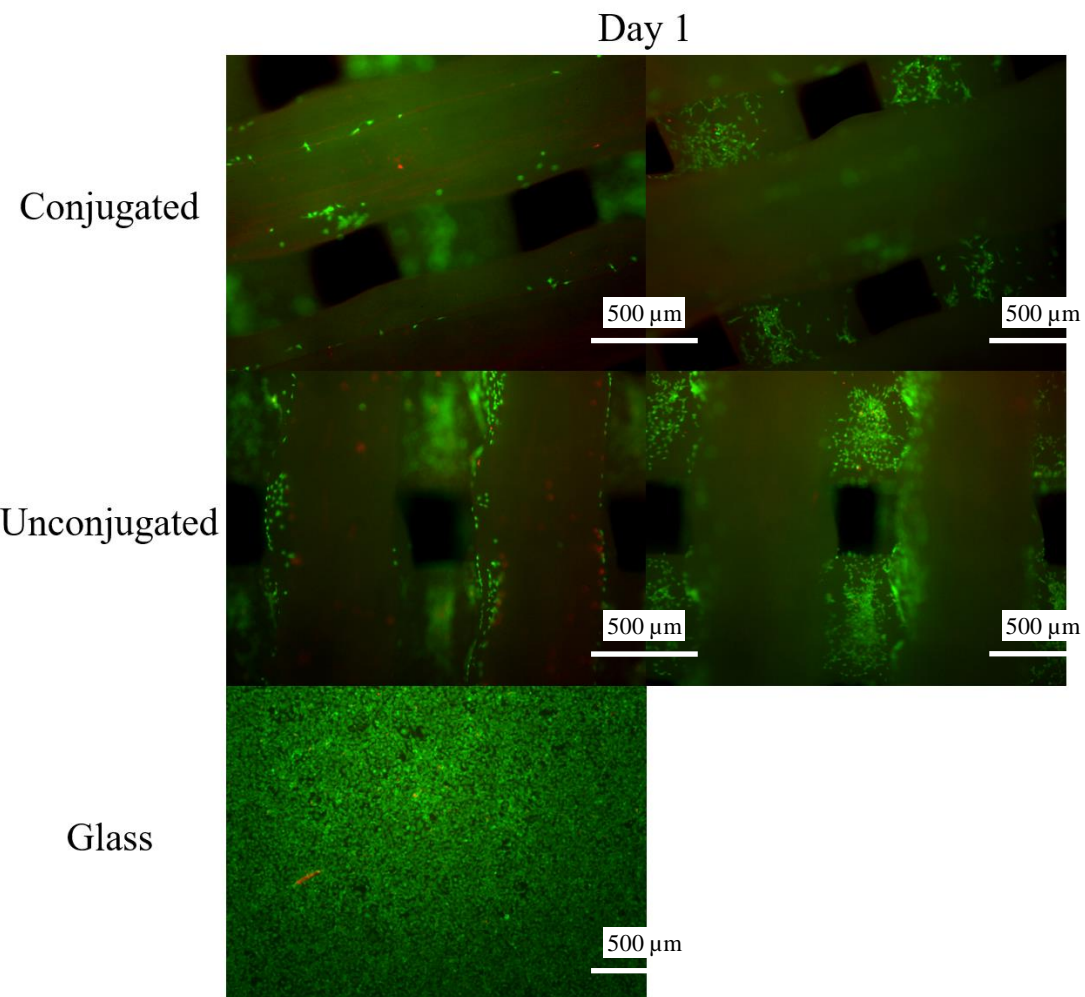


**Figure 6.6 –**LIVE / DEAD Staining of PCL / PHBV and PCL / PHBV-Collagen scaffolds seeded with Tc28a2 chondrocytes on day 1 of the study.

#### **6.4.2. TC28a2 chondrocytes Metabolic Activity by presto blue assay**

Figure 6.7 shows the data gathered from a Presto Blue metabolic activity assay on PCL / PHBV-Collagen and PCL / PHBV scaffold samples.

In day 1, it was observed that conjugated scaffolds showed significantly lower metabolic activity than glass control samples, but not significantly different from unconjugated samples. Unconjugated samples did not show a significant difference in metabolic activity to other samples. Comparison to a calibration curve showed samples were displaying levels of metabolic activity expected of 30,000-35,000 cells. Then, at day 3, there is a trend to increase cellular measured metabolic activity across all samples, however, differences are not statistical significance between samples. Similarly, on day 7, there is a trend to increase the overall metabolic activity across all samples. Control samples registered significantly higher activity than unconjugated scaffolds. While conjugated scaffolds did not show significant differences in metabolic readings when compared to unconjugated or control samples.

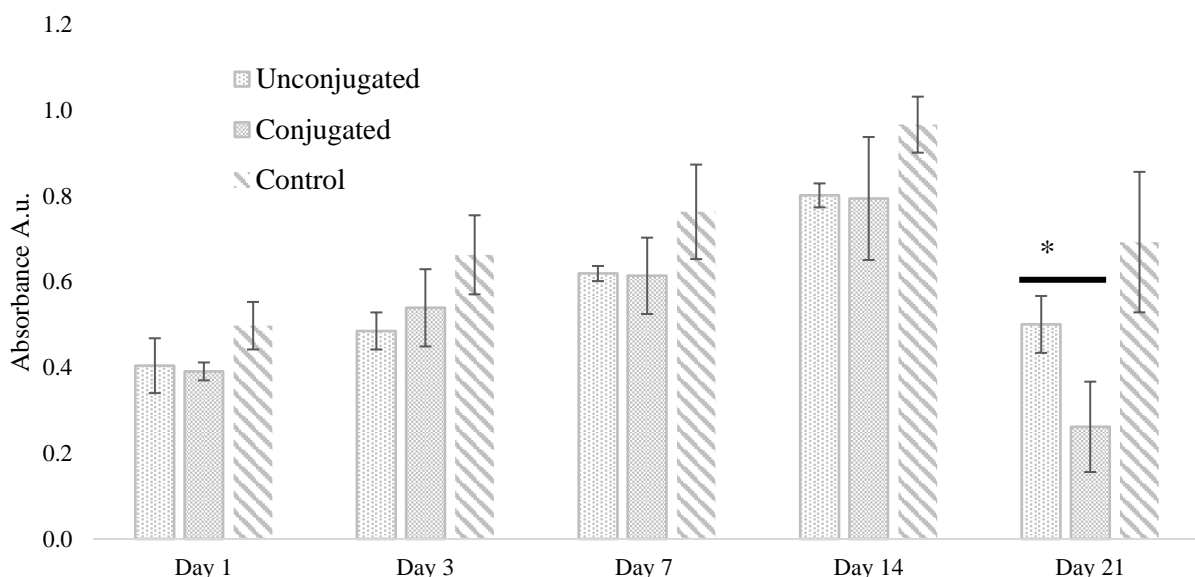


**Figure 6.7** – Graphed data from Presto Blue metabolic assays performed on PCL / PHBV-Collagen scaffolds, PCL / PHBV scaffolds, and Glass control samples seeded with Tc28a2 chondrocytes. Samples were read in absorbance 570/ 600nm.

Another rise in overall metabolic activity across all samples was observed at day 14. Control samples registered significantly higher activity than unconjugated scaffolds. Conjugated scaffolds were not found to have significantly different metabolic readings than unconjugated or control samples. Then, at day 21, samples exhibited a decrease in metabolic activity across all samples. Conjugated samples displayed a significantly lower metabolic activity output than unconjugated or control samples.

#### 6.4.3. Cell Morphology of Tc28a2 chondrocytes onto 3D printed Discs

Figure 6.8 shows a compressed z-stack image of Tc28a2 chondrocytes grown on printed 9 mm discs of PCL / PHBV and PCL / PHBV collagen, after staining with DAPI and Phalloidin. On Day 1 of the study, cells seeded on PCL / PHBV-Collagen samples displayed a higher degree of actin deposition than their counterparts on the unconjugated samples. At this time point, there is no significant difference in the cell density on each sample. On Day 3, the images show a clear difference in both the number of cells growing and the quantity of actin deposition by the cells, PCL / PHBV-Collagen having a significantly higher number of cells present on the surface and with a higher level of visible actin. Images taken on Day 7 of the study display a similar situation to the samples on Day 3, where the PCL / PHBV-Collagen samples have a far greater quantity of cells present than that on PCL / PHBV samples, in addition to a higher level of actin staining.

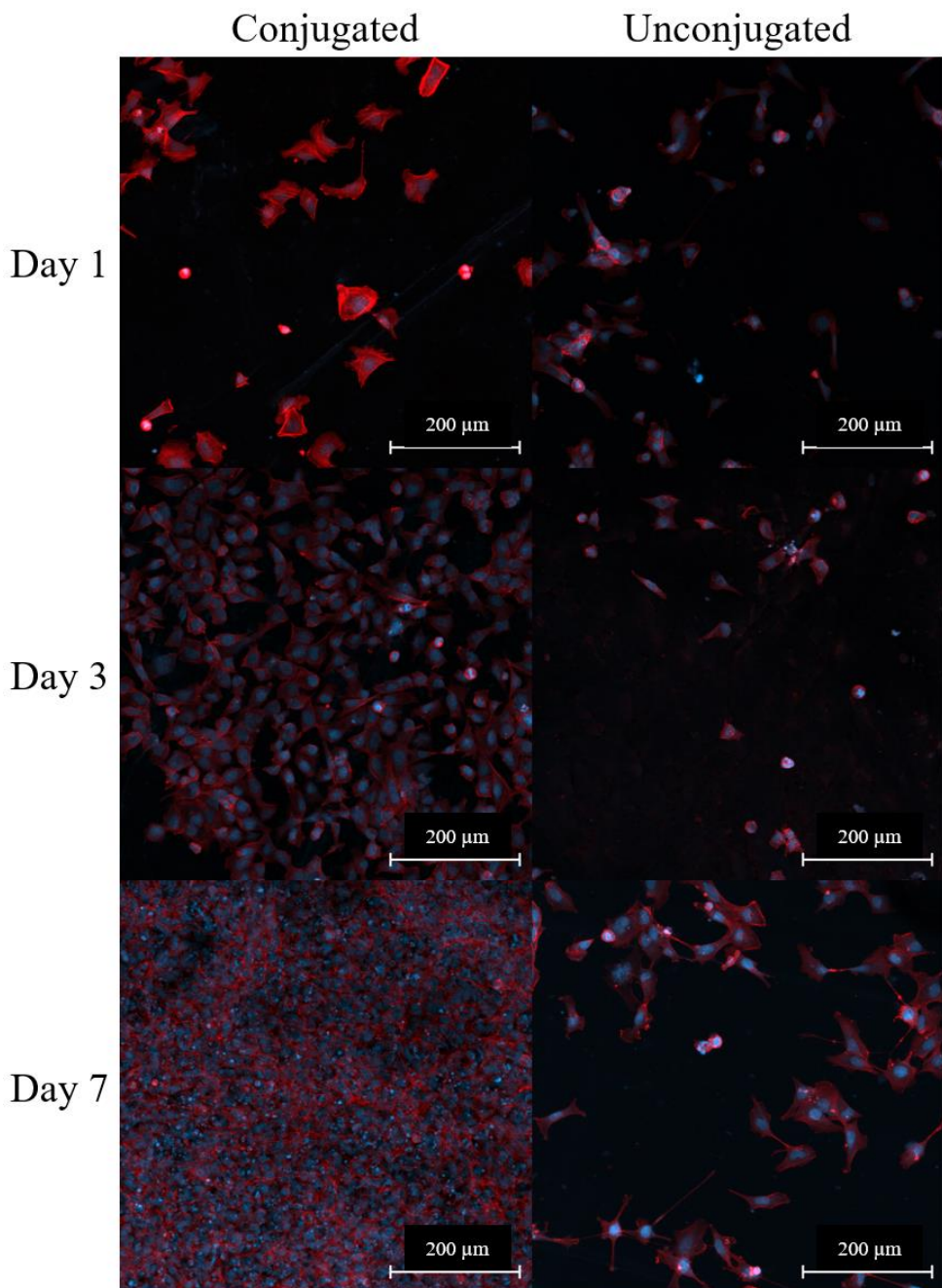


**Figure 6.8** – Confocal microscope images showing the morphology of TC28a2 cells seeded on PCL / PHBV-Collagen and PCL / PHBV scaffolds on Days 1, 3, and 7 (red- phalloidin, and blue – DAPI, 10x magnification).

## 6.5. Discussion

### 6.5.1. 3D printed porous PCL-scaffolds functionalised with Collagen

After the development and analysis of different methods of producing PCL-Collagen scaffolds, it was decided to proceed with using surface conjugation chemistry on printed PCL scaffolds, which will hereby be referred to as PCL-Collagen. The next stage of testing after the initial assessment of physical and mechanical testing was biological studies. These studies were designed to assess the viability of the conjugated scaffolds, using LIVE / DEAD, Presto Blue, and cytoskeleton / nucleus staining assays. With the aim of assessing suitability in the

production of a cartilage regenerating scaffold device, the scaffolds were seeded with TC28a2 chondrocytes.

Initial experiments on PCL-Collagen scaffolds did not allow for the adherence of the original study plan of 1, 3 and 7-day assessments, due to the availability of characterisation equipment. The LIVE / DEAD assay was instead performed on days 5 and 8 of the study, which was further into the growth cycle, meaning initial adherence, proliferation and movement was not captured. The staining on days 5 showed little difference between the conjugated and unconjugated samples, a result not concordant with other studies that captured growth and viability around the same time point, such as in Figure 6.2 B representing disparity at day 7. The day 5 results showed a predominance of dead cells on PCL and PCL-collagen scaffolds, but not on the glass coverslip, a result which was not replicated in other variations of these experiments at various timepoints, as shown in Figures 6.2, 6.3, and 6.6 for printed samples and Figure 7.8 for conjugated fibre scaffolds. The somewhat ambiguous result was replicated on day 8 of the study, where little difference in total growth was observed between conjugated and unconjugated samples, however, it should be noted that a smaller ratio of dead cells was observed on the conjugated samples. It should be noted that samples created from a 100% PCL polymer base displayed a degree of auto-fluorescence when examined after LIVE/DEAD staining. The extent of the visual interference was not so great that useful information and deductions could not be made from the images, however, when observing the images in the previous section, it should be considered that all areas of green fluorescence may not necessarily be due to a high-density growth of cells but from the material itself. Areas of dense cell growth can be determined by granularity in the fluorescence and a higher intensity of green output, rather than a smooth appearance with less green intensity.

The experiment was replicated under the same parameters with a new set of conjugated and unconjugated PCL scaffolds. This time, initial seeding was captured on day 1, showing a clear distinction between the quantities of both live and dead cells imaged on the samples. Stained conjugated samples showed larger numbers of live cells, with fewer dead, and the opposite was observed on the unconjugated samples. This is in concordance with literature observations<sup>73-75</sup> and with the results noted in the PHBV fibre study in Chapter 7.

On day 7 of the second study, cellular proliferation could be observed on both scaffolds. While both are viable, the conjugated scaffolds appear to possess a higher density of live cells situated in clusters in the pores of the scaffold, whereas the unconjugated scaffolds have lower density colonies mainly growing in flat films. This could be due to the formation of a 3D ECM in the scaffold pores, encapsulating the cells, as would be expected for normal cell function. This

accelerated rate of adhesion and proliferation would be expected from cells binding to Collagen substrates<sup>73,84</sup> which is concurrent with literature and with the results of the PHBV fibre study (Figure 7.8).

LIVE / DEAD staining performed on the scaffolds at day 14 of the study showed little difference between the cell behaviour on both sample types, with both displaying dense colonies, both on the surface and in the pores of the scaffolds. What is significant at this time point is the observance of cells existing in an extracellular matrix, as determined by their presence in 3D space, where the scaffold does not have a surface. These ECM structures are more present in the conjugated scaffolds than unconjugated, where the cells appear to adhere directly to the walls of the scaffold's struts. This observation would indicate that the presence of collagen on the surface of scaffolds accelerates the cell adhesion, growth, and ECM deposition process, as indicated in literature<sup>37,38,113</sup>.

#### ***6.5.2 3D printed PCL discs functionalised with Collagen***

After the appearance of inconsistencies across several PCL-Collagen scaffold biological experiments, the decision was made to try and simplify the experiment. Discs of PCL were printed and conjugated to remove the complexity of cellular matrices in 3D space from the analysis. Samples were seeded with Neo-NHDF fibroblasts.

The LIVE / DEAD assay result results shown in Figure 6.3 show a more typical display of the expected results of seeding cells on conjugated and unconjugated PCL. In days 1 and 3, a greater quantity of live cells can be observed on the conjugated samples with a lower ratio of dead, than on unconjugated samples. The cells on conjugated samples are also observed to have a more fibroblastic morphology than those on unconjugated samples, indicating a more rapid adhesion and deposition of actin on conjugated samples. On day 3 of the experiment, LIVE / DEAD staining shows a greater density of live, fibroblastic cells and a lower quantity of dead cells on conjugated samples vs non-conjugated. This result is more in line with the observations in the biological testing component of the PHBV fibres study in Chapter 7.

Analysis of cell metabolism on the PCL / PCL-Collagen discs was assessed by using a Presto Blue assay. Results from day 1 show a significantly higher level of cell metabolism on PCL-collagen discs over PCL and glass samples. This result is concurrent with the expectations of enhanced cellular growth and adhesion in literature and is similar to the performance observed when analysing metabolic activity in the PHBV fibres study, Figure 7.7. Likewise, on day 3, the metabolic activity registered is superior on PCL-Collagen over PCL discs, which is concurrent with the LIVE / DEAD analysis, as well as the results observed in literature. By day

7, there is no significant difference between the activity observed between samples, with both samples having a very similar average fluorescence reading, indicating that the cells on the discs have reached confluence and stabilised.

In addition, another study assessing the cytoskeleton and nucleus of Tc28A2 cells seeded on conjugated and unconjugated PCL discs was conducted, with cells imaged at three timepoints throughout the study. The ability to assess the morphology the cells and quantity of actin deposited is vital to assessing the true effect of the collagen integration on the surface. Like the initial LIVE / DEAD staining experiments on 3D scaffolds, the cell morphology staining showed little difference between conjugated and unconjugated samples. What was observed was the assumption of a star-like morphology and dense levels of actin deposition across both samples. This has been observed in literature with the seeding of chondrocytes on PCL / PHBV blend scaffolds<sup>109</sup>, where the presence of actin filaments and a star-like morphology are indicative of dedifferentiation, where it was also noted that the deposition of “stress-actin” and maintenance of a round chondrocyte morphology was observed on samples containing a higher quantity of PHBV. In addition, a 2020 review by Yao and Wang<sup>114</sup> notes the proclivity of chondrocytes to dedifferentiate after repeated culture in monolayers, a condition in which these Tc28A2 cells would have been exposed during culture in flasks and on printed discs. They cite a change from a characteristically round chondrocytic morphology to a form reminiscent of fibroblast morphology, in addition to the expression of Collagen type I rather than type II. The expression of collagen type I is more aligned with the production of fibrous cartilage, and the expression of collagen type II is indicative of the production of hyaline cartilage<sup>115</sup>. Therefore, retention of the native chondrocyte phenotype could be important to the output of the correct type of cartilage on scaffolds with the proposed purpose of regenerating articular cartilage.

Mirroring some of the observations of the LIVE / DEAD, both samples possessed dense colonies by day 3. This is not the expected observation for this assay testing for conjugated vs unconjugated samples. The expected result would have expected to see a lower level of cellular proliferation on unconjugated scaffolds. The same trend extended to day 7, where both samples reached confluence. A disparity in cell proliferation, as observed in Days 1 and 3 of the PCL / PHBV study shown in Figure 6.8, would have been closer in line with expectations.

#### ***6.5.3. 3D printed PCL / PHBV discs functionalised with Collagen***

In conjunction with the study on printed PCL discs, discs of PCL / PHBV were printed and conjugated with collagen. Discs were seeded with Tc28a2 chondrocytes to assess the efficacy of conjugated polymers with a more mechanically stable base for tissue regrowth. Experiments

on PCL / PHBV scaffolds were performed at a different time and were seeded with Tc28a2 chondrocytes. These were assessed for metabolic activity and cytotoxicity.

The morphology of seeded cells on the discs was more in line with the observations in the PHBV-fibre study, while on day 1, there was a significantly higher observation of deposited actin on Collagen conjugated samples, indicating a more rapid rate of surface adhesion. On day 3 cells on unconjugated scaffolds begin to adopt a more rounded morphology and appear to have proliferated to a higher confluence than those on unconjugated scaffolds. By day 7, the conjugated samples have developed into a confluent tissue layer, by comparison, the chondrocytes on unconjugated samples are displaying levels of actin deposition and fibroblastic morphology observed on the conjugated discs at day 1, indicating they are potentially still in a dedifferentiated form. These results may indicate that there is a significant advantage given to cell growth and proliferation through the conjugation of collagen to the surface of the disc, and potentially the ability to return to a native chondrocyte phenotype faster than those seeded on unconjugated scaffolds. These results, however, do contrast with the those observed in the same study on PCL-Collagen materials. In that study, there was very little observable difference in cell morphology, adherence or proliferation between the conjugated and unconjugated samples.

#### ***6.5.4. 3D printed PCL / PHBV scaffolds functionalised with Collagen***

Analysis of the cytocompatibility and metabolic activity properties of seeded cells on PCL / PHBV based samples were assessed at an earlier stage than the printed discs used in the assessment of morphology. In Figure 6.6, little discernible difference can be observed between the levels of cell adhesion, growth, and the ratio of live to dead cells, on the conjugated and unconjugated samples. This result would indicate there is no advantage to the conjugation of collagen to scaffolds, however, it does contrast with the results of the PHBV-fibre study (Figure 7.8), the morphology assessment on PCL / PHBV discs (Figure 6.8), and with the cytocompatibility and metabolic activity results gained from the study PCL-Collagen discs (Figure 6.3).

The analysis of studies on the metabolic activity of TC28A2 chondrocytes on 3D scaffolds is shown in Figure 6.7. The results show a general trend of increased metabolic activity up until day 14 of the study. Throughout the first 14 days of the study, there was no significant difference in the metabolic activity between scaffold sample types. This however changed on day 21 of the study, where a rapid decline in the metabolic activity of cells seeded on conjugated samples was observed. As cells of a chondrogenic lineage mature from MSCs to chondrocytes, they produce a collagen-rich extracellular matrix and their activity switches from growth to

homeostasis and the maintenance of the ECM<sup>116</sup>. This change in ECM deposition to maintenance may be a possible explanation for the differing levels of chondrocyte metabolism observed at this time point.

#### ***6.5.5. Comparison between cell morphology of Tc28a2 chondrocytes onto 3D printed PCL and PCL / PHBV scaffolds functionalised with Collagen***

In Figures 6.5 (chondrocytes on PCL & PCL-Collagen) 6.8 (chondrocytes on PCL / PHBV & PCL / PHBV-Collagen, it can be observed that adhered chondrocytes adopt a non-fibroblastic, round morphology, characteristic of chondrocytes. This would indicate normal behaviour of the chondrocyte cell on the scaffolds. Contrasted, it is possible to see the fibroblastic morphology, characteristic of the Neo-NHDF fibroblast cell line in Figure 6.3, showing that both cell types adapted to regular function on the scaffold types.

#### ***6.6. Summary and interim conclusions***

Several experiments in these studies indicate that there is a benefit to the conjugation of collagen to scaffolds in terms of boosting levels of cell adhesion, growth, and proliferation. The second study on PCL-Collagen scaffolds, PCL-Collagen discs cytocompatibility and metabolism studies, and morphological study on PCL / PHBV discs showed signals of higher activity on conjugated surfaces. The initial PCL-Collagen scaffolds, PCL-Collagen disc morphology study, and PCL / PHBV scaffolds cytocompatibility and metabolism studies did not indicate a clear advantage to the collagen conjugated materials. It should be noted that while there was not a clear correlation between the study results in all cases, there were no incidences in which unconjugated materials were observed to have higher levels of cellular activity than conjugated materials. If the theory that dedifferentiation due to monolayer culture in cell culture and scaffold seeding is correct, the results of the chondrocyte seeding on PCL / PHBV discs that showed a quicker reversion to chondrocytic morphology, could be an indicator that collagen conjugation may be beneficial to the production of hyaline cartilage on scaffolds.

# Chapter 7: Biomimetic PHBV-Collagen Forcespun Membranes

## 7.1. Introduction

This chapter describes the fabrication, development, and characterisation of micro / nano fibre scaffolds of PHBV fabricated by forcespinning. This chapter has been published under the title “Biomimetic Properties of forcespun PHBV Membranes Functionalised with Collagen as Substrates for Biomedical Application”. Data collection or analysis attributable to authors besides Kegan McColgan-Bannon will be appropriately designated.

## 7.2. Collagen functionalisation of PHBV Forcespun membranes

Previous work by this group<sup>98</sup> optimised the method by which the fibres were produced, which is detailed in Chapter 3, Section 3.3.5.. Large sections of fibre scaffold material fabricated in this manner are shown in Figure 7.1 A. From these large mats, samples were cut into small discs of approximately 1.5 cm diameter, then placed into cell well inserts and subjected to a surface conjugation, introducing collagen to the fibres, detailed in Chapter 3 Section 3.2.2.2.. Scaffolds conjugated with Type-I Collagen stained with Sirius Red dye are shown below in Figure 7.1 B-D.

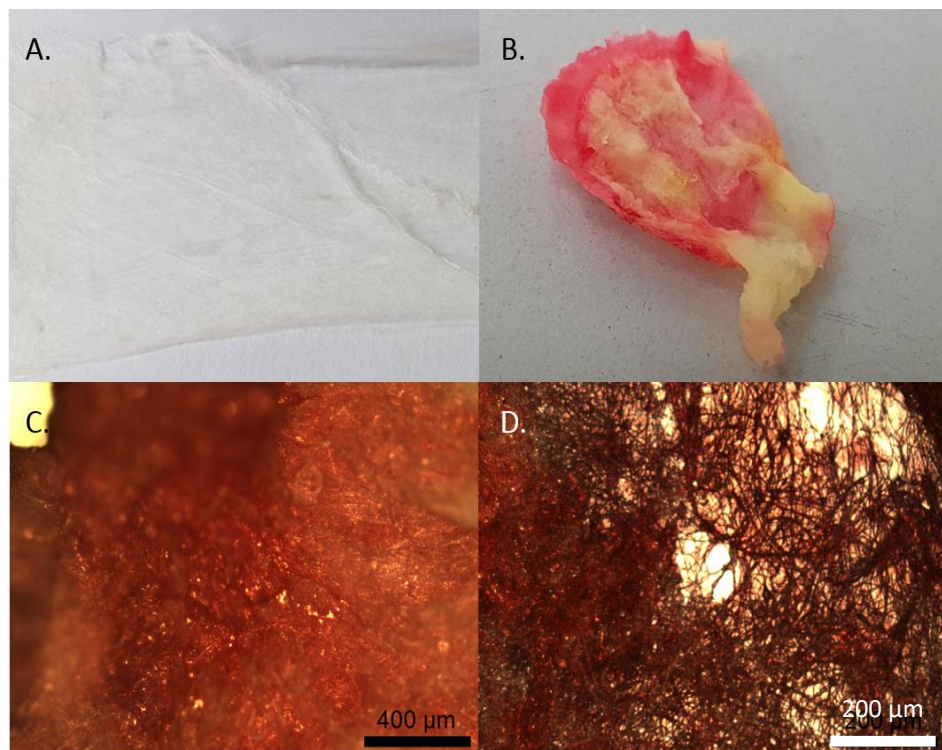


**Figure 7.1** – **A.** Entire PHBV membrane sheet taken from the collecting bars. **B.** A conjugated PHBV-Collagen membrane stained with Sirius Red dye inside of a cell crown, then removed for imaging. **C. & D.** Samples of stained PHBV-Collagen membranes under brightfield microscopy.

Dense red staining can be observed in the PHBV samples in Figure 7.1 B-D. Sirius Red dye binds to structural collagen in a sample, and areas of bright red indicate a high presence of structural collagen<sup>117</sup>, areas of yellow colouring are PHBV that has not been conjugated with collagen. Figure 7.1C and D, display stained samples under microscopy, further clarifying the extent to which collagen conjugation has been effective throughout the scaffold macro-structure.

### **7.3. Physical-chemical characterisation of functionalised PHBV-collagen membranes**

#### **7.3.1. Fibre Collagen Content and Morphology**

Figure 7.2 A & B displays a comparison of the collagen content in PHBV-Collagen fibre scaffolds versus PHBV-Collagen samples produced solid films. Collagen content was measured by Sirus Red assay as a function of surface area and sample mass. Solid conjugated films, produced by solvent casting before functionalisation, were observed to contain  $8.3 \pm 1.1 \mu\text{g} / \text{cm}^2$  of structural collagen, while conjugated fibres were observed to contain  $25.4 \pm 3.1 \mu\text{g}$  of collagen per mg mass of fibre membrane. This experiment displays the ability to load higher levels of collagen onto fibres rather over that of a flat solid surface.

Figure 7.2 C & D depicts fibre morphologies of PHBV membranes via brightfield microscopy before and after collagen conjugation, displaying the extent of collagen integration to the conjugated scaffolds. Conjugated and unconjugated fibre scaffolds were both stained with Sirius Red dye. Following several washes, the unconjugated samples (control) show no red staining when compared to collagen conjugated membranes, as indication of successful collagen grafting onto PHBV membranes surface as well as the efficacy of the staining protocols. Figure 7.2 E & F shows scanning electron microscopy (SEM) images of unconjugated (E) and conjugated (F) fibre scaffolds. ImageJ software was used to analyse the SEM images to determine fibre diameters. Unconjugated fibre samples were observed to possess fibre diameters between 731 nm - 5.40  $\mu\text{m}$  (median 1.67  $\mu\text{m}$ , SD  $\pm 1.27 \mu\text{m}$ ), the range observed in conjugated fibres was between 631 nm - 6.85  $\mu\text{m}$  (median 1.64  $\mu\text{m}$ , SD  $\pm 1.99 \mu\text{m}$ ). No significant change in fibre diameter or membrane structure is attributed to the conjugation process.

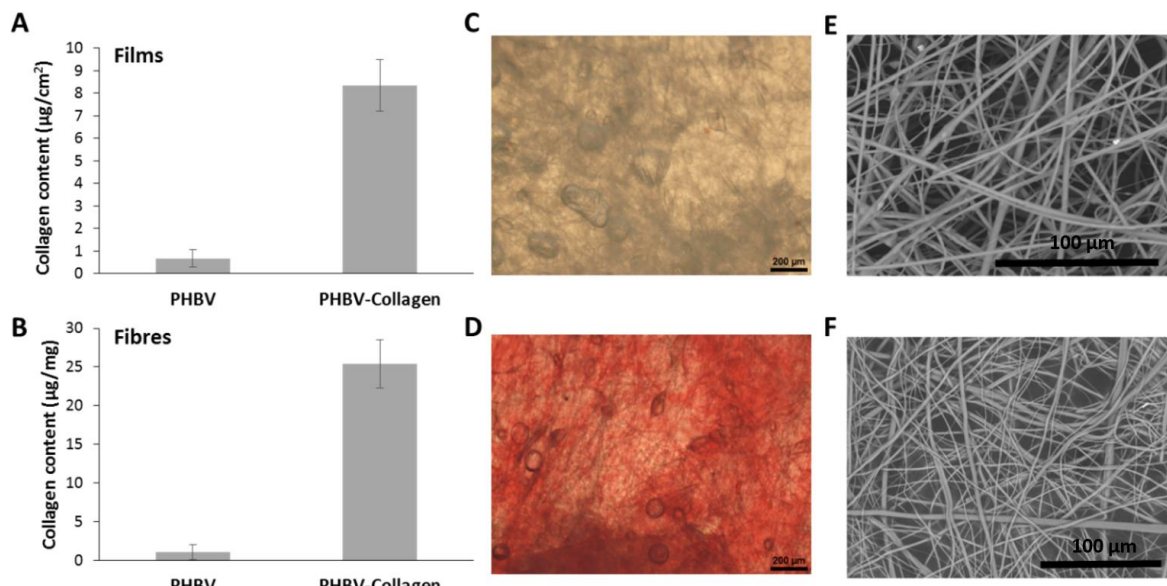


**Figure 7.2** – Quantification of collagen content by Sirius red assay in A. PHBV films (ug of collagen per area) and B. 3D fibre membranes fabricated by forcespinning (ug of collagen per mass of fibres). Microscopy of 3D fibrous PHBV mesh stained with Sirius Red, C before, and D after, collagen functionalisation. SEM image of fabricated scaffolds by forcespinning: E before and F after collagen grafting. Scale bar in SEM corresponds to 100 $\mu\text{m}$ .

### 7.3.2. Chemical analysis by ATR-FTIR

The results from the ATR-FTIR analysis of unconjugated PHBV fibre membranes and collagen conjugated samples are shown in Figure 7.3. The -C=O group present in the PHBV ester functional group is observed as the strong band seen at 1720  $\text{cm}^{-1}$ . The broad band at 3100–3600  $\text{cm}^{-1}$  observed in conjugated samples is representative of -OH groups present in collagen and structural H<sub>2</sub>O. The two most characteristic ATR-FTIR signals used to identify collagen, are the amide bonds observed at 1658  $\text{cm}^{-1}$  and 1558  $\text{cm}^{-1}$ , representing Amide I and Amide II for the PHBV-collagen conjugated sample, respectively. The lack of these bands in unconjugated samples, is evidence of the efficacy of the functionalisation process.

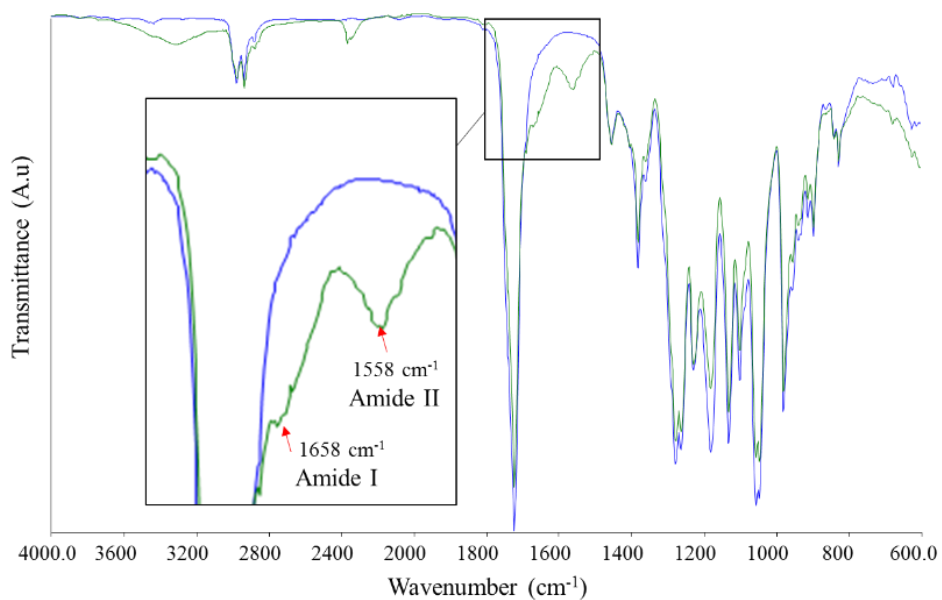


**Figure 7.3 – ATR-FTIR analysis of unconjugated (blue) and conjugated (green) fibre scaffolds. Highlighted in the black box are the Amide I & II peaks, characteristic of the presence of collagen.**

### 7.3.3. Chemical analysis by X-Ray Photoelectron Spectroscopy (XPS)

XPS was used to characterise the surface chemistry of conjugated and unconjugated fibres (Figure 3.4). Unconjugated PHBV samples present two characteristic peaks of C<sub>1s</sub>, 284.5 eV, and O<sub>1s</sub>, 532.0 eV. Upon conjugation of collagen, there is a sharp increase in the N<sub>1s</sub> signal at 398.7 eV, indicating that the conjugation was successful. After conjugation, the relative element content changed from C<sub>1s</sub> 74.5% (SD  $\pm 1.8\%$ ) to 70.5% (SD  $\pm 0.8\%$ ), N<sub>1s</sub> 1.7% (SD  $\pm 0.6\%$ ) to 10.3% (SD  $\pm 0.7\%$ ), and O<sub>1s</sub> 23.9% (SD  $\pm 1.3\%$ ) to 19.2% (SD  $\pm 0.3\%$ ), between unconjugated PHBV and collagen conjugated PHBV samples, showing a proportionally lower carbon and oxygen content, upon the integration of collagen. High resolution XPS analysis of the N<sub>1s</sub> signal detected the presence of C-N (398.3 eV), -NH- and C-NH<sub>2</sub> (~400 eV), and C-N (401.5 eV) bonds in conjugated samples, which are typical chemical motifs within the structure of collagen.

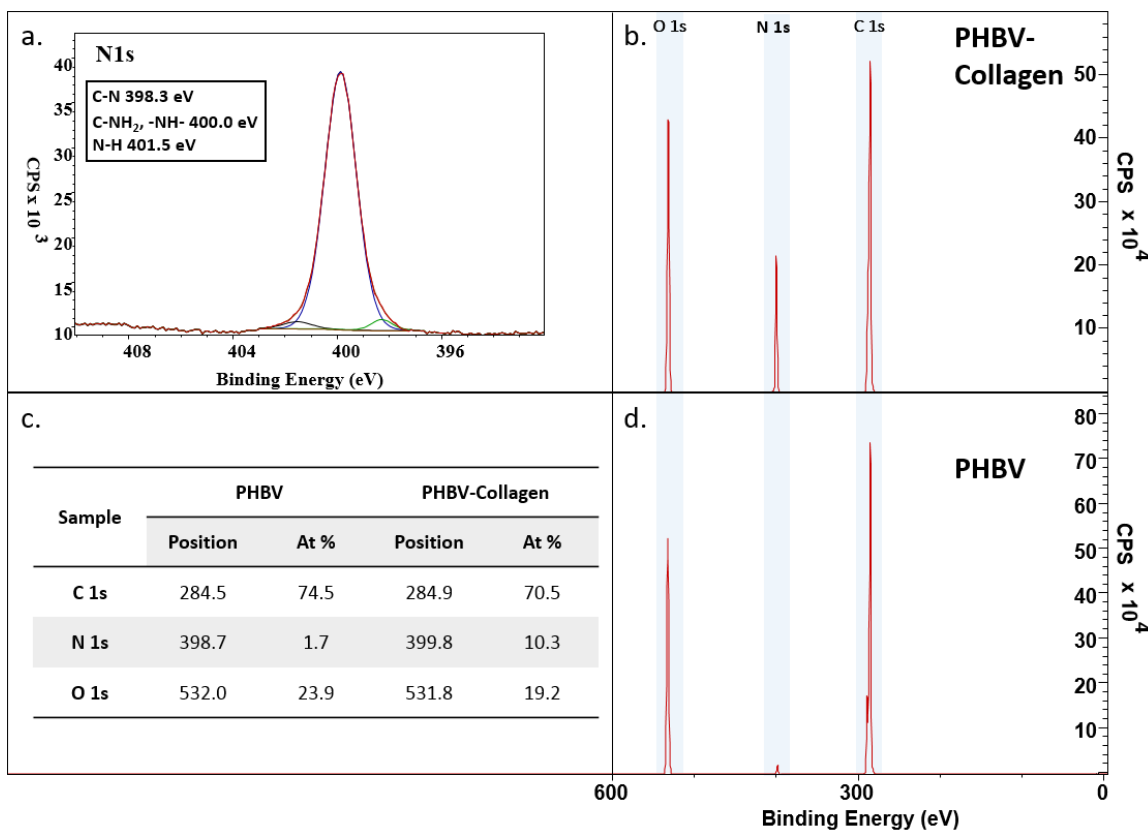
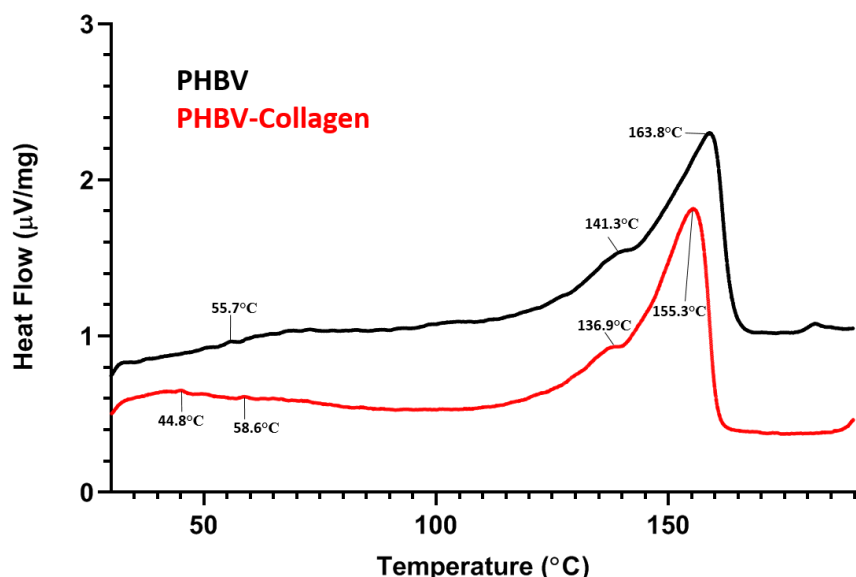


**Figure 7.4** – XPS analysis of PHBV and PHBV-Collagen fibre membranes. (a.) Displays a deconstructed N1s peak at high resolution, observed upon conjugation of collagen. (b.) Shows the low-resolution spectra for PHBV-Collagen. (c.) A table binding energies and % elemental presence from observed peaks. (d.) Low-resolution spectra for unconjugated PHBV.

#### 7.3.4. Thermal analysis by Differential Scanning Calorimetry (DSC)

Differential scanning calorimetry was used to assess the changes in the fine polymer structure of PHBV before and after conjugation. Figure 3.5 shows the DSC thermograms of both conjugated and unconjugated scaffolds, annotated with the peaks of interest, and with the numerical data are summarized in the table below. Both thermograms displayed the characteristic twin melting peaks of PHBV, with a  $T_m$  profile of PHB at 163.8°C and PHV at 141.3°C. However, it was observed for PHBV-collagen fibres, that a decrease in the expected melting temperatures for both PHB and PHV peak upon collagen conjugation had occurred, with a  $T_m$  of 155.3°C for PHB and 136.9°C for PHV. There was little difference in the  $\Delta H_m$  recorded between PHBV and PHBV-collagen melting enthalpies. The crystallisation temperatures,  $T_c$  peaks, were recorded at 55.7°C and 56.9.6°C in unconjugated (PHBV) and collagen conjugated (PHBV-Collagen) samples, respectively, indicating little change in total polymer crystallinity is induced by conjugation. By introducing collagen via surface functionalisation,  $\Delta H_c$  slightly decreased from 0.182 to 0.120  $\mu\text{Vs} / \text{mg}$ . Collagen denaturation temperature was detected as a small peak at 44.8°C for collagen conjugated PHBV, this peak was not observed for pure PHBV scaffolds.



Sample	T <sub>d</sub> (°C)	Collagen T <sub>c</sub> (°C)	PHBV T <sub>c</sub> (°C)	PHV T <sub>m</sub> (°C)	PHB T <sub>m</sub> (°C)	ΔH <sub>d</sub> Collagen (μVs / mg)	ΔH <sub>c</sub> PHBV (μVs / mg)	ΔH <sub>m</sub> PHBV (μVs / mg)
PHBV	-	55.7	141.3	163.8	-	0.182	150.4	
PHBV-Collagen	44.8	56.9	136.9	155.3	0.189	0.120	150.7	

**Figure 7.5 –** Combined thermograms of PHBV and PHBV-Collagen DSC analysis. The main peaks of interest and respective enthalpies are summarized in the table below.

### 7.3.5. Contact Angle

Changes in wettability induced by the conjugation process were characterized by observing the difference in the static contact angle of deionised water on conjugated and unconjugated fibres, shown in Figure 3.6. A. The contact angle of PHBV-collagen fibres was observed to be significantly ( $p<0.001$ ) lower from that of unconjugated fibres, with an initial value of  $92.6^\circ$  ( $SD \pm 7.1^\circ$ ) going to  $54.1^\circ$  ( $SD \pm 9.5^\circ$ ) upon conjugation with collagen.

### 7.3.6. In Vitro Hydrolytic Degradation Study

To emulate the physiological degradation effect of the body on polymeric materials, the change in mass of samples over a six-week time frame was recorded, after incubation in phosphate buffered saline (PBS) (pH 7.4) (intervals T0, T1, T2, T4 & T6 weeks). The dry weight of samples was measured before and after incubation, the analysis of which is displayed in Figure 3.6 B. The results indicate that there is no statistically significant difference in the mass of samples between time points (\*ns) for both, conjugated and unconjugated samples. However, when comparing both samples at same time point (T), it was noticed that PHBV samples showed a significant decrease in mass against PHBV-collagen sample (\* $p < 0.05$ ) at week 6 (T6).

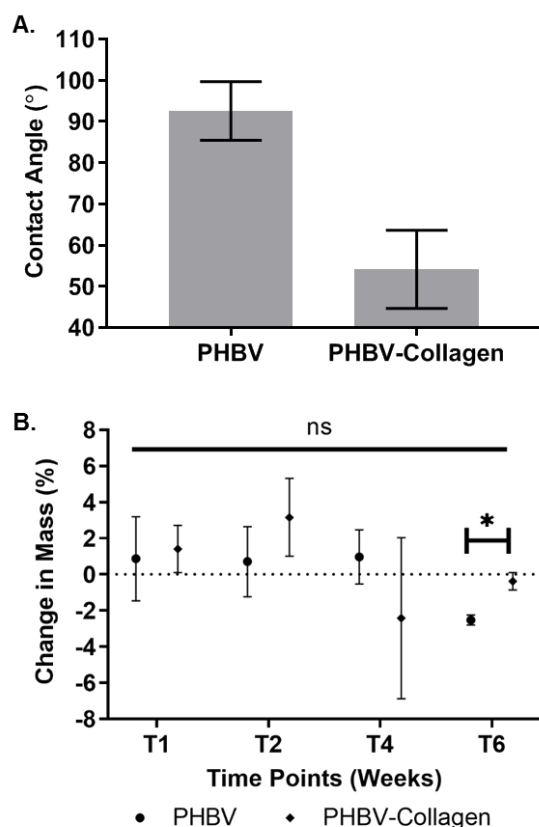


**Figure 7.6 – (A)** Change in PHBV contact angle with collagen conjugation. **(B)** % Change in Mass in conjugated and unconjugated fibres over 6 weeks of incubation at physiological conditions.

#### 7.4. Cytocompatibility studies of functionalised PHBV-collagen membranes

##### 7.4.1. Cellular Metabolic Activity

The relative metabolic activity of Neo-NHDF fibroblasts on the fibre scaffolds was measured using a Presto Blue assay (Figure 3.7). On day 1, there was no significant difference in metabolic activity observed between conjugated, unconjugated and glass control samples. On Day 3 and 7, the cells adhered to PHBV-Collagen membranes showed significantly higher metabolic output than those on unconjugated PHBV scaffolds. For Day 3, comparison of the PHBV-Collagen and glass control samples displayed significantly higher cell metabolic activity on the conjugated fibre membranes, however on Day 7 there was no significant difference in metabolic output detected between the samples.

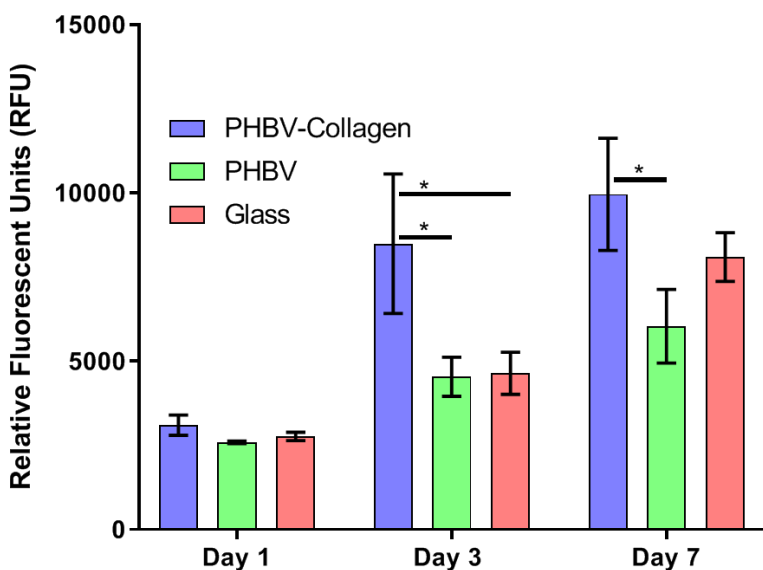


**Figure. 7.7** – Relative fluorescent output of metabolized presto blue, representative of cellular metabolic activity on scaffolds (\* = P<0.05).

#### 7.4.2. Cell viability and morphology

A LIVE / DEAD assay was used to assess the viability of Neo-NHDF cells on the conjugated and unconjugated scaffolds, shown in Figure 3.8. On Day 1, it can be observed that the number of dead cells on PHBV-Collagen scaffolds was fewer than PHBV scaffolds, by a factor of 5x. Simultaneously the PHBV-Collagen scaffolds are observed to host a much higher number of live cells than on PHBV scaffolds, however the excess was not quantified.

To assess cell morphology and cell spreading onto the samples, F-actin cytoskeleton staining of the cells was performed using rhodamine phalloidin. Figure 3.8, in red and blue staining, depicts the morphology of Neo-NHDF cells adhered to the conjugated and unconjugated scaffolds at Day 1, 3, and 7. The F-actin cytoskeleton staining evidenced a typical fibroblast morphology, with an observed increase over time when in presence of collagen conjugation (Figure 3.8.). At each of the individual time points, cells were found to be spread more

widely, both morphologically and geographically, and better attached to the PHBV-collagen scaffolds than in unconjugated PHBV. On PHBV substrates, cell shape was rounded at Day 1 (Figure 3.8.) and more elongated towards Day 7, however, the levels of F-actin deposition observed by Day 7 on unconjugated scaffolds, does not reach the level observed on Day 1 of the PHBV-Collagen scaffolds. Cells seeded onto PHBV-Collagen scaffolds were observed to attach and grow at a faster rate than on PHBV scaffolds. Figure 3.9. depicts a 3D z-stack image of an individual fibre of unconjugated PHBV at day 7. The nuclei and F-actin are observed to adhere to the orientation of the fibre, showing how the scaffolds can be used to direct the growth of cells.

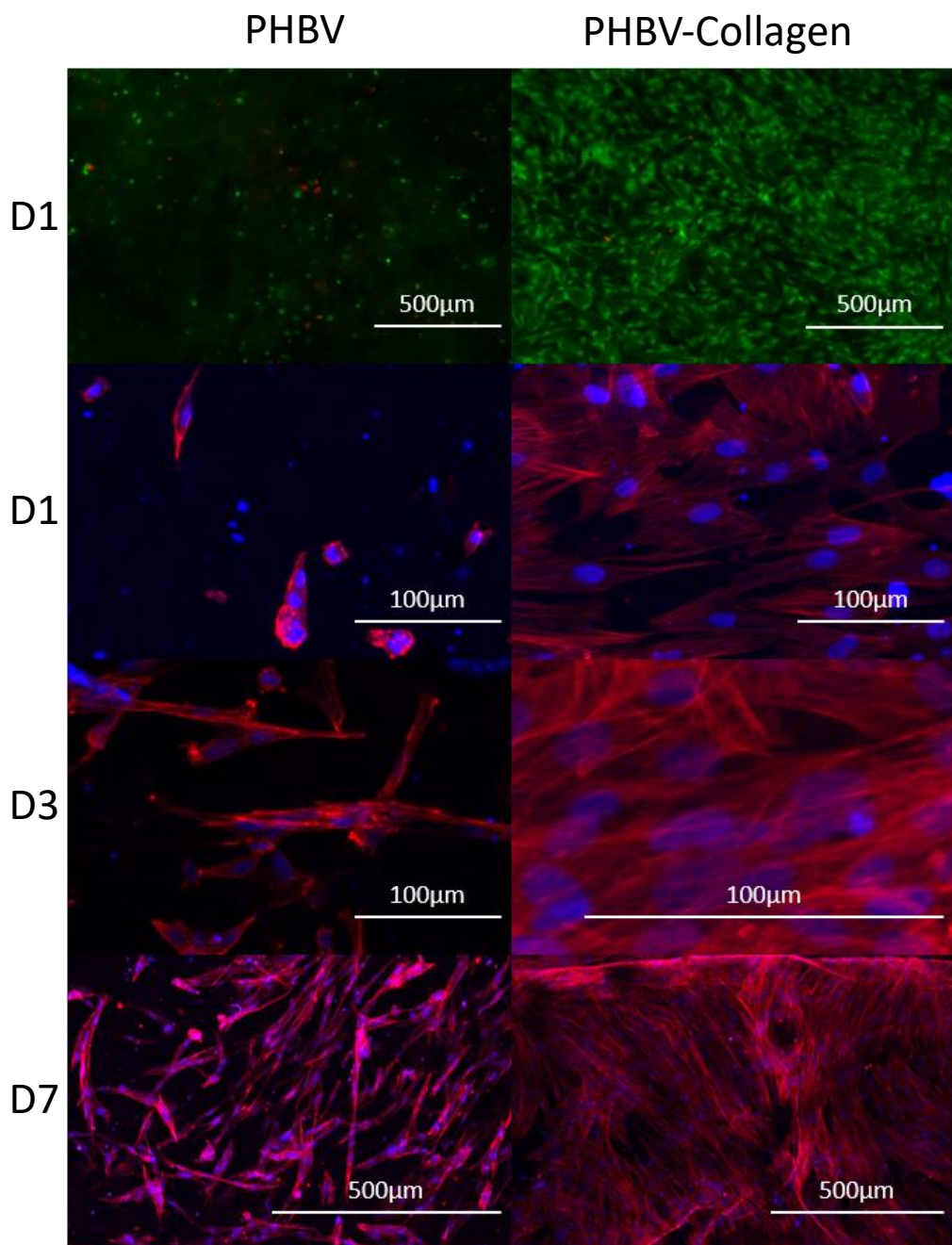


**Figure 7.8** – Cytotoxicity, cell viability and cell morphology of Neo-NHDF cells cultured on forcespun PHBV scaffolds with and without collagen. Fluorescent images of Neo-NHDF cells stained with LIVE / DEAD membrane integrity assay (green – viable cells, red - dead cells, 5x magnification). Confocal microscope images showing the morphology of Neo-NHDF cells seeded on PHBV and PHBV-Collagen scaffolds on days 1 (D1), 3 (D3), and 7 (D7) (red- phalloidin, and blue – DAPI, 5 and 10x magnifications).

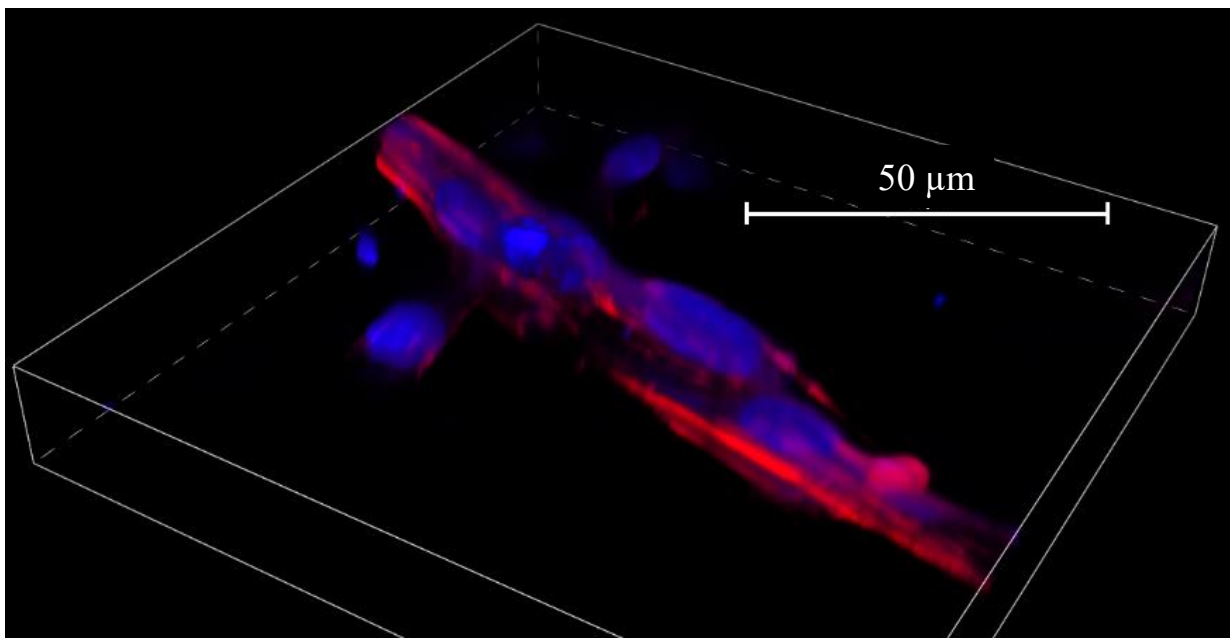


**Figure 7.9** – 3D z-stack confocal microscope image, depicting the orientation of adhered fibroblasts to PHBV fibres. F-actin is depicted in red, while the cell nuclear material is depicted in blue. This image was recorded at a 40x magnification.

### 7.5. Discussion

A cell's microenvironment plays a critical role in cellular function, the endeavour of mimicking the physical and chemical properties of natural extracellular matrices is a key approach in developing biomaterials that control cell behaviour. To this end, a major factor in furthering of tissue engineering and regenerative medicine applications is the design and manufacturing of biocompatible and biodegradable constructs that promote these behaviours. PHBV is a promising biodegradable and non-antigenic biopolymer, as the low molecular weight of PHB exists widely in cells. This biopolymer (and monomers and oligomers) has shown to be an excellent biomaterial candidate for tissue engineering, because of its biocompatibility and suitability for *in vivo* applications<sup>118</sup>. Related works in literature, focusing on nerve and skin tissue engineering have shown improved surface properties and cellular behaviour on collagen-coated nanofibers<sup>46,84,119</sup>. Collagen is a major constituent of the extracellular matrix, and is present in nearly every tissue in the human body; and unsurprisingly its grafting to a base polymer has been shown to increase the adhesion and proliferation of cells onto the polymeric scaffold<sup>120</sup>, making collagen functionalisation treatment an attractive practice for enhancing the biological performance of a material.

In this work, the efficacy of the method used to graft collagen to PHBV forcespun membranes was confirmed by XPS and ATR-FTIR as successful. Characteristic ATR-FTIR collagen signals corresponding to Amide I and Amide II<sup>121</sup> were identified in conjugated samples,

concurrent with the literature and the ATR-FTIR analysis on surface conjugated PCL and PCL / PHBV materials. This result was reinforced by XPS analysis, where an appreciable increase in the N<sub>1s</sub> signal intensity was observed in conjugated samples. Nitrogen in the collagen conjugated PHBV constituted about 10.3% of the overall atomic content. However, an N<sub>1s</sub> signal was detected in the low resolution XPS scan of unconjugated PHBV samples, the signal intensity of 1.7% is within analytical error, and the structure of natural PHBV does not contain nitrogen. Deconvoluted high resolution XPS of the N<sub>1s</sub> peak in conjugated samples revealed the presence of C-N, -NH-, C-NH<sub>2</sub>, and N-H attributable to signals between 398.3 eV and 401.5 eV. The bond signals closely match the expected values for collagen, corresponding with both literature <sup>122-124</sup> and the Thermo Scientific XPS library.

A Sirius Red staining assay was used to qualitatively and quantitatively assess the presence of structural collagen in the fibre scaffolds. The dye functions by binding to the side chains present only in structural collagen; gelatin or otherwise denatured collagen is not bound by the dye <sup>101</sup>. Images of the scaffolds after staining show a high level of collagen conjugation, a result confirmed by the quantitative measurement of collagen content. Fibre membranes were observed to contain a much higher level of collagen content by mass than films of PHBV. The higher levels of collagen present in the fibres can be attributed to the higher surface area <sup>125</sup> exhibited by nano / microfibers in comparison to films, exposing more sites of conjugation in the fibre membranes and allowing for the binding of more collagen molecules per mass of the base polymer.

Analysis of the surface wettability demonstrated an increase in the hydrophilicity of PHBV fibres upon conjugation due to the hydrophilic structural motifs present in the collagen molecule. A significant reduction from 93° to 54° in the contact angle of deionised water with conjugation is indicative of more favourable cellular adhesion properties <sup>103,104</sup>, a result concurrent both with the literature and the observations from wettability assessment of PCL and PCL / PHBV collagen conjugated scaffolds. A general trend is an increase in cellular adhesion on surfaces with a lower wettability value, however, this property consists of multiple factors, such as surface roughness and surface chemistry <sup>106</sup>, which independently affect wettability and cellular adhesion. PHBV is a quite hydrophobic polyester without many functional groups for biomolecules grafting. Therefore, these results suggest that the introduction of chemically favourable motifs present in collagen is responsible for the decrease in contact angle and enhanced cellular adhesion observed <sup>105</sup>.

DSC analysis was used to assess the thermal properties of PHBV and PHBV grafted collagen. Both spectra exhibited typical T<sub>c</sub> and T<sub>m</sub> values for PHBV <sup>126</sup>, with the presence of the

characteristic peak for collagen's denaturation temperature only in conjugated samples<sup>127</sup>. Collagen conjugation led to a small downward shift in peak temperatures for the melting points of PHB and PHV, with peak enthalpies remaining consistent. The surface functionalization or blending of proteins are known to decrease the melting temperature of polymeric based scaffolds, and this study shows the addition of collagen reduced the melting temperature of PHBV<sup>84,128</sup>. However, the T<sub>c</sub> of PHBV membranes remained similar, showing small changes in the total crystallinity. These results indicate that collagen was successfully grafted superficially onto PHBV forcespun fibres, without decreasing or impacting the polymer bulk thermal properties. The thermal stability of the collagen conjugated substrates remains comparable to neat PHBV.

Similarly, analysis of data collected from *in vitro* degradation studies showed no significant change in mass over 6 weeks, in both sample sets. This result is consistent with the observation of similar thermal properties in conjugated and unconjugated samples, in that surface conjugation with collagen presents no significant change to the stability of fibres under degradation conditions; a result consistent with other studies on PHBV fibre scaffolds<sup>84</sup>, and with the results of studies on PCL and PCL / PHBV printed scaffolds. These results are consistent with the measured degradation of PHBV in literature, which exhibits a slow degradation rate under identical conditions, of 5.6% total mass loss after 229 days<sup>129</sup>. In addition, these mass changes are attributed solely to the PHBV, as the mass of collagen would be too low to impact the results. The retention of collagen in its triple helical structure under degradation conditions is a good indicator that conjugated fibres can retain their enhanced biological characteristics over time *in vivo*.

A key component in determining the viability of the scaffold is to observe the behaviour of the fibroblastic cells on the membranes. Collagen is a major constituent of the ECM, bearing the motifs to which cell integrins bind<sup>130</sup>, and as such, scaffolds conjugated with collagen displayed a much higher level of cellular growth and adhesion<sup>37,38,113</sup>. A LIVE / DEAD assay (Figure 7.8) on the same sample area showed a greater quantity of live cells on PHBV-Collagen than PHBV surface. Cellular viability is a key indicator of biological success in living tissues, and thus an important aspect of assessing the efficacy of new materials for TE applications<sup>131</sup>. In this work, it was found a greater number of viable cells growing on PHBV-Collagen conjugated substrates, with an increase in metabolic activity after day 3 (as shown in Figure 7.7). As the adhesion of cells to a surface is key in the mediation of multiple cell functions<sup>103,132</sup> (i.e. structural protein deposition, proliferation, migration, etc.), greater observed viability, mitochondrial activity, cell attachment and spreading is observed in presence of collagen motif

bearing conjugated membranes. Although not in collagen-grafted PHBV membranes, similar results were observed by Prabhakaran et al studies using PC12 neural cells onto electrospun PHBV nanofibers, where cell proliferation improved on blended PHBV / Collagen nanofibers for nerve tissue engineering<sup>84</sup>.

Confocal imaging of the fibroblast cytoskeleton (F-actin) and nuclei evidenced normal fibroblasts morphology with an increased number of cells over time, specifically in presence of collagen. By day 7, cells formed a dense monolayer on the surface of conjugated scaffolds, orienting themselves nearly parallel to each other and the substrate. Whereas cells growing on the unconjugated scaffolds were more sparsely distributed. Human dermal fibroblasts attachment, growth, spreading, and viability was significantly enhanced on PHBV-Collagen, demonstrating the positive effect of collagen conjugation to promote tissue growth and overcome relatively poor cell adhesion properties of the PHBV material. Similar works for cartilage tissue engineering showed that collagen-modified PHBV provided a more favourable surface for chondrocytes adhesion, spread, and proliferation than PHBV<sup>85</sup>. With the conjugation of collagen, there are a greater number of focal adhesion points available for cells to adhere to, allowing for the cells to begin proliferation sooner than without focal adhesion points. The results in quicker tissue formation of tissue, ideal for TE scaffolds, where rapid regeneration of the host tissue is a primary goal.

### **7.6. Summary and interim conclusion**

PHBV fibre scaffolds were successfully prepared by forcespinning and covalently conjugated with type I collagen by using carbodiimide chemistry. Collagen surface functionalization was evidenced by the presence of amide I and II bands in ATR-FTIR and nitrogen contents detected by XPS scan of about 10.3 at % of the total atom, which was not observed in pure PHBV scaffolds. Surface functionalization significantly improved the surface properties of PHBV substrates by rendering it hydrophilic, evidenced by the significant reduction of PHBV contact angle from 93° to 54° by grafting collagen. The amount of collagen was successfully quantified in (2D) films by obtaining a superficial amount 8 ug / cm<sup>-2</sup> collagen and in (3D) membranes 25ug of collagen per mg of porous membranes. Collagen grafting onto PHBV forcespun membranes does not significantly change the morphology and fibres diameters ranged between 631nm and 6.85 µm. Moreover, collagen conjugated PHBV fibres showed physiological stability as pure PHBV scaffolds, as degradation assays showed no changes of mass over 6 weeks of incubation and thermal properties of PHBV polymer are maintained post chemical conjugation. Collagen-modified PHBV forcespun membranes provided a more favourable surface for human fibroblasts adhesion, spread, and growth than PHBV. Forcespun PHBV fibre

membranes conjugated with type I collagen present promising characteristics for use as scaffolds for tissue engineering, as an alternative and scalable method of creating nano / micro fibres with enhanced biological properties in a more efficient and less toxic manner than current technologies.

# **Chapter 8: Summary Discussion, Conclusions, and Future Work**

## ***8.1. Introduction***

This chapter discusses the higher-level comparisons between the different scaffold production projects, focusing more on the end products. As such, processes that were not used in biological testing (such as thermal moulded films from PCL-g-Collagen) are not discussed. The chapter concludes with a Conclusions and Future Work section, discussing the impact of the work and how the research may be carried forward.

## ***8.2. Summary Discussion***

### ***8.2.1. Material Processing***

Central to the theme of this thesis is the development and optimisation of materials processing. Understanding the capabilities and needs of each material used in the experiments was key to reaching a concord in defining the processing route from base polymers to biosynthetic scaffold product. Melting, compressing, dissolving, shearing, reforming, extruding, hydrolysing, and conjugation all played critical roles in the examination and development of the biomaterial scaffolds. To these processes, each material reacted more or less favourably, requiring a balance to be struck and a specific route for each end product. When considering experiments holistically, PCL was considerably easier to work with than natural polymers or PHBV blends.

### ***8.2.2. Route to the Scaffold***

The experimental endpoint of each study was the creation of a biosynthetic scaffold, for which the cellular compatibility characteristics could be examined and considered within the proposed treatment paradigm. The journey from base material to product for each scaffold came with individual challenges and opportunities, which will be discussed in the following sections.

### ***8.2.3. Building logpiles and spinning fibers***

With the same base polymers and conjugation process, the main point of difference between the scaffolds in the studies was the advanced manufacturing techniques applied to generate the scaffold macro structure; FFF vs. Forcespinning. The product of the two processes creates structures with vastly different physical properties. As demonstrated in Chapters 4 & 5, logpile structures are durable and regular in construction with a relative modulus in line with the base polymer. Forcespun PHBV fibre scaffolds by comparison are extremely fragile, possess a more variable macrostructure, and have a large surface area.

From base polymer, logpile scaffolds pass through 4 significant formative processes: Extrusion, Printing, Laser Cutting, and Surface Conjugation. Forcespun fibres by comparison pass through

2, Spinning and Conjugation. With fewer steps involved in creation, Forcespun biosynthetic material scaffolds may seem simpler to create, however, the highly fragile nature of the fibre scaffolds lead to difficulties in maintaining the integrity of the scaffolds throughout the process; e.g. capture during spinning and when introduced to the multiple solution exchanges of the surface conjugation. This fragile nature resulted in many destroyed samples while completing the experiments. For instance, if the fibres folded, the high surface area scaffolds would become self-entangled and impossible to separate.

While requiring a greater number of processes to reach completion, the methods used to create logpile scaffolds created successful products more with greater repeatability. In the case of PCL, once optimised, the fabrication process would yield scaffolds with consistent geometries, as seen in Figure 4.8. PCL-PHBV scaffolds by comparison had greater variability in construction, which was primarily attributable to the extrusion process, which resulted in filament of varying width.

Variations in the morphology of the two different scaffold types was reflected in the mechanical properties. As the measurement of the mechanical properties of PCL and PCL / PHBV logpile scaffolds showed no significant difference in the compressive modulus, it is assumed that under similar usage circumstances in a hypothetical therapeutic situation, the two types of scaffold would behave in a similar manner. Attempts were made to quantify the tensile properties of the PHBV fibre scaffolds, however, the apparatus available was not sensitive enough to detect the value of the tensile strength. As it was possible to destroy the fibre scaffold's by gently rubbing them between a finger and thumb, it can be observed that they are significantly last durable than the 3D printed FFF scaffolds. From this contrast in mechanical properties, it is reasonable to assume that the scaffold types would be suited to different applications, perhaps using the logpile scaffolds in a therapy where mechanical integrity under compressive stress is vital and the fibre scaffolds in treatment where sheer or compression would not be involved.

Even though the consistency observed in the macro structure of the fibre scaffolds was of higher variability than that of logpile scaffolds, the higher surface area of the fibres grants the scaffold the ability to bond a high quantity of collagen during the conjugation process. The effects of which can be seen in contrast between fibre scaffolds and conjugated polymer films in Figure 4.6. & Figure 7.1.

The two advanced manufacturing processes, Forcespinning and FFF, both had advantages and disadvantages. In the Forcespinning process, it was not necessary to expose the base polymers to thermal decomposition, as the pellets were placed into solution before spinning. The

drawback being a product that was less repeatable and more difficult to handle. To create scaffolds using a FFF method, it was necessary to put polymer pellets through two thermal processes using temperatures that may induce decomposition, and / or a change in the crystalline structure of the materials. The advantage being much greater control in the final geometry of the printed scaffold. For the purposes of this project, discs of printed scaffolds were cut with a laser, introducing a further thermal process and risk of physical change. While necessary for the purposes of this experiment, it can be envisioned that this process may not always be necessary in the production of polymer scaffolds, for instance if they were printed directly to specification, rather than as a large template block used to obtain multiple samples.

The conjugation of PHBV pellets prior to spinning was considered to increase the ease of handling by avoiding the conjugation of delicate fibres. In Chapter 4, the solubility properties of PCL-Collagen materials were discussed, and it was found that bulk conjugated PCL-Collagen was not fully soluble, in even strong fluorinated solvents. Though the solubility of PHBV-Collagen was not directly examined, it is reasonable to suspect a similar result. The process of forcespinning the PHBV fibres before surface conjugation avoids the potential issue of insolubility.

The ATR-FTIR examination of each scaffold type showed little variation in intensity of collagen signals. As the ATR-FTIR was not utilised in a quantitative manner, this would not be a quantitative reading, rather a directional observation. The main observable difference was in the total staining visually observed between scaffolds, demonstrating the utility of a high surface area for collagen conjugation, as shown in Figures 4.6 and 7.1.

Another key indicator of the change in surface properties upon collagen conjugation is wettability. The contact angle of DI water on each material was observed to decrease upon conjugation with Collagen. The decrease in contact angle was notably higher in materials containing PHBV, with a 41.6% and 47.9% decrease observed in conjugated fibres and films respectively, contrasted with a 10.3% drop for bulk-conjugated PCL, though the solubility of PCL-g-collagen spin coated samples may have influenced the results of testing wettability in PCL and PCL-g-Collagen samples.

In the observation of hydrolytic degradation, there was little variance between scaffold types. The overarching result is that during the experiment duration, there was no significant change in mass within each sample type. These results are consistent with the literature for the PCL<sup>32</sup> and PHBV<sup>84</sup>.

#### **8.2.4. Cytocompatibility, morphology, and metabolism studies**

Analysis of cytocompatibility using LIVE / DEAD staining showed overall good compatibility across scaffold types, with low numbers of dead cells observed at the different time points, with the exception of the experiment reported in Chapter 6, Section 6.2.1. It can be observed that in most experiments, there was a higher number of live cells adhered to collagen conjugated samples, though the difference became less pronounced after day 7. It should also be noted that Neo-NHDF cells adopted a more fibroblastic morphology when seeded on conjugated scaffolds, as seen on PCL log pile scaffolds in Chapter 6, Section 6.3.1. and PHBV fibre scaffolds Chapter 7, Section 7.4.2.

Examination of cell morphology with DAPI / Phalloidin staining on PHBV fibre scaffolds showed a pronounced difference in the morphology and quantity of actin deposited by fibroblasts between conjugated and unconjugated scaffolds. Neo-NHDF Cells seeded on conjugated fibre scaffolds were highly fibroblastic in nature and had deposited significantly higher quantities of actin onto scaffold surfaces, as seen in Chapter 7, Section 7.4.2. This effect is congruent in materials containing PHBV, however, in Chapter 6, Section 6.4.3. little difference can be observed in the morphology or in actin deposition between conjugated and unconjugated PCL samples.

The metabolism of fibroblastic and chondrocyte cells seeded onto scaffolds was assessed by a Presto Blue assay. The behaviour of Neo-NHDF cells on PCL / PCL-Collagen logpile scaffolds and PHBV / PHBV-Collagen fibre scaffolds was broadly analogous, with both experiencing similar increases in output over the course of 7-days. On PCL printed film scaffolds, fibroblasts seeded on conjugated samples showed a significantly higher rate of metabolism than unconjugated samples on days 1 & 3 of a 7-day trial. By contrast fibroblasts seeded onto PHBV-fibre scaffolds showed higher rates of metabolism on conjugated scaffolds on days 3 and 7 of the 7-day trial. Chondrocytes seeded on PCL / PHBV logpile scaffolds did not display a significant difference in the metabolism of cells seeded on conjugated / unconjugated scaffolds at time points between days 1 and 14, though a trend of increasing metabolism was observed in this period. At day 21, there was a significant drop in the metabolic reading on PCL / PHBV logpile scaffolds, and a significantly lower readout on conjugated scaffolds. This may be attributable to the maturation of chondrocytes in a localised deposited ECM<sup>116</sup>.

#### **8.3. Conclusions**

The thesis objectives state the intention to develop new biosynthetic polymer materials and to develop novel conjugation methods to functionalise the base polymers with proteins relevant to cartilage tissue engineering applications. To this end, new synthetic protocols were developed

to create bulk and surface conjugated PCL-Collagen were devised and applied to multiple scaffolds fabrication routes. The scope of creation for new biosynthetic materials was also expanded through the development of polymer blending processes used in the creation of PCL / PHBV-Collagen scaffolds. The optimised conjugation methods developed in Chapter 4 were applied to create 3D printed scaffolds of PCL-Collagen and PCL / PHBV-Collagen, and Forcespun scaffolds of PHBV-Collagen. The physicochemical and biological testing of biosynthetic vs unconjugated scaffolds showed that collagen conjugation improved the biocompatibility properties of the scaffolds under examination. It was determined that surface conjugation was the most efficient method to use in conjunction with the FFF and Forcespinning processes to create a 3D biosynthetic scaffold with enhanced cellular compatibility properties. The objectives also state the intent to assess the fabrication strategies through which biosynthetic materials can be processed into 3D scaffolds. This was investigated through experimentation and optimisation of techniques involving hot-moulding, extrusion, Fused Filament Fabrication, Spin Coating, and Forcespinning. Each of these techniques created scaffolds which displayed distinct physical and mechanical characteristics, indicating different potential end applications for the scaffold types. In particular, the optimisation of PCL filament production and FFF printing created a set of parameters with high repeatability not seen elsewhere in literature where materials were fabricated from base materials rather than purchased, especially when considering the difficulties in processing medical grade high molecular weight PCL. The repeatability of the parameter optimisation was carried over to the FFF printing of PCL / PHBV scaffolds, however, greater variability in output was introduced through the difficulties in producing blended filaments from polymers with such drastically different thermal and mechanical properties. The techniques of FFF and Forcespinning were examined in more detail as they delivered greater versatility than those of hot moulding or spin coating, specifically regarding the control of output. Forcespun and FFF printed scaffolds fit the requirements of consistently distributed high porosity scaffolds, whereas hot moulding and blending produced solid isotropic (by comparison) surfaces. Scaffolds created by FFF are potentially more suited to an application in load bearing cartilage tissue engineering applications, due to higher mechanical strength, in addition to the ability to maintain cellular growth. Scaffolds fabricated from Forcespun fibres displayed quick cellular proliferation, the formation of dense tissue layers, and high levels of maintained cellular activity, however, due to the weak structural properties, it would be suited to superficial or non-loadbearing TE applications. While the objectives were satisfied in the manner of creating new biosynthetic materials, conjugation methods, and developing scaffold fabrication strategies, assigning a specific purpose for the scaffolds was challenging based on the evidence generated. Further

evidence that would expand the knowledge base of these scaffolds will be addressed in the future work. These results are significant in that it delivers new methodologies to the fabrication of enhanced biosynthetic 3D scaffolds to the field of biomaterials. Multiple synthetic strategies were assessed and contrasted for potential application in tissue engineering, with rationale provided to efficacy and efficiency of the techniques in conjunction with selected advanced 3D fabrication techniques. Biological testing on the 3D scaffolds of PCL, PHBV, and PCL / PHBV further evidenced the potential future use of the biosynthetic scaffolds produced through the developed fabrication strategies. To conclude, using chemical conjugation techniques to enhance the surfaces of FFF printed and Forcespun 3D polymer scaffolds with collagen proved a reliable method of improving biocompatibility, and the combination of materials and fabrication process can strongly dictate scaffold applicability in the potential use of these biosynthetic scaffolds for musculoskeletal applications.

#### **8.4. Future work**

##### **8.4.1. Continued support**

In terms of developing the current knowledge base on the biosynthetic materials and scaffolds developed throughout this thesis, the following work could be done to provide a more complete view on the properties.

###### *Mechanical properties of PHBV fibres.*

The geometry and mechanical properties of a scaffolds play a large part in the overall applicability of a scaffold to a potential purpose. Where 3D printed logpile scaffolds were mechanically characterised, PHBV-Collagen fibre scaffolds were unable to be characterised due to equipment sensitivity. Further characterisation of the mechanical properties of fibre scaffolds would give insight to areas of applicability and allow the research to be carried forward.

###### *Scaffold morphology optimisation.*

Literature analysis of studies on the effect of pore size on cell growth and proliferation steered the design of the scaffolds investigated in this thesis. The biological testing carried out showed that the pore size range was sufficient for the growth and proliferation of the cells seeded onto the varying scaffold types. With additional time to experiment, examination of the effect of varying pore size on cell behaviour could give a view to optimising the macrostructure of the scaffolds. Factors easily modified in the FFF printed scaffolds through design alteration and requiring modification of the operating protocol for forcespun fibre scaffolds.

### Cell assay examination

In the chapters describing examination of cells seeded onto the different scaffold types, cell morphology, metabolism, and cytocompatibility are discussed. While this serves as a basis to comment on the success of the biosynthetic scaffolds over unconjugated polymer scaffolds, it does not further elucidate the state of the tissue forming on the scaffolds. An examination of the properties of the tissue formed on scaffolds would be of benefit to future studies, especially in the situation where chondrocytes were used. As was theorised chapter 6, the metabolic activity drop of chondrocytes observed at later time points could be due to chondrocyte maturation, and a technique such as Alcian blue, could be used to quantify the deposition of ECM proteins to confirm. Quantification of Collagen Type I vs Type 2 presence on scaffolds would also help to further elucidate the phenotype of chondrocytic cells on scaffolds. This would give further support to the proposed application of the scaffolds in a cartilage TE environment.

#### **8.4.2. Wider application**

The new biosynthetic material scaffolds developed in this thesis may go on to be used in Osteoarthritis / cartilage repair TE therapeutics with additional supporting evidence. The research shows the potential of the biosynthetic scaffold approach through demonstrating the enhanced growth of cells on the conjugated scaffolds. One could envision an approach, similar to that of Autologous Chondrocyte Implantation, whereby a patient can donate chondrocytes or a less differentiated stem cell, expanded in vitro, and incubated on the scaffolds before reimplantation. The enhanced cell growth coupled with the support matrix of the scaffold could lead to a more successful therapeutic option over that of current therapies, offering those with cartilage damage or mid-stage osteoarthritis a regenerative therapy before the condition worsens to require more drastic surgical intervention. The field of biomaterial research now has gained additionally characterised material synthetic strategies, and characterisation of the resulting materials. In addition, the advanced manufacturing processing strategies for PCL and PHBV have been characterised and optimised in a 3D printing and Forcespinning context, leaving room for further optimisation of scaffold geometries and cellular characterisation. With both 3D log pile scaffolds and 3D fibre scaffolds developed, there is scope for the development of the work to multiple therapeutic targets in load bearing and non-load bearing capacities.

## Appendix: References

1. A., V. C. The history of tissue engineering. *J. Cell. Mol. Med.* **10**, 569–576 (2007).
2. Langer, R. & Vacanti, J. P. - ARTICLES Tissue Engineering. *Science (80-. ).* **260**, 920–926 (1993).
3. Hao, L. & Harris, R. Customised Implants for Bone Replacement and Growth. in *Bio-Materials and Prototyping Applications in Medicine* 79–107 (2008).
4. UK, A. OSTEOARTHRITIS IN GENERAL PRACTICE Data and perspectives. 1–36 (2013).
5. Chen, A., Gupte, C., Akhtar, K., Smith, P. & Cobb, J. The Global Economic Cost of Osteoarthritis: How the UK Compares. *Arthritis* **2012**, 1–6 (2012).
6. Bitton, R. The economic burden of osteoarthritis. *Am. J. Manag. Care* **15**, S230–S235 (2009).
7. Hafez, A. R. & Mohammed, A. Knee Osteoarthritis : A Review of Literature Physical Medicine and Rehabilitation - Knee Osteoarthritis : A Review of Literature. (2019).
8. Cooper, G. M. *et al.* Testing the ‘critical-size’ in calvarial bone defects: revisiting the concept of a critical-size defect (CSD). *Plast Reconstr Surg.* **125**, 1685–1692 (2011).
9. Is 2 cm 2 the Correct Threshold Size to Dictate Articular Cartilage Repair ? Poster No . 1092 • 55th Annual Meeting of the Orthopaedic Research Society. *Poster No. 1092 • 55th Annu. Meet. Orthop. Res. Soc.* **20**, 2008 (2008).
10. The State of Musculoskeletal Health 2019. (2019).
11. Sophia Fox, A. J., Bedi, A. & Rodeo, S. A. The basic science of articular cartilage: Structure, composition, and function. *Sports Health* **1**, 461–468 (2009).
12. Herman, A. R. The history of skin grafts. *J. Drugs Dermatol.* **1**, 298—301 (2002).
13. Maguire, T. J. & Yarmush, M. L. Tissue Engineering and Regenerative Medicine : History , Progress , and Challenges Franc. (2011). doi:10.1146/annurev-chembioeng-061010-114257
14. Rheinwald, J. G. & Green, H. Seria cultivation of strains of human epidemal keratinocytes: the formation keratinizin colonies from single cell is. *Cell* **6**, 331–343 (1975).

15. Burke, J. F., Yannas, O. V., Quinby, W. C., Bondoc, C. C. & Jung, W. K. Successful use of a physiologically acceptable artificial skin in the treatment of extensive burn injury. *Ann. Surg.* **194**, 413–427 (1981).
16. Vacanti, J. P. *et al.* Selective cell transplantation using bioabsorbable artificial polymers as matrices. *J. Pediatr. Surg. Off. J. [the] Surg. Sect. Am. Acad. Pediatr. Br. Assoc. Paediatr. Surg. Am. Pediatr. Surg. Assoc. Can. Assoc. Pediatr. Surg.* **23**, 3–9 (1988).
17. Sundelacruz, S. & Kaplan, D. L. Stem cell- and scaffold-based tissue engineering approaches to osteochondral regenerative medicine. *Semin. Cell Dev. Biol.* **20**, 646–655 (2009).
18. Murphy, C. M., Haugh, M. G. & O'Brien, F. J. The effect of mean pore size on cell attachment, proliferation and migration in collagen-glycosaminoglycan scaffolds for bone tissue engineering. *Biomaterials* **31**, 461–6 (2010).
19. Karageorgiou, V. & Kaplan, D. Porosity of 3D biomaterial scaffolds and osteogenesis. *Biomaterials* **26**, 5474–5491 (2005).
20. Lien, S. M., Ko, L. Y. & Huang, T. J. Effect of pore size on ECM secretion and cell growth in gelatin scaffold for articular cartilage tissue engineering. *Acta Biomater.* **5**, 670–679 (2009).
21. Loh, Q. L. & Choong, C. Three-dimensional scaffolds for tissue engineering applications: Role of porosity and pore size. *Tissue Eng. - Part B Rev.* **19**, 485–502 (2013).
22. Kundu, J., Shim, J.-H., Jang, J., Kim, S.-W. & Cho, D.-W. An additive manufacturing-based PCL–alginate–chondrocyte bioprinted scaffold for cartilage tissue engineering. *J. Tissue Eng. Regen. Med.* **9**, 1286–1297 (2015).
23. Jiao, Z. *et al.* 3D printing of HA / PCL composite tissue engineering scaffolds. *Adv. Ind. Eng. Polym. Res.* **2**, 196–202 (2019).
24. Scaffaro, R., Lopresti, F., Botta, L., Rigogliuso, S. & Ghersi, G. Integration of PCL and PLA in a monolithic porous scaffold for interface tissue engineering. *J. Mech. Behav. Biomed. Mater.* **63**, 303–313 (2016).
25. Sajesh, K. M., Kiran, K., Nair, S. V. & Jayakumar, R. Sequential layer-by-layer electrospinning of nano SrCO<sub>3</sub>/PRP loaded PHBV fibrous scaffold for bone tissue

- engineering. *Compos. Part B Eng.* **99**, 445–452 (2016).
- 26. Hutmacher, D. W. *et al.* Mechanical properties and cell cultural response of polycaprolactone scaffolds designed and fabricated via fused deposition modeling. *J. Biomed. Mater. Res.* **55**, 203–216 (2001).
  - 27. Dhanaraju, M. D., Gopinath, D., Ahmed, M. R., Jayakumar, R. & Vamsadhara, C. Characterization of polymeric poly(??-caprolactone) injectable implant delivery system for the controlled delivery of contraceptive steroids. *J. Biomed. Mater. Res. - Part A* **76**, 63–72 (2006).
  - 28. Sinha, V. R., Bansal, K., Kaushik, R., Kumria, R. & Trehan, A. Poly-??-caprolactone microspheres and nanospheres: An overview. *Int. J. Pharm.* **278**, 1–23 (2004).
  - 29. Vert, M. Degradable and bioresorbable polymers in surgery and in pharmacology: Beliefs and facts. *J. Mater. Sci. Mater. Med.* **20**, 437–446 (2009).
  - 30. Middleton, J. C. & Tipton, A. J. Synthetic biodegradable polymers as orthopedic devices. *Biomaterials* **21**, 2335–2346 (2000).
  - 31. Vert, M., Li, S. M., Spenlehauer, G. & Guerin, P. Bioresorbability and biocompatibility of aliphatic polyesters. *J. Mater. Sci. Mater. Med.* **3**, 432–446 (1992).
  - 32. Woodruff, M. A. & Hutmacher, D. W. The return of a forgotten polymer - Polycaprolactone in the 21st century. *Prog. Polym. Sci.* **35**, 1217–1256 (2010).
  - 33. Bergsma, J. Late degradation tissue response to poly(L-lactide) bone plates and screws. *Biomaterials* **16**, 25–31 (1995).
  - 34. Zein, I., Hutmacher, D. W., Tan, K. C. & Teoh, S. H. Fused deposition modeling of novel scaffold architectures for tissue engineering applications. *Biomaterials* **23**, 1169–1185 (2002).
  - 35. Lam, C. X. F., Hutmacher, D. W., Schantz, J.-T., Woodruff, M. A. & Teoh, S. H. Evaluation of polycaprolactone scaffold degradation for 6 months in vitro and in vivo. *J. Biomed. Mater. Res. A* **90**, 906–919 (2009).
  - 36. Chang, K. Y., Hung, L. H., Chu, I. M., Ko, C. S. & Lee, Y. Der. The application of type II collagen and chondroitin sulfate grafted PCL porous scaffold in cartilage tissue engineering. *J. Biomed. Mater. Res. - Part A* **92**, 712–723 (2010).
  - 37. Kiran, S., Nune, K. C. & Misra, R. D. K. The significance of grafting collagen on

- polycaprolactone composite scaffolds: Processing-structure-functional property relationship. *J. Biomed. Mater. Res. - Part A* **103**, 2919–2931 (2015).
- 38. Sousa, I., Mendes, A. & Bárto, P. J. PCL scaffolds with collagen bioactivator for applications in tissue engineering. *Procedia Eng.* **59**, 279–284 (2013).
  - 39. Uematsu, K. *et al.* Cartilage regeneration using mesenchymal stem cells and a three-dimensional poly-lactic-glycolic acid (PLGA) scaffold. *Biomaterials* **26**, 4273–4279 (2005).
  - 40. Malinauskas, M. *et al.* 3D microporous scaffolds manufactured via combination of fused filament fabrication and direct laser writing ablation. *Micromachines* **5**, 839–858 (2014).
  - 41. Cui, M., Liu, L., Guo, N., Su, R. & Ma, F. Preparation, cell compatibility and degradability of collagen-modified poly(lactic acid). *Molecules* **20**, 595–607 (2015).
  - 42. Reddy, C. S. K., Ghai, R., Rashmi & Kalia, V. C. Polyhydroxyalkanoates: An overview. *Bioresour. Technol.* **87**, 137–146 (2003).
  - 43. Williams, S. F., Martin, D. P., Horowitz, D. M. & Peoples, O. P. PHA applications: Addressing the price performance issue I. Tissue engineering. *Int. J. Biol. Macromol.* **25**, 111–121 (1999).
  - 44. Han, I. *et al.* Effect of poly(3-hydroxybutyrate-co-3-hydroxyvalerate) nanofiber matrices cocultured with hair follicular epithelial and dermal cells for biological wound dressing. *Artif. Organs* **31**, 801–808 (2007).
  - 45. Chen, G. Q. & Wu, Q. The application of polyhydroxyalkanoates as tissue engineering materials. *Biomaterials* **26**, 6565–6578 (2005).
  - 46. Ghebi, A., Khoshnevisan, K., Katabchi, N., Derakhshan, M. A. & Babadi, A. A. Application of Electrospun Nanofibrous PHBV Scaffold in Neural Graft and Regeneration : A Mini-Review. *Nanomed Res J* **1**, 107–111 (2016).
  - 47. Keshel, S. H. *et al.* The healing effect of unrestricted somatic stem cells loaded in collagen-modified nanofibrous PHBV scaffold on full-thickness skin defects. *Artif. Cells, Nanomedicine Biotechnol.* **42**, 210–216 (2014).
  - 48. Sultana, N. & Wang, M. PHBV Tissue Engineering Scaffolds Fabricated via Emulsion Freezing / Freeze-drying : Effects of Processing Parameters. *Int. Conf. Biomed. Eng.*

*Technol.* **11**, 29–34 (2011).

49. Chun, Y. S. & Kim, W. N. Thermal properties of poly(hydroxybutyrate-co-hydroxyvalerate) and poly(??-caprolactone) blends. *Polymer (Guildf.)*. **41**, 2305–2308 (2000).
50. Janik, H. & Marzec, M. A review: Fabrication of porous polyurethane scaffolds. *Mater. Sci. Eng. C* **48**, 586–591 (2015).
51. Gogolewski, S. & Pennings, A. J. An artificial skin based on biodegradable mixtures of polylactides and polyurethanes for full-thickness skin wound covering. *Die Makromol. Chemie, Rapid Commun.* **4**, 675–680 (1983).
52. Gogolewski, S., Galletti, G. & Ussia, G. Polyurethane vascular prostheses in pigs. *Colloid Polym. Sci.* **265**, 774–778 (1987).
53. Chiono, V. *et al.* Poly(ester urethane) Guides for Peripheral Nerve Regeneration. *Macromol. Biosci.* **11**, 245–256 (2011).
54. Tetteh, G., Khan, A. S., Delaine-Smith, R. M., Reilly, G. C. & Rehman, I. U. Electrospun polyurethane/hydroxyapatite bioactive Scaffolds for bone tissue engineering: The role of solvent and hydroxyapatite particles. *J. Mech. Behav. Biomed. Mater.* **39**, 95–110 (2014).
55. Kon, E. *et al.* Biodegradable polyurethane meniscal scaffold for isolated partial lesions or as combined procedure for knees with multiple comorbidities: clinical results at 2 years. *Knee Surgery, Sport. Traumatol. Arthrosc.* **22**, 128–134 (2014).
56. Yang, X. *et al.* Collagen-alginate as bioink for three-dimensional (3D) cell printing based cartilage tissue engineering. *Mater. Sci. Eng. C* **83**, 195–201 (2018).
57. Rhee, S., Puetzer, J. L., Mason, B. N., Reinhart-King, C. A. & Bonassar, L. J. 3D Bioprinting of Spatially Heterogeneous Collagen Constructs for Cartilage Tissue Engineering. *ACS Biomater. Sci. Eng.* **2**, 1800–1805 (2016).
58. Noh, I., Kim, N., Tran, H. N., Lee, J. & Lee, C. 3D printable hyaluronic acid-based hydrogel for its potential application as a bioink in tissue engineering. *Biomater. Res.* **23**, 3 (2019).
59. Kutlusoy, T., Oktay, B., Apohan, N. K., Süleymanoğlu, M. & Kuruca, S. E. Chitosan-co-Hyaluronic acid porous cryogels and their application in tissue engineering. *Int. J.*

*Biol. Macromol.* **103**, 366–378 (2017).

60. Nair, L. S. & Laurencin, C. T. Biodegradable polymers as biomaterials. *Prog. Polym. Sci.* **32**, 762–798 (2007).
61. Altman, G. H. *et al.* Silk-based biomaterials. *Biomaterials* **24**, 401–416 (2003).
62. Ferreira, A. M., Gentile, P., Chiono, V. & Ciardelli, G. Collagen for bone tissue regeneration. *Acta Biomater.* **8**, 3191–3200 (2012).
63. Castillo-Briceño Patricia, P. *et al.* A role for specific collagen motifs during wound healing and inflammatory response of fibroblasts in the teleost fish gilthead seabream. *Mol. Immunol.* **48**, 826–834 (2011).
64. Ferreira, A. M., Gentile, P., Chiono, V. & Ciardelli, G. Collagen for bone tissue regeneration. *Acta Biomater.* **8**, 3191–3200 (2012).
65. Gaudet, I. D. & Shreiber, D. I. Characterization of methacrylated Type-I collagen as a dynamic, photoactive hydrogel. *Biointerphases* **7**, 1–9 (2012).
66. Brodsky, B. & Persikov, A. V. B. T.-A. in P. C. Molecular Structure of the Collagen Triple Helix. in *Fibrous Proteins: Coiled-Coils, Collagen and Elastomers* **70**, 301–339 (Academic Press, 2005).
67. Lloyd, C., Besse, J. & Boyce, S. Controlled-rate freezing to regulate the structure of collagen-glycosaminoglycan scaffolds in engineered skin substitutes. *J. Biomed. Mater. Res. - Part B Appl. Biomater.* **103**, 832–840 (2015).
68. Matsiko, A., Levingstone, T. J., O'Brien, F. J. & Gleeson, J. P. Addition of hyaluronic acid improves cellular infiltration and promotes early-stage chondrogenesis in a collagen-based scaffold for cartilage tissue engineering. *J. Mech. Behav. Biomed. Mater.* **11**, 41–52 (2012).
69. Woodhouse, K. A. *et al.* Investigation of recombinant human elastin polypeptides as non-thrombogenic coatings. *Biomaterials* **25**, 4543–4553 (2004).
70. Kosir, M. A., Quinn, C. C., Wang, W. & Tromp, G. Matrix glycosaminoglycans in the growth phase of fibroblasts: more of the story in wound healing. *J. Surg. Res.* **92**, 45–52 (2000).
71. JLC, van S. *et al.* Linkage of chondroitin-sulfate to type I collagen scaffolds stimulates the bioactivity of seeded chondrocytes in vitro. *Biomaterials* **22**, 2359–2369 (2001).

72. Shi, C. *et al.* Therapeutic Potential of Chitosan and Its Derivatives in Regenerative Medicine1 1 This work was supported by ‘973’ programs on severe trauma (NO. 1999054205 and NO. 2005CB522605) from the Ministry of Science and Technology of China. *J. Surg. Res.* **133**, 185–192 (2006).
73. Jia, L., Prabhakaran, M. P., Qin, X. & Ramakrishna, S. Guiding the orientation of smooth muscle cells on random and aligned polyurethane/collagen nanofibers. *J. Biomater. Appl.* **29**, 364–377 (2014).
74. Yin, D. *et al.* Fabrication of composition-graded collagen/chitosan-polylactide scaffolds with gradient architecture and properties. *React. Funct. Polym.* **83**, 98–106 (2014).
75. Shin, Y. C. *et al.* Stimulated myoblast differentiation on graphene oxide-impregnated PLGA-collagen hybrid fibre matrices matrices. *J. Nanobiotechnology* **13**, 1–11 (2015).
76. Holmes, B., Zhu, W., Li, J., Lee, J. D. & Zhang, L. G. Development of novel three-dimensional printed scaffolds for osteochondral regeneration. *Tissue Eng. Part A* **21**, 403–15 (2015).
77. Veleirinho, B. *et al.* Nanofibrous poly(3-hydroxybutyrate-co-3-hydroxyvalerate)/chitosan scaffolds for skin regeneration. *Int. J. Biol. Macromol.* **51**, 343–350 (2012).
78. Veleirinho, B., Ribeiro-Do-Valle, R. M. & Lopes-Da-Silva, J. A. Processing conditions and characterization of novel electrospun poly (3-hydroxybutyrate-co-hydroxyvalerate)/chitosan blend fibers. *Mater. Lett.* **65**, 2216–2219 (2011).
79. Peschel, G. *et al.* Growth of keratinocytes on porous films of poly(3-hydroxybutyrate) and poly(4-hydroxybutyrate) blended with hyaluronic acid and chitosan. *J. Biomed. Mater. Res. - Part A* **85**, 1072–1081 (2008).
80. Wang, X., Yan, H., Zhou, Y., Lou, X. & Zhang, Y. Fabrication of fibrous PLLA/PHBV scaffolds with shape memory capability. *J. Control. Release* **259**, e144–e145 (2017).
81. Thadavirul, N., Pavasant, P. & Supaphol, P. Fabrication and Evaluation of Polycaprolactone-Poly(hydroxybutyrate) or Poly(3-Hydroxybutyrate- co -3-Hydroxyvalerate) Dual-Leached Porous Scaffolds for Bone Tissue Engineering Applications. *Macromol. Mater. Eng.* **302**, 1600289 (2017).

82. Li, W., Nooeaid, P., Roether, J. A., Schubert, D. W. & Boccaccini, A. R. Preparation and characterization of vancomycin releasing PHBV coated 45S5 Bioglass??-based glass-ceramic scaffolds for bone tissue engineering. *J. Eur. Ceram. Soc.* **34**, 505–514 (2014).
83. Li, W. *et al.* Preparation and characterization of PHBV microsphere/45S5 bioactive glass composite scaffolds with vancomycin releasing function. *Mater. Sci. Eng. C* **41**, 320–328 (2014).
84. Prabhakaran, M. P., Vatankhah, E. & Ramakrishna, S. Electrospun aligned PHBV/collagen nanofibers as substrates for nerve tissue engineering. *Biotechnol. Bioeng.* **110**, 2775–2784 (2013).
85. Wang, Y. *et al.* Surface engineering of PHBV by covalent collagen immobilization to improve cell compatibility. *J. Biomed. Mater. Res. - Part A* **88**, 616–627 (2009).
86. Bazar, E. *et al.* Fabrication of coated-collagen electrospun PHBV nanofiber film by plasma method and its cellular study. *J. Nanomater.* **2011**, (2011).
87. Zeugolis, D. I. *et al.* Electro-spinning of pure collagen nano-fibres - Just an expensive way to make gelatin? *Biomaterials* **29**, 2293–2305 (2008).
88. Lin, K. *et al.* Advanced Collagen-Based Biomaterials for Regenerative Biomedicine. *Adv. Funct. Mater.* **29**, 1–16 (2019).
89. Chau, D. Y. S., Collighan, R. J., Verderio, E. A. M., Addy, V. L. & Griffin, M. The cellular response to transglutaminase-cross-linked collagen. *Biomaterials* **26**, 6518–6529 (2005).
90. Yeung, T. *et al.* Effects of substrate stiffness on cell morphology, cytoskeletal structure, and adhesion. *Cell Motil. Cytoskeleton* **60**, 24–34 (2005).
91. Trappmann, B. *et al.* Extracellular-matrix tethering regulates stem-cell fate. *Nat. Mater.* **11**, 742–742 (2012).
92. Gentile, P., Carmagnola, I., Nardo, T. & Chiono, V. Layer-by-layer assembly for biomedical applications in the last decade. *Nanotechnology* **26**, 422001 (2015).
93. He, X., Wang, Y. & Wu, G. Layer-by-layer assembly of type i collagen and chondroitin sulfate on aminolyzed PU for potential cartilage tissue engineering application. *Appl. Surf. Sci.* **258**, 9918–9925 (2012).

94. Vasita, R. & Katti, D. S. Nanofibers and their applications in tissue engineering. *Int. J. Nanomedicine* **1**, 15–30 (2006).
95. Esfahani, H., Jose, R. & Ramakrishna, S. Electrospun ceramic nanofiber mats today: Synthesis, properties, and applications. *Materials (Basel)*. **10**, (2017).
96. Sarkar, K. *et al.* Electrospinning to Forcespinning<sup>TM</sup>. *Mater. Today* **13**, 12–14 (2010).
97. Padron, S., Fuentes, A., Caruntu, D. & Lozano, K. Experimental study of nanofiber production through forcespinning. *J. Appl. Phys.* **113**, (2013).
98. Upson, S. J., O'Haire, T., Russell, S. J., Dalgarno, K. & Ferreira, A. M. Centrifugally spun PHBV micro and nanofibres. *Mater. Sci. Eng. C* **76**, 190–195 (2017).
99. Hernández, A. R., Contreras, O. C., Acevedo, J. C. & Moreno, L. G. N. Poly( $\epsilon$ -caprolactone) Degradation Under Acidic and Alkaline Conditions. *Am. J. Polym. Sci.* **3**, 70–75 (2013).
100. McColgan-Bannon, K. I. S. *et al.* Biomimetic properties of force-spun PHBV membranes functionalised with collagen as substrates for biomedical application. *Coatings* **9**, (2019).
101. Dapson, R. W., Fagan, C., Kiernan, J. A. & Wickersham, T. W. Certification procedures for sirius red F3B (CI 35780, Direct red 80). *Biotech. Histochem.* **86**, 133–9 (2011).
102. Zhang, Y. Z., Venugopal, J., Huang, Z. M., Lim, C. T. & Ramakrishna, S. Characterization of the surface biocompatibility of the electrospun PCL-Collagen nanofibers using fibroblasts. *Biomacromolecules* **6**, 2583–2589 (2005).
103. Khalili, A. A. & Ahmad, M. R. A Review of cell adhesion studies for biomedical and biological applications. *Int. J. Mol. Sci.* **16**, 18149–18184 (2015).
104. Keshel, S. H. *et al.* The relationship between cellular adhesion and surface roughness for polyurethane modified by microwave plasma radiation. *Int. J. Nanomedicine* **6**, 641–647 (2011).
105. Yuan, S., Xiong, G., Wang, X., Zhang, S. & Choong, C. Surface modification of polycaprolactone substrates using collagen-conjugated poly(methacrylic acid) brushes for the regulation of cell proliferation and endothelialisation. *J. Mater. Chem.* **22**, 13039–13049 (2012).

106. Dowling, D. P., Miller, I. S., Ardhaoui, M. & Gallagher, W. M. Effect of surface wettability and topography on the adhesion of osteosarcoma cells on plasma-modified polystyrene. *J. Biomater. Appl.* **26**, 327–347 (2011).
107. Little, C. J., Bawolin, N. K. & Chen, X. Mechanical properties of natural cartilage and tissue-engineered constructs. *Tissue Eng. - Part B Rev.* **17**, 213–227 (2011).
108. Wang, Y. *et al.* Biosynthesis and Thermal Properties of PHBV Produced from Levulinic Acid by Ralstonia eutropha. *PLoS One* **8**, 4–11 (2013).
109. Kosorn, W. *et al.* PCL/PHBV blended three dimensional scaffolds fabricated by fused deposition modeling and responses of chondrocytes to the scaffolds. *J. Biomed. Mater. Res. - Part B Appl. Biomater.* **105**, 1141–1150 (2017).
110. Shuai, C. *et al.* Calcium silicate improved bioactivity and mechanical properties of poly(3-hydroxybutyrate-co-3-hydroxyvalerate) scaffolds. *Polymers (Basel)*. **9**, 1–15 (2017).
111. Sultana, N. & Khan, T. H. In vitro degradation of PHBV scaffolds and nHA/PHBV composite scaffolds containing hydroxyapatite nanoparticles for bone tissue engineering. *J. Nanomater.* **2012**, (2012).
112. Beck, E. C., Barragan, M., Tadros, M. H., Gehrke, S. H. & Detamore, M. S. Approaching the compressive modulus of articular cartilage with a decellularized cartilage-based hydrogel. *Acta Biomater.* **38**, 94–105 (2016).
113. Sousa, I., Mendes, A., Pereira, R. F. & Bártolo, P. J. Collagen surface modified poly( $\epsilon$ -caprolactone) scaffolds with improved hydrophilicity and cell adhesion properties. *Mater. Lett.* **134**, 263–267 (2014).
114. Yao, Y. & Wang, C. Dedifferentiation: inspiration for devising engineering strategies for regenerative medicine. *npj Regen. Med.* **5**, (2020).
115. Bianchi, V. J. *et al.* Redifferentiated Chondrocytes in Fibrin Gel for the Repair of Articular Cartilage Lesions. *Am. J. Sports Med.* **47**, 2348–2359 (2019).
116. Akkiraju, H. & Nohe, A. Role of chondrocytes in cartilage formation, progression of osteoarthritis and cartilage regeneration. *J. Dev. Biol.* **3**, 177–192 (2015).
117. Assay, S. C. Sircol.
118. Lü, L. X., Wang, Y. Y., Mao, X., Xiao, Z. D. & Huang, N. P. The effects of PHBV

- electrospun fibers with different diameters and orientations on growth behavior of bone-marrow-derived mesenchymal stem cells. *Biomed. Mater.* **7**, (2012).
119. Keshel, S. H. *et al.* The healing effect of unrestricted somatic stem cells loaded in collagen-modified nanofibrous PHBV scaffold on full-thickness skin defects. *Artif. Cells, Nanomedicine Biotechnol.* **42**, 210–216 (2014).
120. Gentile, P. *et al.* Biosynthetic PCL-graft-collagen bulk material for tissue engineering applications. *Materials (Basel)*. **10**, (2017).
121. De Campos Vidal, B. & Mello, M. L. S. Collagen type I amide I band infrared spectroscopy. *Micron* **42**, 283–289 (2011).
122. Zhang, X. Y., Zheng, Y., Liu, C. H., Wang, P. H. & Zhu, Y. Y. Facile and large scale in situ synthesis of the thermal responsive fluorescent SiNPs/PNIPAM hydrogels. *RSC Adv.* **6**, 55666–55670 (2016).
123. Dementjev, A. P. *et al.* X-ray photoelectron spectroscopy reference data for identification of the C<sub>3</sub>N<sub>4</sub> phase in carbon-nitrogen films. *Diam. Relat. Mater.* **9**, 1904–1907 (2000).
124. Diller, K. *et al.* Temperature-dependent templated growth of porphine thin films on the (111) facets of copper and silver. *J. Chem. Phys.* **141**, 1–8 (2014).
125. Yong, T. *et al.* Electrospun nanofibers: solving global issues. *Mater. Today* **9**, 40–50 (2006).
126. Wang, X. Z. *et al.* Thermal Properties and Biodegradability Studies of Poly(3-hydroxybutyrate-co-3-hydroxyvalerate). *J. Polym. Environ.* **20**, 23–28 (2011).
127. Leikina, E., Mertts, M. V., Kuznetsova, N. & Leikin, S. Type I collagen is thermally unstable at body temperature. *Proc. Natl. Acad. Sci.* **99**, 1314–1318 (2002).
128. Ke, Y., Wang, Y., Ren, L., Wu, G. & Xue, W. Surface Modification of PHBV Films with Different Functional Groups: Thermal Properties and In Vitro Degradation. *J. Appl. Polym. Sci.* **116**, 2658–2667 (2010).
129. Amass, W., Amass, A. & Tighe, B. A review of biodegradable polymers: Uses, current developments in the synthesis and characterization of biodegradable polyesters, blends of biodegradable polymers and recent advances in biodegradation studies. *Polym. Int.* **47**, 89–144 (1998).

130. Heino, J. The collagen family members as cell adhesion proteins. *BioEssays* **29**, 1001–1010 (2007).
131. Insomphun, C., Chuah, J. A., Kobayashi, S., Fujiki, T. & Numata, K. Influence of Hydroxyl Groups on the Cell Viability of Polyhydroxyalkanoate (PHA) Scaffolds for Tissue Engineering. *ACS Biomater. Sci. Eng.* **3**, 3064–3075 (2017).
132. Beck, U. *et al.* Cell architecture–cell function dependencies on titanium arrays with regular geometry. *Biomaterials* **31**, 5729–5740 (2010).